Adsorption Calorimetry Measurements of the Energetics of Catalytic Intermediates: Empirical Trends and Benchmarks for Theory

Eric M. Karp

A dissertation

submitted in partial fulfillment of the

requirements for the degree of

Doctor of Philosophy

University of Washington

2012

Reading Committee:

Charles T. Campbell, Chair

Stuart B. Adler

David G. Castner

Program Authorized to Offer Degree:

Chemical Engineering

Abstract

Energetics of Catalytic Intermediates from Single Crystal Adsorption Calorimetry, Empirical Trends, and Benchmarks for DFT

Eric M. Karp

Chair of the Supervisory Committee:

Professor Charles T. Campbell

Chemical Engineering

Catalysts enable chemical reactions to occur with less energy input than would be required without a catalyst, simultaneously increasing the rate and selectivity of a reaction. Thus, catalysts are important industrial materials crucial for the production of commodity chemicals and fuels. In particular, solid, heterogeneous catalysts are of great interest in the chemical industry, because the reactants and products can be easily separated from the catalyst. Much effort is dedicated to the discovery and development of new catalytic materials capable of facilitating important industrial reactions, however these materials are mainly discovered through a trial and error approach, which can be a time-consuming and expensive process. A quicker and more efficient way to develop the future generation of catalysts is to understand the fundamental energetics that control catalytic activity and selectivity and understand how those energetics depend on catalyst surface structure and composition. The most important parameters that

determine the activity of a catalyst material are the bond strengths with which it binds a few key chemical intermediates and transition states. There are many computational approaches (mainly based on Density Functional Theory, DFT) that calculate these parameters and how they depend on the material. This provides a wonderful opportunity for computational screening of potential new catalytic materials that has already led to the discovery of a few new catalysts. However, prior calorimetry results suggest that even the best of these methods may not yet be accurate enough to achieve anywhere near its full potential for catalyst discovery. Unfortunately, accurate experimental values are still not available for the bond strengths of even the simplest adsorbates to catalyst materials, like -OH, $-OCH_3$, -CH and $-CH_3$, which are very widely recognized to be key intermediates in a broad variety of catalytic reactions used in energy and environmental technology.

In this dissertation, I detail the results of experimental measurements of the energetics of these important adsorbates on Pt(111), using Single Crystal Adsorption Calorimetry (SCAC). The results provide important benchmarks for assessing the accuracy of new calculational methods based on DFT that are being designed to achieve higher energy accuracy. Thus, these experimental energies are compared to published DFT results throughout these chapters. Earlier measurements of oxygen adsorption energies on Pt(111) both from TPD and calorimetry data are reexamined also in light of our group's calorimeter calibration methods, and it is shown that a calibration error was made in that calorimetry data. We present corrected values for the calorimetric adsorption energy of oxygen on Pt(111), show that it agrees with prior TPD results, and use it to amend previously-reported energetics of adsorbed OH.

Finally, SCAC results for several oxygen-containing ligands on Pt(111) which bind to the Pt through an oxygen atom are shown to follow a trend, whereby their O-Pt(111) bond strength

is proportional to the strength with which these ligands bind H in gas-phase molecules, with a slope of 1.0. This trend allows the prediction of the bond strengths for other adsorbates that cannot or have not been measured. This trend is identical to one observed previously for the bond strength in organometallic complexes between metal centers and ligands. Here this trend is shown, for the first time, to also hold for metal surfaces and adsorbates bound through a single bond, and is hopefully the first step in developing trends for design rules for catalytic materials based on fundamental parameters.

Table of Contents

List of Tables

List of Figures

Acknowledgements

Funding for the work presented in this dissertation comes from the National Science Foundation under CHE-1010287. E. M. Karp foremost thanks Professor Charles Campbell for his guidance and wisdom throughout the completion of the work presented here and would like to acknowledge several others including: Trent Silbaugh for many thought provoking conversations and invaluable help with both data analysis and lab work, Dr. Matthew Crowe for taking the time and effort to educated me on the basics of ultrahigh vacuum technology, Brian Holm and John Heutink for their instruction in the Chemistry machine shop, and finally the entire Chemical Engineering faculty for admission into a doctoral program that provided me a truly world class education.

Chapter 1 Introduction

The industrially important properties of solid catalysts (selectivity, activity, poisoning resistance, etc.) depend on the adsorption energies of key chemical intermediates on the surfaces of catalytic materials. Knowledge of how these energies (heats of formation, and bond strengths) depend upon the atomic-level structure and composition of the surface is needed to understand the structure / function relationships in catalytic materials, crucial for the development of the next generation of catalysts for energy and environmental catalysts.

Much effort is dedicated to the discovery and development of new catalytic materials capable of facilitating important industrial reactions, however these materials are mainly discovered through a trial and error approach, which can be a time-consuming and expensive process. A quicker and more efficient way to develop the future generation of catalysts is to understand the fundamental energetics that control catalytic activity and selectivity and how those energetics depend on catalyst surface structure and composition. That is, the most important parameters that determine the activity of a catalyst material are the bond strengths with which it binds a few key chemical intermediates and transition states. As such, it is important that the energetics of adsorbates be measured on model systems with well-defined surface structures and compositions. However, there are also many computational approaches (mainly based on Density Functional Theory, DFT) that calculate these parameters and how they depend on the material. This provides a wonderful opportunity for computational screening of potential new catalytic materials that has already led to the discovery of a few new catalysts.[1-4] However, prior calorimetry results suggest that even the best of these methods may not yet be accurate

enough to achieve anywhere near its full potential for catalyst discovery. Yet accurate experimental values are still not available for the bond strengths of even the simplest adsorbates to catalyst materials, like -OH, -OCH_3, -CH and -CH_3, which are very widely recognized to be key intermediates in a broad variety of catalytic reactions used in energy and environmental technology. Thus, it is still difficult to assess the accuracy of these DFT calculations for some of the simplest and most important adsorbates. This dissertation presents calorimetric results for many of these species in well-defined structures on Pt(111), and thus provide key benchmarks for testing and improvement of new DFT methods that can potentially greatly accelerate the computational discovery of new catalysts.

Chapter 3 reports the adsorption energy (heat of formation and bond strength) of adsorbed methoxy, on Pt(111). Methoxy was chosen to study because it is the simplest adsorbed alkoxy species, which are ubiquitous adsorbates in catalytic combustion, selective oxidation and steam reforming reactions that take place on Pt and/or Pt group metals. These reactions have attracted much attention for application in direct alcohol fuel cells and for the production of high purity hydrogen. Methanol is an appealing oxygenate for these reactions because it has a high H/C ratio, lacks a C-C bond allowing good selectivity at lower temperatures, and is a liquid under standard conditions that can be easily transported. As such, much work has been dedicated to elucidating the chemical pathway methanol follows on Pt surfaces. Microkinetic models have been developed[5,6] in which many intermediates have been proposed, but only a few have been directly observed. One of the more stable intermediates in these pathways is surface bound methoxy, which has been observed under reaction conditions on Pt supported catalysts[7-10] and in ultrahigh vacuum (UHV) conditions on Pt single crystal surfaces[11-15] and thus because of its stability is thought to play an important role in the rate limiting steps of these reactions. Since

the important catalytic parameters of selectivity and activity depend on the thermodynamic stability of adsorbed intermediates, it is important that the energetics (heat of adsorption, bond strength, etc.) of methoxy be measured. Using these values, reaction energies for several surface reactions of methanol decomposition on Pt(111) can be obtained. This yields much fundamental insight into the interaction between methanol (and other simple alcohols) on Pt surfaces. These reaction energies give thermodynamic insight into the reactions that may be occurring under reaction conditions in direct alcohol fuel cells and in Pt based catalytic processes for the production of high purity hydrogen from methanol.

In Chapter 4, the adsorption energies of adsorbed $CH_{3,ad}$ (where the subscript ad represents an adsorbed species) and CH_{ad} are reported. These adsorbates where chosen to be measured because they are simple hydrocarbon fragments that are known to be key intermediates in energy-related catalysis over late transition metals, including: partial oxidation of methane, steam reforming, combustion and selective oxidations of methane and various other hydrocarbons and oxygenates, methanation, Fischer-Tropsch, methanol decomposition, and several fuel cells reactions. Similarly to methoxy, these simple hydrocarbon fragments ($CH_{3,ad}$, $CH_{2,ad}$, and CH_{ad}) are stable enough to have been isolated on both Pt supported catalysts[16] and Pt(111) single crystal surfaces in ultrahigh vacuum (UHV) conditions[17-19], and because of their stability are likely involved in rate limiting steps of the above reactions at industrial conditions. Measuring the adsorption energies of $CH_{3,ad}$ and CH_{ad} allows the reaction energies of several surface reactions involving methane on Pt(111), and knowing these values gives insight into the chemical pathways hydrocarbons undergo on Pt based catalysts in industrial reactions.

There have been many techniques developed to measure adsorption energies of molecules on surfaces, such as Temperature Programmed Desorption (TPD) and equilibrium

adsorption isotherms. However, these techniques are indirect measurements and have drawbacks in that they require the adsorbate to adsorb and desorb reversibly from the surface. This is an unfortunate limitation, because many chemical intermediates that are stable enough to be observed under reaction conditions do not adsorb and desorb reversibly, this is unfortunately true for the adsorbates listed above (methoxy, methyl, and methylidyne) which we have chosen to study due to their prevalence in industrial reactions. Therefore, the best approach to make these measurements is to directly measure the heat released upon production of these chemical intermediates using Calorimetry. Calorimetry is the experimental science of measuring the energy of physical changes. The energy of a physical change is a fundamental quantity that allows us to calculate enthalpies of formation, entropic values, and free energies of a system. However, in these types of experiments a reactant gas must react with the surface of a single crystal to cleanly produce a well-defined adsorbate. This is a difficult system to apply Calorimetry, because the cleanliness necessary for production of a specific adsorbate requires one to work in Ultrahigh Vacuum (UHV) conditions and since the adsorption energy of chemical intermediates is known to vary with surface coverage, submonolayer amounts of reactant gas must be dosed. This makes the heat released upon reaction very small (1-10 mK even for very thin crystals (1000 nm)) and design of a heat detector sensitive enough for this task is challenging. Additionally, during each dose of reactant gas to the surface, the probability that the molecules stick and react is not always unity and thus the molecules reflected after each dose must be simultaneously measured in order to extract an accurate heat of reaction in kJ per mole *adsorbed*.

In the 1990's, Sir David King's research group at Cambridge first pioneered Single Crystal Adsorption Calorimetry (SCAC) by using an optical pyrometer to detect the heat

released when a dose of reactant gas was impinged on the surface of a single crystal.[20-22] This technique was used to successfully measure the energetics of adsorbed oxygen, carbon monoxide, and nitric oxide among others (a review of their work can be found in Ref. [23]). However, their technique had limitations. The signal from the optical pyrometer relies on the black body radiation from the single crystal, which has a strong dependence on temperature dictated by the Stefan-boltzmann law; $j = \sigma T^4$ (where j is the emitted power). The signal dependence on temperature constrained this technique to use at ambient temperatures or above and because many chemical intermediates can only be isolated on single crystal surface at cryogenic temperatures (~77 - 200 K), in UHV, this technique only provided interesting results for a few adsorbates. As an example, adsorbed methoxy is an important intermediate thought to be involved in rate limiting steps in methanol reforming and synthesis reactions over Pt catalysts. Although it is stable on Pt(111) at 150 K in UHV[11,12], any higher temperatures result in its rapid decomposition. Therefore the King group's optical pyrometer technique could not be used to measure the energetics of this adsorbate.

To extend the temperature range of SCAC, the King group experimented with a pyroelectric heat detection scheme where a single crystal of Ni(100) was cold welded onto solid $LiTaO_3$ (lithium tantalate).[24] Oxygen was then pulsed onto the Ni(100) surface and the adsorption event released heat. As the heat transferred to the substrate the $LiTaO_3$ produced a voltage change resulting from the pyroelectric effect. The voltage change was recorded and calibrated by impinging a pulse of known energy onto the Ni(100) surface with a HeNe laser. This allowed each recorded signal to be converted to a value in kJ/mol. While this was the first successful attempt using a pyroelectric detector to measure a heat of adsorption on a single crystal[24] as a function of surface coverage, the technique's major drawback was that the Ni(100)

surface was cold welded to solid $LiTaO_3$ and could not be annealed to the high temperatures necessary for achieving surface order on most catalytic metals without damaging the heat detector.

To improve upon this technique, Prof. Campbell's group here at the University of Washington developed a new microcalorimetric method that utilizes a β-Polyvinylidene fluoride (PVDF) heat detector. A cartoon depiction and a photo of the instrumentation are shown in Figure 1.1 below. Pulses of reactant gas from a molecular beam are dosed onto the front face of a thin (1 μm) single crystal foil shown in Figure 1.1 (for the results presented in this dissertation that metal foil is Pt(111)) and the β-PVDF heat detector is pressed onto the back face of the single crystal foil. The heat released during each dose of reactant gas is measured by conduction of the evolved heat to the PVDF heat detector. The advantage of this technique is that the heat detector can be retracted from the sample, allowing the single crystal to be cleaned and annealed easily. Additionally, the sample can be flash heated just prior to an experiment. This ensures the sample surface is free of any adsorbates that may have accumulated from background gases in the chamber that could affect the results. The PVDF heat detector is functional at cryogenic temperatures from 77 K up to 350 K, but at temperatures greater than 350 K the β-PVDF ribbon will lose its pyroelectric properties.

As mentioned above the third and fourth chapters of this dissertation present two projects that utilize the Campbell SCAC technique to measure the energetics of adsorbed methoxy, methyl, and methylidyne on Pt(111). Methoxy, the simplest alkoxy, was chosen to be measured because has been observed under reaction conditions on several transition metal catalysts and because it is stable enough to be observed it is thought to be an important chemical intermediate in catalytic reactions involving alcohols (e.g. alcohol reforming and synthesis reactions). As

such, it is important that its energetics be measured since they are useful values for constructing microkinetic models that can be used to optimize these types of catalytic processes and can aid in new catalyst development. To measure the energetics of methoxy on Pt(111) the Campbell SCAC technique is the only available method since methoxy is isolated on Pt(111) at cryogenic temperatures (150 K) and decomposes upon heating, making it impossible to measure by other techniques like TPD.

The methyl and methylidyne chemical intermediates were chosen to be measured because these hydrocarbon fragments have been observed on transitional metal catalysts that facilitate hydrocarbon reforming and synthesis reactions. Again, because these intermediates are stable enough to be observed they are thought to be involved in the rate limiting steps of these types of reactions. The direct calorimetric measurement of these fragments (detailed in chapter 4) provides their heats of formation and bond strength to the Pt(111) surface. Here again the Campbell SCAC method is the only available technique to make these measurements since methyl and methylidyne decompose upon heating, making their measurement inaccessible by techniques like TPD. The energetics measured here are useful for constructing microkinetic models that can be used to optimize catalytic hydrocarbon processing reactions and can aid in new catalyst development. An example of an enthalpy landscape for surface reactions of methane on Pt(111) is shown in Figure 1.2. Here the energies for each reaction step are found using the measured values is chapter 4.

In addition to providing thermodynamic values for these adsorbates, these measurements are crucial benchmarks for theoretical methods like Density Functional Theory (DFT) that attempt to calculate energetic parameters of adsorbates to predict catalytic pathways of molecules on surfaces. DFT is an important tool for accelerating the discovery of new catalytic

materials. However, its accuracy for these types of energetic parameters must be improved if it is to make accurate predictions. The measurements made in Chapters 3 and 4 are directly compared to calculations from DFT and shed light on how these computational methods are performing. In Chapter 5 a study of binding energies from adsorbed oxygen both from TPD and from Calorimetry from King's group are compared to DFT calculations. In this work an error was discovered in a previous measurement made be Fiorin et. al., a correction was applied and the results are compared to findings from other studies of the same system. This chapter also provides further comparisons between DFT and experiments for water and hydroxyl on Pt(111) this is shown to have a large impact on predicting the thermodynamics of some reactions (e.g. 2 hydroxyls combining to form adsorbed water and an oxygen adatom), which are important steps in water gas shift catalysis over late transition metals. Figure 1.3 shows the enthalpy landscape for water dissociation reactions on Pt(111). These types of reaction energies are important for industrial Pt based catalysts that exhibit water gas shift activity.

Finally, in Chapter 6 I report our discovery of a trend in the bond strengths measured by SCAC of several adsorbates bound through their oxygen atom to the Pt(111) surface. This trend plots the gas phase hydrogen-ligand bond strength versus the Pt(111) to adsorbate bond strength. When plotted in this fashion the adsorbates fall on a line with a slope equal to 1. This relationship allows the bond strength of many other important adsorbates, that cannot or have not been measured, to be predicted simply by knowing the gas phase hydrogen-ligand bond strength, for which much data exists. This trend is identical to the trend developed by Bryndza et. al.[25] for ligand bonding to metal centers in organometallic complexes, but it is the first time it has been shown to also hold for metal surfaces. The value of this trend is that it relies on gas phase

thermodynamic data, which is readily available, to predict surface to adsorbate bond strengths so that difficult SCAC experiments do not need to be performed to find these values.

1.1 Figures

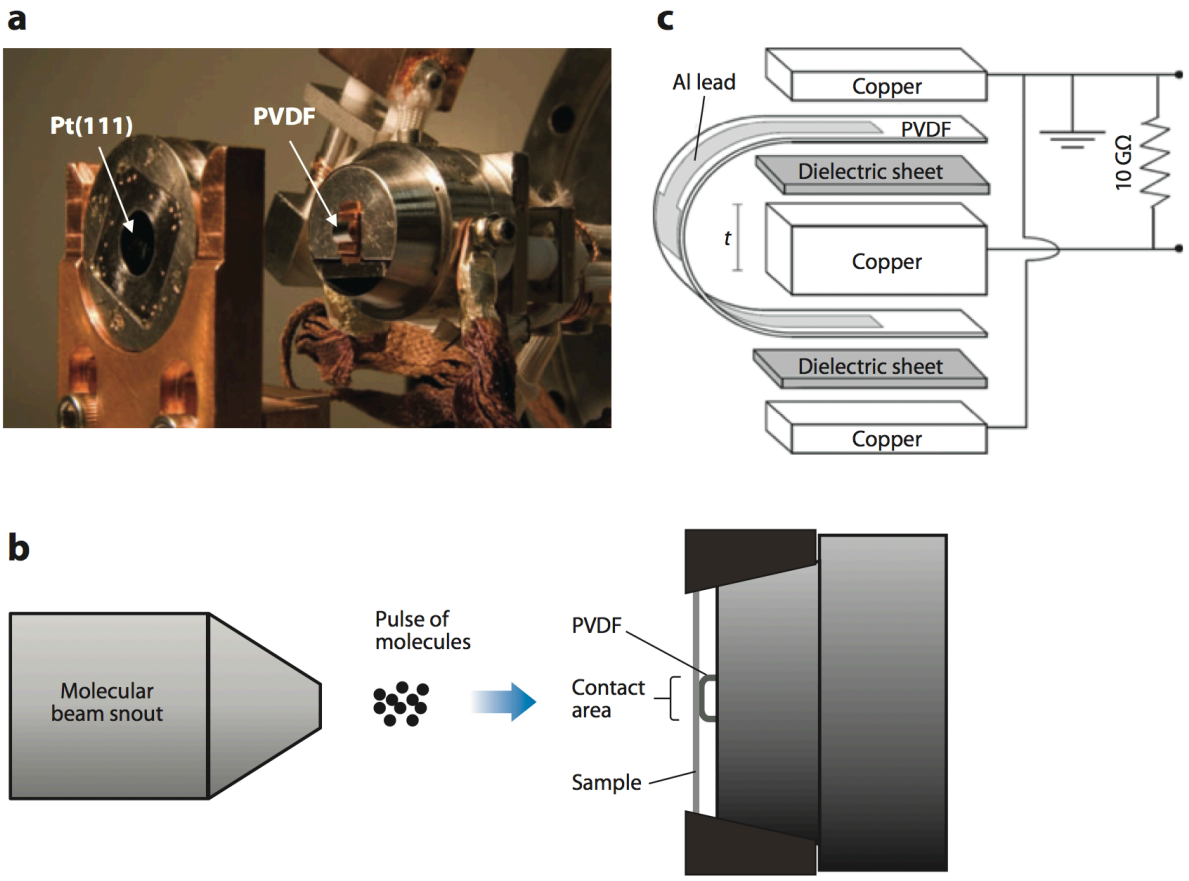

Figure 1.1: (*a*) The Campbell group's single-crystal adsorption calorimetry (SCAC) pyroelectric heat detector assembly, which houses a polyvinylidene fluoride (PVDF) ribbon (4 mm wide, held in a 6-mm-diameter arc), shown retracted from a single-crystal sample holder that exposes an 8-mm-diameter area of the Pt(111) sample's surface. A linear translator is used to press the pyroelectric detector into thermal contact with the back face of the sample during heat measurement. The ribbon is fully coated on the front and back faces with a thin layer of aluminum, as received from the manufacturer (Goodfellow) (*b*) Schematic of an SCAC experiment. The molecular beam emits spatiotemporally resolved pulses of gas-phase atoms or molecules that impinge on the sample surface; the pyroelectric heat detector, shown pressed into contact with the back face of a single-crystal sample, measures temperature changes associated with adsorption events. (*c*) Exploded view of the detector assembly, showing the PVDF ribbon with patterned aluminum electrodes, ribbon-mounting hardware, and a portion of the associated electronic circuitry. (Figure and caption taken with permission from ref. [26])

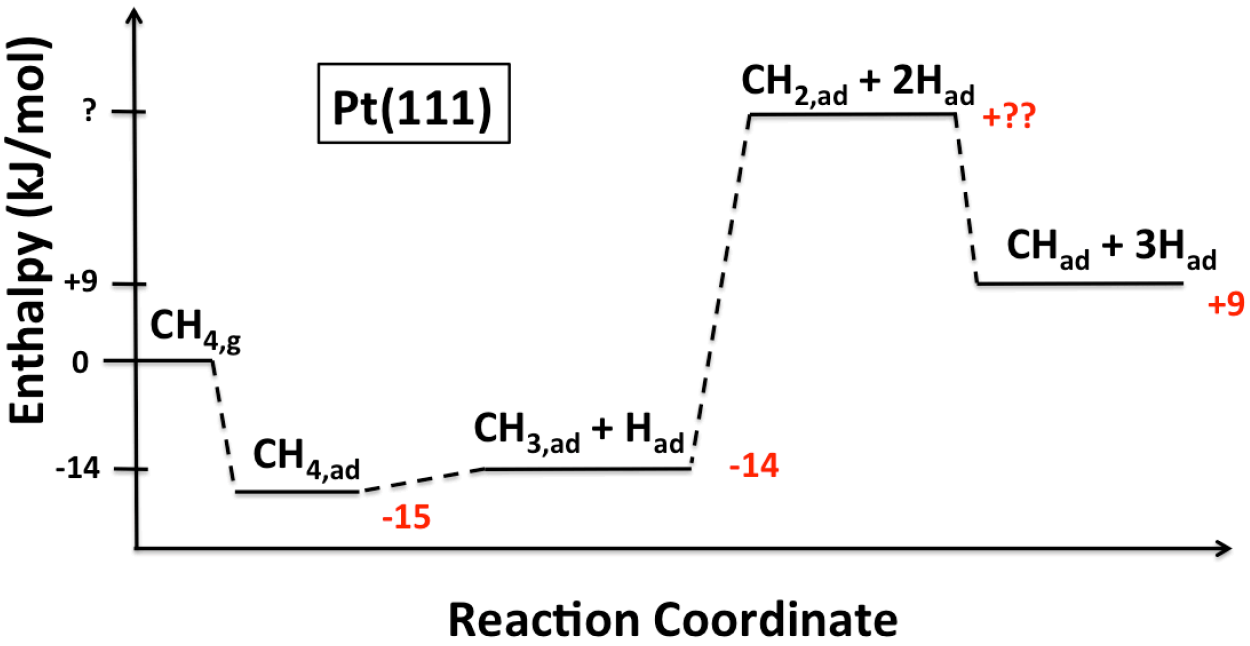

Figure 1.2:. Reaction enthalpy landscape for three steps of methane dehydrogenation on Pt(111) calculated from the heats of formation of methyl fragments measured in chapter 4 and referenced to methane gas. Note here that the enthalpy for dehydrogenation of methane gas to to $CH_{2,ad}$ and 2 hydrogen adatoms is unknown, but is shown here higher than $CH_{ad} + 3H_{ad}$ since methylene is known to decompose at low temperatures (~130 K) to $CH_{ad} + H_{ad}$.

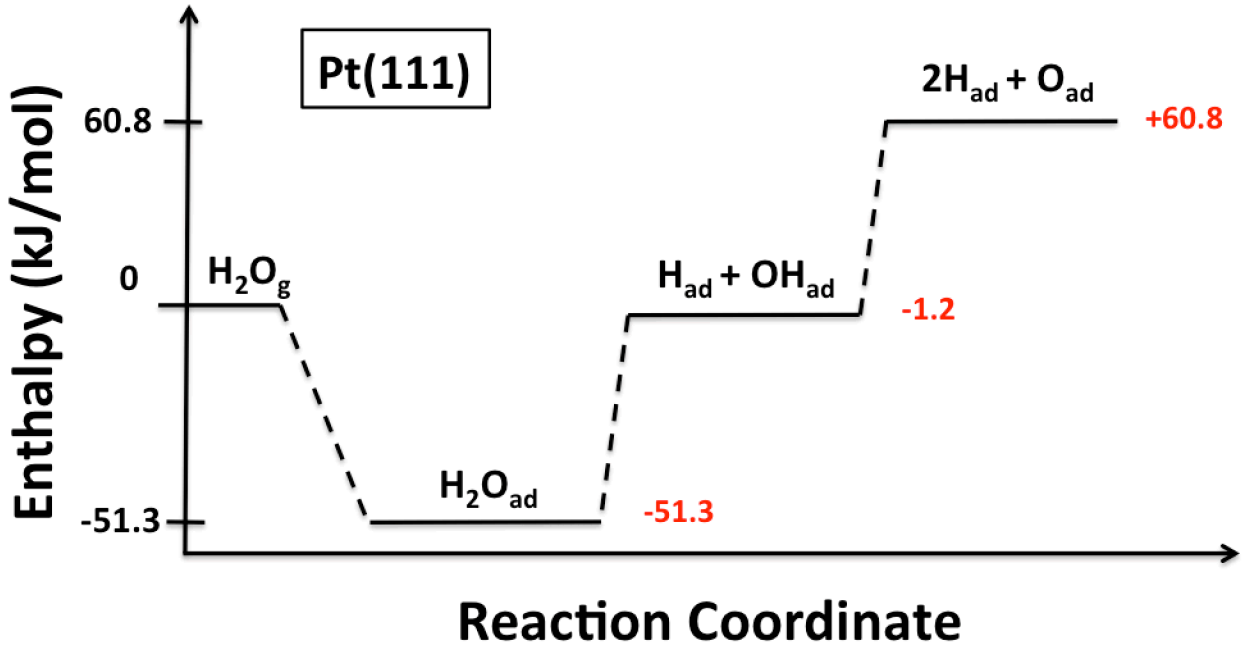

Figure 1.3:. Reaction enthalpy landscape for three steps of water dissociation on Pt(111) calculated from the heats of formation of water, hydroxyl and oxygen adsorbates, each measured calorimetrically.

Chapter 2 Experimental

The experiments in chapters 3 and 4 were performed in a UHV chamber (base pressure <2 x 10^{-10} mbar) equipped with X-ray photoelectron spectroscopy (XPS), Auger electron spectroscopy (AES), low energy ion scattering spectroscopy (LEIS), low energy electron diffraction (LEED), and SCAC. The apparatus and procedures for SCAC have been described in previous publications.[27,28]

The sample used was a 1 μm thick Pt(111) single crystal foil, supplied by Jacques Chevallier at Aarhus University in Denmark. The sample surface was cleaned by 1.25 kV Ar^+ ion sputtering, annealing at 1123 K, then gently heating at 773 K in $1x10^{-8}$ mbar $O_{2,g}$ for 1 minute to remove any surface carbon, and finally flash heating to 1123 K (<1 s). After this treatment, impurities were below the detection limit of AES, and the surface gave a very sharp Pt(111) LEED pattern.

Before calorimetry, the clean Pt(111) sample was brought to thermal equilibrium with the calorimeter and then flash heated to 1123 K (<1 s) to ensure a clean surface. The sample was then brought back into contact with the pyroelectric detector and thermal equilibrium was re-established (in about 5 minutes), after which the experiment was performed. Note that in Chapter 3, to produce the Pt(111) surface predosed with 0.25 ML of O adatoms (p(2x2) over-layer), the surface was exposed to $1x10^{-7}$ mbar of $O_{2,g}$ for 60 seconds from a directed doser immediately after this heating so that the sample was still above 150 K during dosing to dissociate all of the adsorbed O_2.

Calorimetry was performed by exposing the surface to a pulsed molecular beam of methanol (CH_3OH) gas for the work in Chapter 3 and methyl iodide (CH_3I) gas in chapter 4. Each pulse was 102 ms long and repeated every 2 seconds for methanol and every 5 seconds for

CH_3I_g. The liquid reactant (methanol or methyl iodide) was purified by several freeze-pump-thaw cycles after being put into its reservoir on the vacuum chamber. Its purity was checked with a mass spectrometer and found to be consistent with the manufacturer's claim. The beam was created by expanding ~1.3 mbar of methanol or 2.0 mbar or CH_3I_g through a microchannel array at 299±6 K (defining the gas temperature) and then collimated through a series of five liquid nitrogen cooled orifices as described previously.[29] A schematic of the molecular beam is shown in Figure 2.1, below. Coverages of adsorbates are reported in monolayers (ML) and are defined as the number of adsorbate molecules that adsorb to the surface irreversibly, normalized by the number of platinum surface atoms in the Pt(111) surface (1.50×10^{19} Pt atoms / m^2). A typical methanol dose was ~0.01 ML (1.88×10^{12} molecules) per pulse and a typical CH3Ig dose was ~0.004 ML (4.64×10^{12} molecules) with a beam spot size previously determined to be 4.36 mm in diameter.[29] In a given run, the dose per pulse was highly precise (<1% pulse-to-pulse variation, determined by the reproducibility of the chopper's beam-open time). The absolute accuracy of the measurement of the number of molecules per pulse was better than the measured 3% accuracy of the combined heat measurement, but how much better is difficult to determine. A more detailed description of the experimental principles and implementation of the molecular beam can be found elsewhere.[29,30] The flux of methanol and / or methyl iodide from the molecular beam is measured by impinging the beam onto a liquid nitrogen cooled quartz crystal microbalance (QCM), pre-covered with multilayers of methanol or methyl iodide. Calibration of the QCM has been described previously.[29]

The heat released from the adsorption of one gas pulse is measured with a pyroelectric polymer ribbon gently pressed against the back side of the Pt(111) sample (Figure 1.1).[27,31] The

sensitivity of the pyroelectric detector was calibrated after each experiment by depositing a known amount of energy into the sample using a HeNe (632.8 nm) laser. The absolute accuracy of the calorimetric heats is estimated to be better than 3% (i.e., any systematic errors are less than 3%) for systems like those studied here, which have sticking probabilities above 0.8. This is based on comparisons to literature values for standard enthalpies of sublimation of the bulk solid when forming solids with known enthalpies, specifically multilayers of adsorbed cyclohexene,[30] methanol (Chapter 3), methyl iodide (Chapter 4),[32] and water[28] on Pt(111). For these molecules, the differences between the measured value and the estimated heat of sublimation based on the literature values for the standard enthalpies of phase transition (after correcting for temperature differences using literature values for heat capacities) were -5.6%, -3.3%, <1%, and -5.1%, respectively. Note these differences from bulk sublimation values may be due to errors in the literature values or the possibility that we were not producing exactly the most stable phase at these low temperatures (possibly explaining the fact that our heats are lower than the literature values in the two cases where they differ most). However, these differences are all within the error bars (at 95% confidence) of the two values being compared and therefore they do not really differ in any statistically significant way. Relative measurements (for example, differences in heat with changes in coverage or temperature) can be much more accurate. The precision of energy calibration can be improved as much as desired by averaging multiple runs.

Sticking probabilities were measured simultaneously with calorimetric measurements, using the King and Wells method.[33] A mass spectrometer, without line-of-sight to the sample, measured the background pressure increase of methanol (Chapter 3), CH_3OH_g (m/z = 31) or CH_3I_g (Chapter 4) (m/z = 142) in the chamber. A gold flag was positioned in front of the sample and used to determine the mass spectrometry signal corresponding to full reflection of a gas

pulse. The gold flag was used because methanol and methyl iodide do not stick to gold at room temperature.[34] The sticking probability of a pulse of gas is calculated by integrating the mass spectrometer signal measured from the increase in gas partial pressure above background when the molecular beam is pulsed onto the sample surface in comparison with the increase in gas partial pressure resulting when pulsed onto the inert gold flag. We report two types of sticking probabilities, the long-term sticking probability and the short-term sticking probability.[30] The long-term sticking probability, S_∞, is the probability that a gas molecule strikes the Pt(111) surface, sticks, and remains until the next gas pulse starts ~2 seconds later (5 seconds later in Chapter 4). This measurement is used to calculate the adsorbate coverage remaining at the start of the next gas pulse. The short-term sticking probability, $S_{140\ ms}$, is the probability that a gas molecule strikes the Pt(111) surface, sticks, and remains at least throughout the timeframe of our heat measurement (i.e. the first 140 ms). This is used to calculate the moles of gas phase reactant that contribute to the measured heat of adsorption, so we can report that value in kJ per mole adsorbed. When there is no desorption between pulses, the two sticking probabilities are the same.

The calorimeter and Pt(111) sample are cooled by a large thermal reservoir, but one cannot mount a thermocouple directly on the ultrathin single crystal used for calorimetry, nor on the sample platen to which it is mounted (because this whole platen is removed from its manipulator and mounted on the thermal reservoir during calorimetry to achieve better signal stability). Therefore, the sample temperature was monitored by two alumel/chromel thermocouples spot-welded to the two closest locations, one spot-welded to the holder of the pyroelectric detector and another to the thermal reservoir. We took the average of these two temperature readings as the sample temperature here. For the sample temperatures used here

(100 to 210 K), the readings of these two thermocouples differed by ~20 K on average.

2.1 Figures

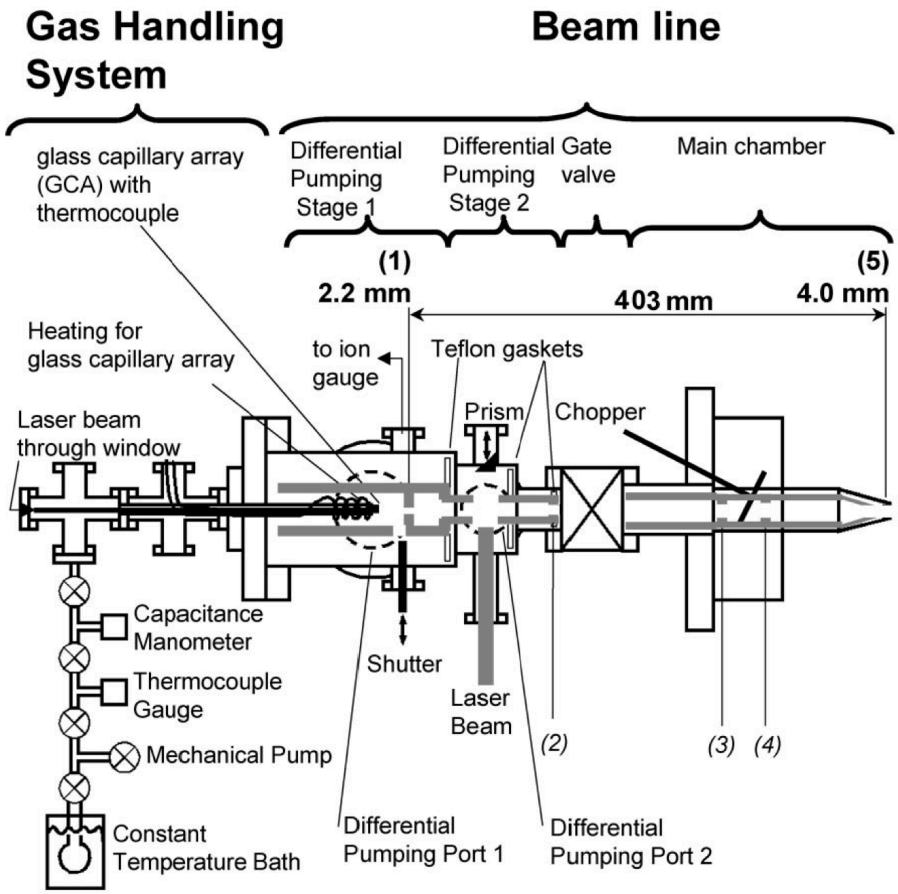

Figure 2.1: Schematic of the effusive molecular beam and its separate elements: gas handling system and beam line, with five orifices indicated by numbers: (1)–(5). The beam line consists of two differential pumping stages separated from the main chamber by a gate valve. The purpose of the gas handling system is to deliver the low vapor pressure molecules in the constant temperature bath, kept at 280 K, to the glass capillary array (GCA). The temperature of the GCA is monitored by a thermocouple and is resistively heated to maintain a temperature of 300 K. The line between the constant temperature bath and the GCA is maintained at 290 K, using heating tape, to prevent condensation of the low vapor pressure molecules along the way. The beam line consists of five orifices, only two of which are beam defining: (1) and (5). The inner diameter (ID) of (1) and (5) are 2.2 and 4.0 mm, respectively, and the distance between them is 403 mm. Orifices (2), (3), and (4) which are not beam defining, but only slightly larger, have IDs of 2.8, 3.8, and 4.0 mm, respectively. Also indicated are ports for the laser and prism for calibration with the laser beam, the shutter, used to block the molecular beam, and the chopper, used to chop both the laser and molecular beams. (Figure and caption taken with permission from Ref [29])

Chapter 3

The Energetics of Adsorbed Methanol and Methoxy on Pt(111) by Microcalorimetry

The heat of adsorption and sticking probability of methanol were measured on clean Pt(111) at 100, 150, and 210 K and on oxygen pre-covered Pt(111) at 150 K using Single Crystal Adsorption Calorimetry (SCAC). On clean Pt(111) at 100 K, the heat of methanol adsorption was found to be 60.5±0.8 kJ/mol in the limit of low coverage, resulting in a standard enthalpy of formation (ΔH_f^0) of CH_3OH_{ad} of -263±0.8 kJ/mol; at 150 and 210 K on clean Pt(111) the results were indistinguishable from the energetics measured at 100 K in the same coverage range. Calorimetry of methanol on oxygen-precovered Pt(111) at 150 K yielded the energetics of adsorbed methoxy, giving $\Delta H_f^0(CH_3O_{ad})$ = -170±10 kJ/mol and a CH_3O-Pt(111) bond enthalpy of 187±11 kJ/mol. Using these enthalpies, the dissociation of adsorbed methanol on Pt(111) to form methoxy and a hydrogen adatom is found to be uphill by +57 kJ/mol. At coverages below 0.2 ML, the sticking probability for methanol on both surfaces at or below 150 K was >0.95. At 210 K, ~80% of the methanol beam pulse transiently adsorbs to clean Pt(111) with a surface residence time of 238 ms and heat of adsorption of 61.2±2.0 kJ/mol, giving a prefactor for methanol desorption of $4 \times 10^{15\pm0.5}$ s^{-1}. These measured energetics for methoxy and methanol were compared to DFT calculations from previous literature, showing DFT to routinely underestimate the bond energy of both adsorbed methanol and methoxy by 15 to 52 kJ/mol.

3.1 Introduction

The catalytic reforming and decomposition of oxygenates has attracted much attention for the production of high-purity hydrogen and for applications in direct alcohol fuel cells. The transition metals Pt, Rh, Ni and Pd are typical catalysts used to facilitate these reactions, with Pt being the most active metal. Methanol is an appealing oxygenate for these reactions because it has a high H/C ratio, lacks a C-C bond allowing good selectivity at lower temperatures, and is a liquid under standard conditions that can be easily transported. As such, much work has been dedicated to elucidating the chemical pathway methanol follows on Pt surfaces. Microkinetic models have been developed[5,6] in which many intermediates have been proposed, but only a few have been directly observed. One of the more stable intermediates in these pathways is surface bound methoxy, which has been observed under reaction conditions on Pt supported catalysts[7-10] and in ultrahigh vacuum (UHV) conditions on Pt single crystal surfaces[11-15] and thus because of its stability is thought to play an important role in the rate limiting steps of these reactions. Adsorbed alkoxy species, of which methoxy is the simplest, are also ubiquitous intermediates in many catalytic combustion, selective oxidation and steam reforming reactions that take place on Pt and/or Pt group metals.

Since the important catalytic parameters of selectivity and activity depend on the thermodynamic stability of adsorbed intermediates, it is important that the energetics (heat of adsorption, bond strength, etc.) of methoxy be measured. Typically, such measurements are made on single crystal surfaces, since only on such surfaces can well-defined adsorbed intermediates be cleanly produced. On such surfaces, heats of adsorption are often measured using techniques like Temperature Programmed Desorption (TPD) and equilibrium adsorption isotherms. However, those techniques require the adsorbate to adsorb and desorb reversibly,

which methoxy does not, but instead decomposes upon heating. Therefore we employ the only technique available, single crystal adsorption calorimetry (SCAC), to provide a direct measurement of the energetics of methoxy as a function of coverage on Pt(111).

There are two known ways to cleanly produce methoxy species on Pt(111) in UHV conditions. One method involves dosing methyl nitrite on Pt(111) at ~165 K[14,15] to yield methoxy co-adsorbed with NO, the second requires dosing methanol on an oxygen pre-covered Pt(111) surface at 150 K producing methoxy co-adsorbed with hydroxyl.[11-13] In this work, we measure the energetics of adsorbed methoxy using the latter method, because the energy of the co-adsorbed hydroxyl can be accounted for using our previous SCAC measurements of adsorbed hydroxyl on Pt(111)[35,36] allowing the energetics of adsorbed methoxy to be extracted. We also present SCAC results of methanol on clean Pt(111) at 100, 150, and 210 K to provide the energetics of molecularly adsorbed methanol and its surface residence time at 210 K, giving the pre-factor for methanol desorption from the Pt(111) surface. Finally, we use our measured values to calculate heats of reaction for methanol dissociation on Pt(111), and compare the methoxy and methanol bond energies to Density Functional Theory (DFT) calculations, providing benchmarks for its improvement.

3.2 Experimental

Experiments were performed in a UHV chamber (base pressure $<2 \times 10^{-10}$ mbar) equipped with X-ray photoelectron spectroscopy (XPS), Auger electron spectroscopy (AES), low energy ion scattering spectroscopy (LEIS), low energy electron diffraction (LEED), and SCAC. The apparatus and procedures for SCAC have been described in previous publications and in detail in Chapter 2.[27,28]

Calorimetry was performed by exposing the Pt(111) surface to a pulsed molecular beam of methanol (CH_3OH) gas. Each pulse was 102 ms long and repeated every 2 seconds. The methanol (Alfa Aesar, anhydrous, 99.9%) was outgassed by several freeze-pump-thaw cycles after being put into its reservoir on the vacuum chamber. Its purity was checked with a mass spectrometer and found to be consistent with the manufacturer's claim. The beam was created by expanding ~1.3 mbar of methanol through a microchannel array at 299±6 K (defining the gas temperature) and then collimated through a series of five liquid nitrogen cooled orifices as described previously[29] and in Chapter 2. Coverages are reported in monolayers (ML) and are defined as the number of methanol molecules that adsorb to the surface irreversibly, normalized by the number of platinum surface atoms in the Pt(111) surface (1.50×10^{19} Pt atoms / m^2). A typical methanol dose was ~0.01 ML (1.88×10^{12} molecules) per pulse with a beam spot size previously determined to be 4.36 mm in diameter.[29] The flux of methanol from the molecular beam is measured by impinging the beam onto a liquid nitrogen cooled quartz crystal microbalance (QCM), pre-covered with multilayers of methanol. Calibration of the QCM has been described previously.[29]

The heat released from the adsorption of one methanol pulse is measured with a pyroelectric polymer ribbon gently pressed against the back side of the Pt(111) sample.[27,31] The sensitivity of the pyroelectric detector was calibrated after each experiment by depositing a known amount of energy into the sample using a HeNe (632.8 nm) laser.

Sticking probabilities were measured simultaneously with calorimetric measurements, using the King and Wells method.[33] A mass spectrometer, without line-of-sight to the sample, measured the background pressure increase of methanol, CH_3OH_g (m/z = 31) in the chamber. A

gold flag was positioned in front of the sample and used to determine the mass spectrometry signal corresponding to full reflection of methanol. The gold flag was used because methanol does not stick to gold at room temperature.[34] The sticking probability of methanol is calculated by integrating the mass spectrometer signal measured from the increase in methanol partial pressure above background when the molecular beam is pulsed onto the sample surface in comparison with the increase in methanol partial pressure resulting when pulsed onto the inert gold flag. We report two types of sticking probabilities, the long-term sticking probability and the short-term sticking probability.[30] The long-term sticking probability, S_∞, is the probability that a gas molecule strikes the Pt(111) surface, sticks, and remains until the next gas pulse starts ~2 seconds later. This measurement is used to calculate the adsorbate coverage remaining at the start of the next gas pulse. The short-term sticking probability, $S_{140\ ms}$, is the probability that a gas molecule strikes the Pt(111) surface, sticks, and remains at least throughout the timeframe of our heat measurement (i.e. the first 140 ms). This is used to calculate the moles of gas phase reactant that contribute to the measured heat of adsorption, so we can report that value in kJ per mole adsorbed. When there is no desorption between pulses, the two sticking probabilities are the same.

3.3 Results

Sticking probability. As described previously[30] and above, we measured two types of sticking probabilities; the long-term sticking probability, S_∞, and the short-term sticking probability, $S_{140\ ms}$. Figure 3.1 shows both of these sticking probabilities for methanol versus coverage on clean and oxygen precovered Pt(111) at 100 K and 150 K. Both start at 0.95 and approach unity in the coverage range 0 to 0.2 ML. The high sticking probability at low coverage

indicates a precursor-mediated adsorption mechanism. This type of adsorption has also been observed for benzene[37], naphthalene[38], cyclohexene[30], and water[28] on Pt(111). The slight increase in sticking probability from 0.95 to 1 as the coverage increases in the first 0.2 ML may be due to temporary attachment of the mobile precursor to a previously adsorbed methanol molecule, which may prevent it from desorbing before it can reorient and achieve the more stable bonding structure required to keep it permanently on the Pt. After 0.2 ML, the sticking probabilities for the different surfaces and temperatures diverge.

For the clean Pt(111) surface at 100 K, the sticking probability is near unity for all coverages, in agreement with the observations of White and coworkers[13]. At these conditions, methanol adsorbs molecularly in the first layer through its oxygen atom to atop sites[11,39] and at higher coverages forms an amorphous multilayer[39]. Previous TPD experiments have observed this multilayer to desorb at ~140 K[11] and therefore, a multilayer is not expected to form when methanol is dosed on a clean Pt(111) surface at 150 K. Figure 3.1 confirms that a multilayer does not form on a clean Pt(111) surface at 150 K and instead a saturation coverage of 0.33 ML is reached. The third experiment shown in Figure 3.1 is the sticking probability of methanol on a Pt(111) surface at 150 K pre-covered with 0.25 ML of oxygen adatoms. When methanol is dosed onto this surface, adsorbed oxygen acts as a lewis base to abstract a hydrogen from the adsorbed methanol, leaving methoxy and hydroxyl adsorbates on the surface.[11-13] Even though this surface reaction is occurring, the same saturation coverage of 0.33 ML is obtained as for the clean Pt(111) surface at 150 K. Note that the coverage axis in Figs. 3.1-3.4 is the total coverage of methanol which stuck to the surface (measured using the long-term sticking probability multiplied by the beam flux and pulse duration), irrespective of the final products it produces. The observed total surface coverage of 0.33 ML is in good agreement with the saturation

coverage of 0.36 ML for methanol on the oxygen pre-covered surface reported by White and coworkers[13].

The sticking probability versus coverage for methanol on clean Pt(111) at 210 K is shown in Fig. 3.2. Since TPD experiments have shown that the 1st layer of methanol desorbs from Pt(111) at 180 K, methanol is not expected to adsorb on a clean Pt(111) surface at 210 K. The results of Fig. 3.2 confirm this, showing that the saturation coverage is only 0.008 ML, which builds up in the first few pulses and might be associated with adsorption of methanol on defect sites. In contrast, the short term sticking probability remains high (~0.8) after hundreds of pulses, proving that ~80% of the molecules stick initially but desorb again before the next pulse.

Heat of adsorption at 100 K on clean Pt(111). In this paper we define the term *heat of adsorption* as the negative of the differential standard molar enthalpy change for the adsorption reaction, with the gas and the Pt(111) surface being at the same temperature as the Pt(111) surface. During our experiments, the temperature of the molecular beam is ~300 K, while the Pt(111) sample is held at cryogenic temperatures (e.g 100 K). Thus, the measured heat is corrected by the small difference in the internal energy of the gas in the *directed* molecular beam at 300 K and in a Boltzmann distribution at the sample temperature, and then by RT to convert from internal energy change to enthalpy change for the adsorption reaction, as described elsewhere.[30]

The heat of adsorption of methanol on clean Pt(111) at 100 K is shown in Fig. 3.3. Initially, methanol adsorbs molecularly through its oxygen atom with a heat of adsorption of 60.5±0.8 kJ/mol in the limit of low coverage. As coverage increases to 0.5 ML, the heat of adsorption decreases, which is not surprising since TPD has shown the 1st layer peak desorption temperature to decrease with increasing coverage.[40] For the first 1/3 ML, the heat of adsorption

is well described by a best-fit line (60.5 - 19.3 θ) kJ/mol, where θ is coverage, in ML, yielding an average heat of 57.3 kJ/mol.

Insight into the nature of the repulsive adsorbate-adsorbate interactions which give rise to this decreasing heat can be obtained by estimating the footprint of an adsorbed methanol from the van der Waal's radius of methane (1.70 Å),[41] giving a diameter of adsorbed methanol of ~3.4 Å. Since this is much smaller than the next nearest neighbor Pt-Pt distance (4.8 Å)[42], the decrease in adsorption energy up to 1/3 ML coverage is probably due to dipole-dipole repulsions. However, the distance between nearest neighbor sites (2.77Å)[42] is less than the footprint of methanol (3.4Å), so there will be stronger steric repulsions at nearest neighbor sites. Thus, it is likely that methanol saturates next nearest neighbor sites first, to avoid these steric repulsions, forming a local (√3x√3) structure at 1/3 ML.

Following Persson's model,[43] this linear decrease in adsorption energy in the first 1/3 ML can be explained by immobile adsorbates which randomly populate next nearest neighbor sites (but not closer) with repulsive interactions between adsorbates at next nearest neighbor sites (but not further) and no relaxation of this repulsion by slight movement apart for an isolated pair (i.e., Persson's ε = 0). Adapting Persson's model to a hexagonal lattice, the initial heat of adsorption (60.5 kJ/mol) is the heat of adsorption for a single isolated adsorbate (Persson's μ) and the slope (-19.3 kJ/mol per ML) is equal to $-6V_0$ per 1/3 ML, where V_0 is the pairwise repulsion between adsorbates at next nearest neighbor sites (1.1 kJ/mol here).

This decrease in heat below 0.33 ML could be the result of a much more complex situation than the simple model above, as suggested by recent STM and DFT studies of methanol on Cu(111) and Au(111).[44,45] On both surfaces, the methanol molecules lie sideways on the surface and cluster together into hydrogen-bonded hexamers and/or chains, with the methyl

groups pointing outwards. Chains are formed at 145 K on Cu(111), and there are repulsive interactions between the chains such that the saturation coverage is 1/3 ML.[45] If the same chains and/or hexamers form here on Pt(111) already at 100 K, then this decrease in heat may be due to hexamer-hexamer or chain-chain repulsions, instead of the simple molecule-molecule repulsions suggested above.

After 0.33 ML and up to 0.5 ML, the heat of adsorption decreases much more rapidly, and is well described by the best-fit line (74.6 - 62.0 θ) kJ/mol. The abrupt change in slope at 0.33 ML suggests that as the (√3x√3) structure completes, methanol continues to adsorb but now must populate nearest neighbor sites, completing a c(2x2) structure at ½ ML. The stronger steric repulsions between adsorbates at nearest neighbor sites explains this more rapid decrease in adsorption energy. The integral heat of adsorption at 0.5 ML is 54.2±0.8 kJ/mol from Fig. 3.3. This can be compared to heats of adsorption of 47 kJ/mol[12] and 48 kJ/mol[40] reported for the saturated first layer based on TPD. (For comparison to heats of adsorption, we added ½ RT here to the reported desorption activation energies, as described elsewhere[23].) These heats are 7-8 kJ/mol lower than our measured integral heat of adsorption; a discrepancy that is due to the assumption of 10^{13} s^{-1} as the desorption prefactor in ref [12] and [40] to extract desorption energies. We show below that this prefactor is instead 4 x $10^{15\pm0.5}$ s^{-1}, which would increase these enthalpies by ~9 kJ/mol and bring the values within ~1-2 kJ/mol.

At coverages greater than 0.5 ML, the heat of adsorption becomes constant at 43.8±0.8 kJ/mol, implying that additional methanol adsorbs on top of methanol adsorbates, growing as a multilayer above 0.5 ML at 100 K. This multilayer adsorption energy of 43.8±0.8 kJ/mol is in good agreement with the heat of sublimation of bulk methanol (solid) at 100 K, 45.3 kJ/mol, calculated from bulk thermodynamic data,[46-48] and results from a detailed TPD study of

multilayer methanol on Au(111) that employed leading-edge analysis to determine a sublimation enthalpy of 42.1 - 44.6 kJ/mol[49] (after correction using bulk solid and gas phase heat capacities from 150 K down to 100 K).

Heat of adsorption at 150 K on clean and oxygen pre-covered Pt(111). Figure 3.4 displays heat of adsorption versus coverage for two experiments at 150 K; one where methanol is dosed on clean Pt(111) and a second where methanol is dosed on a Pt(111) surface at 150 K that had been pre-saturated with 0.25 ML of oxygen adatoms.

At 150 K on clean Pt(111), methanol does not form a multilayer and is known to adsorb molecularly through its oxygen atom at atop sites.[11] Figure 3.4 shows that the heat of adsorption of methanol on Pt(111) at 150 K is relatively constant, giving an average heat of adsorption of 57.0 kJ/mol in the coverage range 0 to 0.33 ML, which is the statistically identical (i.e. within the 95% confidence interval) to the average heat of adsorption of 57.3 kJ/mol in the same coverage range measured at 100 K (Fig. 3.3). Note the maximum coverage is 0.33 ML at 150 K, meaning only the ($\sqrt{3}$x$\sqrt{3}$)-like structure is formed, with methanol in next nearest neighbor sites. Any coverage greater than 0.33 ML would require methanol to adsorb in nearest neighbor sites with strong steric repulsions; a structure too unstable to form at this temperature.

Next, we studied the heat of methanol adsorption on the Pt(111) surface pre-dosed with oxygen adatoms under conditions where it is known to produce adsorbed methoxy and hydroxyl species. Previous TPD[11-13] and HREELS[11,12] studies have shown that pre-dosed oxygen adatoms on the Pt(111) surface, at O_{ad} coverages up to 0.25 ML, abstract a hydrogen atom from adsorbed methanol to form adsorbed methoxy and hydroxyl species above 140 K (Reaction 1):

$$CH_3OH_g + O_{ad} \rightarrow CH_3O_{ad} + OH_{ad} \quad . \qquad (1)$$

At temperatures greater than 150 K, the methoxy adsorbates become unstable and decompose, ultimately evolving $H_{2,g}$, $CO_{2,g}$, CO_g, and H_2O_g in TPD experiments.[13] In SCAC experiments, it is best to choose a temperature where the reaction of interest occurs as fast as possible, to avoid complications in heat signal analysis from slow heat deposition due to slow kinetics of the surface reactions, H abstraction here.[28] Thus, experiments are done at the highest temperature where the reaction occurs cleanly. Therefore, methanol was dosed on the oxygen pre-dosed Pt(111) surface at 150 K, which is the maximum temperature at which methoxy and hydroxyl species are formed without further decomposition of the adsorbed methoxy[13]. The oxygen adatoms where pre-dosed using an exposure of ~$1x10^{-7}$ mbar of $O_{2,g}$ for 60 seconds to the clean Pt(111) surface at 150 K, which is known to produce a saturation coverage of 0.25 ML of oxygen adatoms in a p(2x2) structure.[50-52] During this experiment, no broadening in the heat signal lineshape was observed, indicating that the kinetics of the reaction are indeed fast within the timeframe of our heat measurement.

The results of this experiment (Fig. 3.4) show the heat of adsorption is approximately 19 kJ/mol higher than on the clean Pt(111) surface. The higher heat, associated with the methanol reacting to form methoxy and hydroxyl adsorbates, is only apparent in the coverage range 0 – 0.25 ML. At higher coverages, the heat of adsorption is the same on the clean and O-predosed Pt surfaces: 56.8 and 58.9 kJ/mol, respectively, in the coverage range 0.25 – 0.33 ML. This is consistent with the reaction stoichiometry (one methanol reacts per O_{ad}) and the oxygen precoverage of 0.25 ML. Any additional coverage of methanol greater than 0.25 ML simply adsorbs molecularly. In the coverage region from 0 to 0.25 ML on the O-predosed surface, where methoxy and hydroxyl species are being produced, the integral heat of adsorption is 76.4 kJ/mol.

The heat and surface residence time of transiently adsorbed methanol on clean Pt(111) at 210 K. The sticking probabilities for methanol dosed onto Pt(111) at 210 K (Fig. 3.2) show that ~80% of a pulse of methanol adsorbs transiently during the timeframe of our heat measurement and then desorbs shortly thereafter, and this occurs repeatedly for many pulses. While no permanent accumulation of methanol occurs, the 80% that does stick during our heat measurement allows us to measure a heat of adsorption of 61.2±2.0 kJ/mol, a value that is within the error bar of the zero-coverage limit of methanol adsorption on clean Pt(111) measured at 100 K, 60.5±0.8 kJ/mol (Fig. 3.3). If we take this measured heat of adsorption at 210 K and assume non-activated adsorption, the activation energy for desorption at this temperature is 60.3 kJ/mol (subtracting ½RT from the heat of adsorption, where T is the temperature of the sample)[23].

Figure 3.5 displays the lineshape of the methanol signal (m/e 31) measured with our mass spectrometer for a single pulse period of methanol gas on the Pt(111) surface at 210 K, averaged over 30 pulses. For reference, the mass spectrometer signal of a pulse of methanol gas impinged on an Au flag, where methanol desorbs very rapidly, is also shown. The long tail seen in the line shape for methanol desorption from the 210 K Pt(111) surface is well fit with an exponential decay function of the form $y = e^{-t/\tau}$, representing first order kinetics of the desorption process, giving τ = 238 ms. Here τ represents the average surface residence time, which is equal to $1/k_{des}$, where k_{des} is the rate constant of methanol desorption from Pt(111). This τ = 238 ms gives k_{des} = 4.2 s^{-1}. Using the Arrhenius equation for k_{des} in conjunction with the desorption activation energy of 60.3 kJ/mol from the measured heat gives a pre-exponential factor for methanol desorption from Pt(111) of $4 \times 10^{15\pm0.5}$ s^{-1}.

3.4 Discussion

Energetics of adsorbed methoxy on Pt(111). For the experiment of methanol dosed onto oxygen pre-covered Pt(111) at 150 K, we attribute the integral heat of adsorption of 76.4 kJ/mol in the coverage range 0 - 0.25 ML (Fig. 3.4) to the heat of reaction (1). Using this measured enthalpy of reaction (1) at 150 K (-76.4 kJ/mol), a thermodynamic cycle is constructed to extract the standard heat (enthalpy) of formation (ΔH_f^0) of adsorbed methoxy and the CH_3O-Pt(111) bond enthalpy (Fig. 3.6). ("Standard" here simply refers to 1 bar pressure.) The enthalpy of formation of adsorbed methoxy is found by first starting on the left hand side of the cycle with the elements in their standard states and following the pathway of the bottom half of the cycle. The enthalpy for the lower left hand step is found by adding the known enthalpy of formation of gas phase methanol[53] with the known enthalpy of formation of adsorbed oxygen on Pt(111) at a coverage of 0.25 ML.[36] The lower right-hand step is the measured integral enthalpy of reaction (1), -76.4 kJ/mol from Fig. 3.4. By adding the energies of the lower left and right hand steps, a total value of -377±8 kJ/mol is found. This is the total enthalpy change in taking the elements in their standard states to methoxy co-adsorbed with hydroxyl (both at 0.25 ML coverage), and therefore is equal to the sum of the enthalpy of formation of adsorbed hydroxyl with the enthalpy of formation of adsorbed methoxy. The standard enthalpy of formation of adsorbed hydroxyl on Pt(111) is known: $\Delta H_f^0(OH_{ad})$ = -207±7 kJ/mol[36]. This reported value is for OH_{ad} coadsorbed with H_2O in a very stable $(H_2O\text{-}OH)_{ad}$ adlayer, where the OH_{ad} was estimated to be 38 kJ/mol more stable than isolated OH_{ad} on Pt(111) due to hydrogen bonding. We use this value (rather than that for isolated OH_{ad}) since we assume that hydrogen bonding will stabilize the OH_{ad} coadsorbed with CH_3O_{ad} to a similar magnitude. Subtracting this enthalpy of formation of

adsorbed hydroxyl from -377±8 kJ/mol results in the enthalpy of formation of adsorbed methoxy: -170±10 kJ/mol.

By following the pathway depicted in the upper part of this thermodynamic cycle (Fig. 3.6), the bond enthalpy of methoxy can be extracted. This is accomplished by again starting on the left hand side of the cycle with the elements in their standard states, but now following the upper left-hand step that takes the elements in their standard states to gas phase methoxy radical and adsorbed hydroxyl. The enthalpy for this step is determined by adding the known enthalpies of formation of gas phase methoxy (17±4 kJ/mol)[54] and adsorbed hydroxyl (-207±7 kJ/mol)[36], giving an enthalpy for this step of -190±8 kJ/mol. The next step in the upper pathway is the adsorption of gas phase methoxy onto the hydroxylated Pt(111) surface, depicted in the upper right-hand side of the cycle in Fig. 3.6. The enthalpy for this step is found by summing the rest of the steps in the cycle, giving -187±11 kJ/mol. Thus, the CH_3O-Pt(111) bond enthalpy of methoxy on Pt(111) is 187 ± 11 kJ/mol based on our heat measurements in Fig. 3.4 and other known thermodynamic data.

These methoxy species are co-adsorbed with an equal amount of hydroxyl on the Pt(111) surface. In this situation, the adsorbates are expected to form hydrogen bonds that stabilize the overall structure. We compensated for this as described above with our choice of enthalpy of formation for OH_{ad}. Since this may overestimate the magnitude of this stabilization, we also performed the same cycle using the estimated enthalpy of formation of isolated OH_{ad} on Pt(111), -169 kJ/mol[36]. This results in a 38 kJ/mol stabilization in both the standard enthalpy of formation of adsorbed methoxy and the CH_3O-Pt(111) bond enthalpy compared to the values in Fig. 3.6. The real situation is somewhere between these two limits, probably closer to the values in Fig. 3.6.

Comparisons to DFT calculations and evaluation of the enthalpy for methanol dissociation on Pt(111).

The bond strengths measured in this work provide a benchmark for comparison to DFT calculations of methanol and methoxy on Pt(111). It is important to note that DFT calculations report integral bond energies of adsorbates at specific coverages, therefore the fitted line in the coverage range 0 – 0.33 ML of methanol on Pt(111) at 100 K (Fig. 3.3) is used to extract integral heats of adsorption at specific methanol coverages to compare to DFT calculations. Adsorption energies of methanol to Pt(111) of 31.8 kJ/mol[55,56] and 20 kJ/mol[57] at 1/9 ML of coverage were calculated by two different groups using the GGA-PW91 functional. These values are ~27 kJ/mol and ~39 kJ/mol weaker, respectively, than our measured adsorption energy of 58.6 kJ/mol at 1/9 ML (calculated by subtracting RT from our integral heat of adsorption of 59.4 kJ/mol at 1/9ML of methanol coverage at T = 100 K). A similar calculation was performed by Desai et. al. also using the GGA-PW91 functional, but at ¼ ML of methanol coverage. This group found an adsorption energy of 43.2 kJ/mol[58] for molecularly adsorbed methanol; only ~14 kJ/mol weaker than the measured 57.3 kJ/mol at this coverage.

The papers cited above also calculated DFT values for the bond energy of isolated methoxy species on Pt(111) using the same GGA-PW91 functional. At 1/9 ML of methoxy coverage, bond energies of 149 kJ/mol[55,56] and 134 kJ/mol[57] were reported, and at ¼ ML of coverage a value of 161 kJ/mol[58] was reported. All of these calculated values are considerably less stable than the methoxy bond enthalpy measured in this work of 187±11 kJ/mol, which gives a bond energy of 186 kJ/mol.

The measured heats of formation of methanol and methoxy allow estimation of the following reaction enthalpy on Pt(111):

$$CH_3OH_{ad} \rightarrow CH_3O_{ad} + H_{ad} \qquad \Delta H^0_2 = +57\pm10 \text{ kJ/mol} \qquad (2)$$

This heat of reaction is calculated from the measured enthalpy of formation of methoxy of -170±10 kJ/mol at 150 K (Fig. 3.6), the known enthalpy of formation of H_{ad} on Pt(111) of -36 kJ/mol[30], and the enthalpy of formation of molecularly adsorbed methanol on Pt(111). For molecularly adsorbed methanol, the enthalpy of formation is found by adding the zero-coverage limit of the enthalpy of methanol adsorption on Pt(111) of -60.5±0.8 kJ/mol from Fig. 3.3 at 100 K (which was indistinguishable from measurements at 150 and 210 K) to the known enthalpy of formation of methanol gas of -202±0.2 kJ/mol[53] giving $\Delta H_f^0(CH_3OH_{ad})$ = -263±0.8 kJ/mol. Note that reaction (2) is rather endothermic (ΔH^0_2 = +57±10 kJ/mol) and therefore should be very slow, perhaps even the rate-limiting step in catalytic reactions like methanol decomposition on Pt-based catalysts.

3.5 Conclusion

At 100 K on clean Pt(111) methanol adsorbs molecularly through its oxygen atom at atop sites, forming a local (√3x√3) structure with repulsive dipole-dipole interactions resulting in a decreasing heat of adsorption that is well fit by (60.5 - 19.3 θ) kJ/mol in the first 1/3 ML of coverage. Above 1/3 ML, the heat of adsorption drops much more rapidly until 1/2 ML, probably corresponding to the population of a c(2x2) structure with strong steric repulsions between adsorbates. Above ½ ML, methanol adsorbs with a constant heat of adsorption equal to the multilayer sublimation enthalpy. At 150 K on clean Pt(111), only the first 1/3 ML adsorbs, giving identical heats of adsorption as those measured at 100 K. These results provide the

standard enthalpy of formation of adsorbed methanol $\Delta H_f^0(CH_3OH_{ad})$ = -263±0.8 kJ/mol and the methanol-Pt(111) bond enthalpy of 60.5±0.8 kJ/mol. At 210 K on clean Pt(111), methanol adsorbs transiently with a surface residence time of 238 ms and a heat of ~61 kJ/mol, giving a pre-factor for methanol desorption of $4 \times 10^{15\pm0.5}$ s^{-1}.

At 150 K, methanol reacts with a Pt(111) surface pre-covered with 0.25 ML of oxygen adatoms to form adsorbed methoxy and hydroxyl in the first 0.25 ML, giving an average enthalpy of reaction of -76.4 kJ/mol. Using known enthalpies of formation of gas phase species, we find the standard enthalpy of formation of adsorbed methoxy to be $\Delta H_f^0(CH_3O_{ad})$ = -170±10 kJ/mol and the CH_3O-Pt(111) bond enthalpy of 187±11 kJ/mol.

The measured energetics for adsorbed methanol and methoxy on the Pt(111) surface were compared to DFT calculations from several different groups that used the PW-91 functional. DFT calculations consistently underestimated the bond strength of methanol and methoxy to the Pt(111) surface, compared to measured values, in one case by 52 kJ/mol.

From these measured heats, the heat of reaction for the dissociation of adsorbed methanol to form H_{ad} and methoxy on Pt(111) was found to be +57±10 kJ/mol.

3.6 Figures

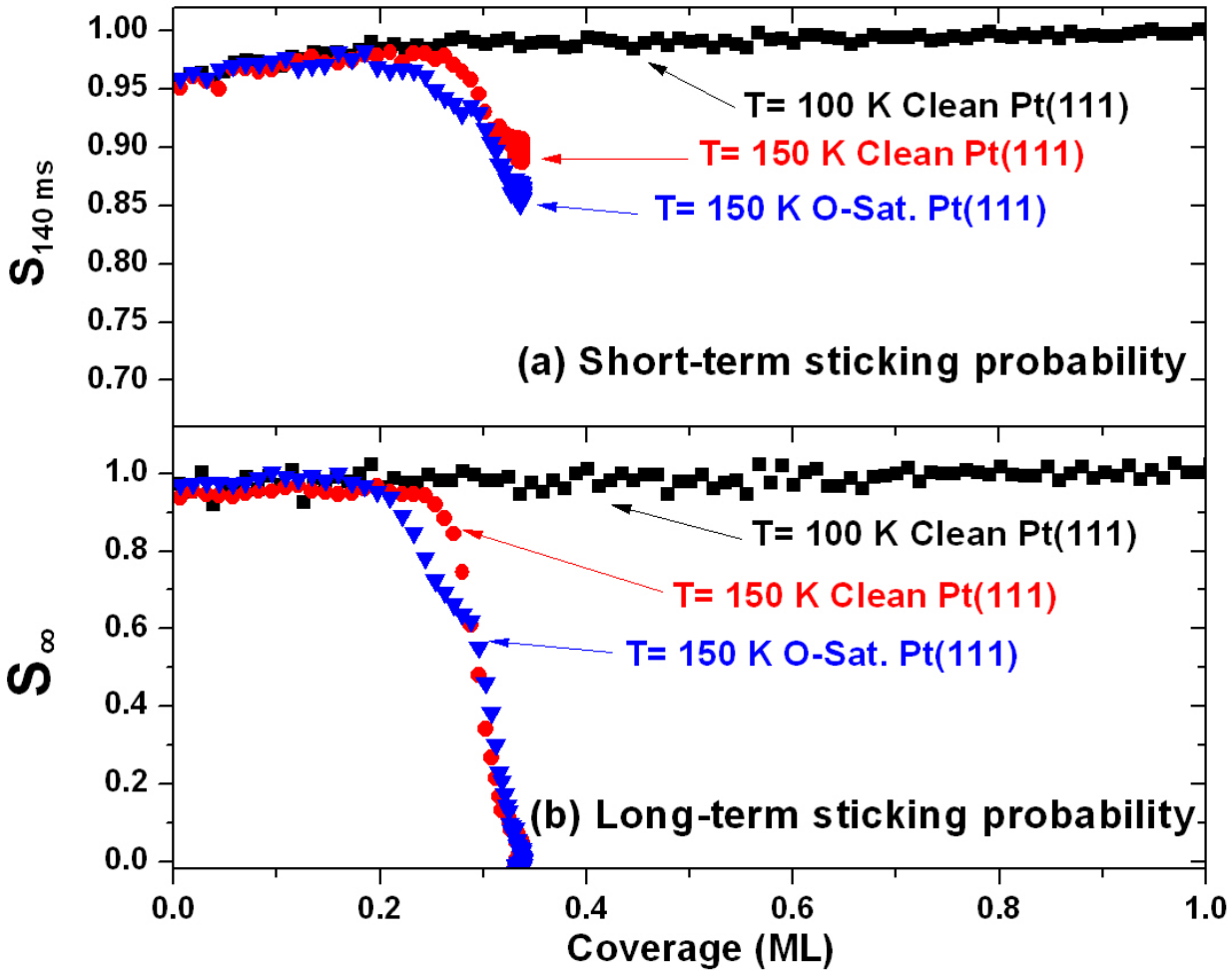

Figure 3.1: The average short term (a) and long-term (b) sticking probability of methanol versus total methanol coverage on clean Pt(111) at 100 K (squares), on clean Pt(111) at 150 K (circles), and on oxygen pre-covered Pt(111) at 150 K (triangles).

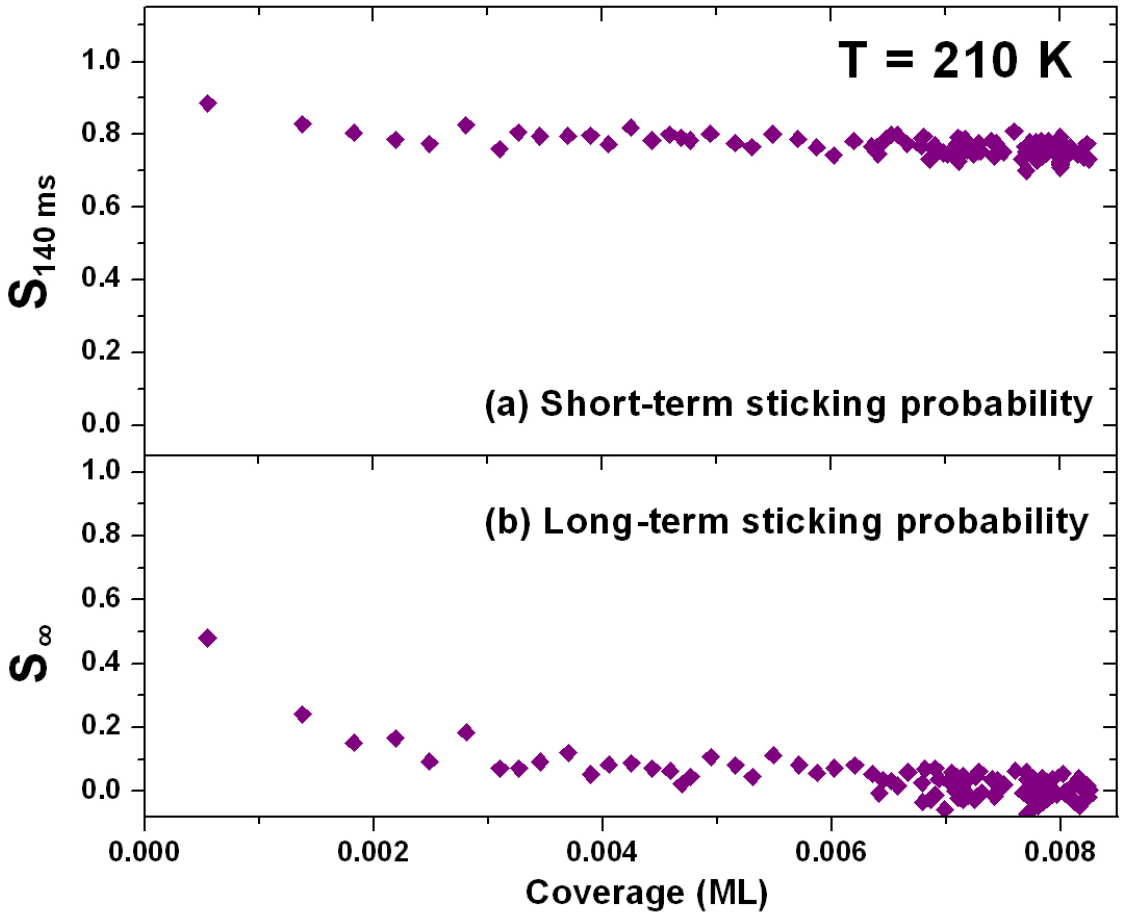

Figure 3.2: The average short-term (a) and long-term sticking probability (b) of methanol gas pulses versus total methanol coverage on clean Pt(111) at 210 K. Here the short-term sticking indicates that approximately 80% of the gas pulse sticks to the surface during the timescale of our heat measurement (140 ms). At times longer than 140 ms, all of the methanol desorbs at coverages above 0.008, as seen in the long-term sticking probability of 0.0.

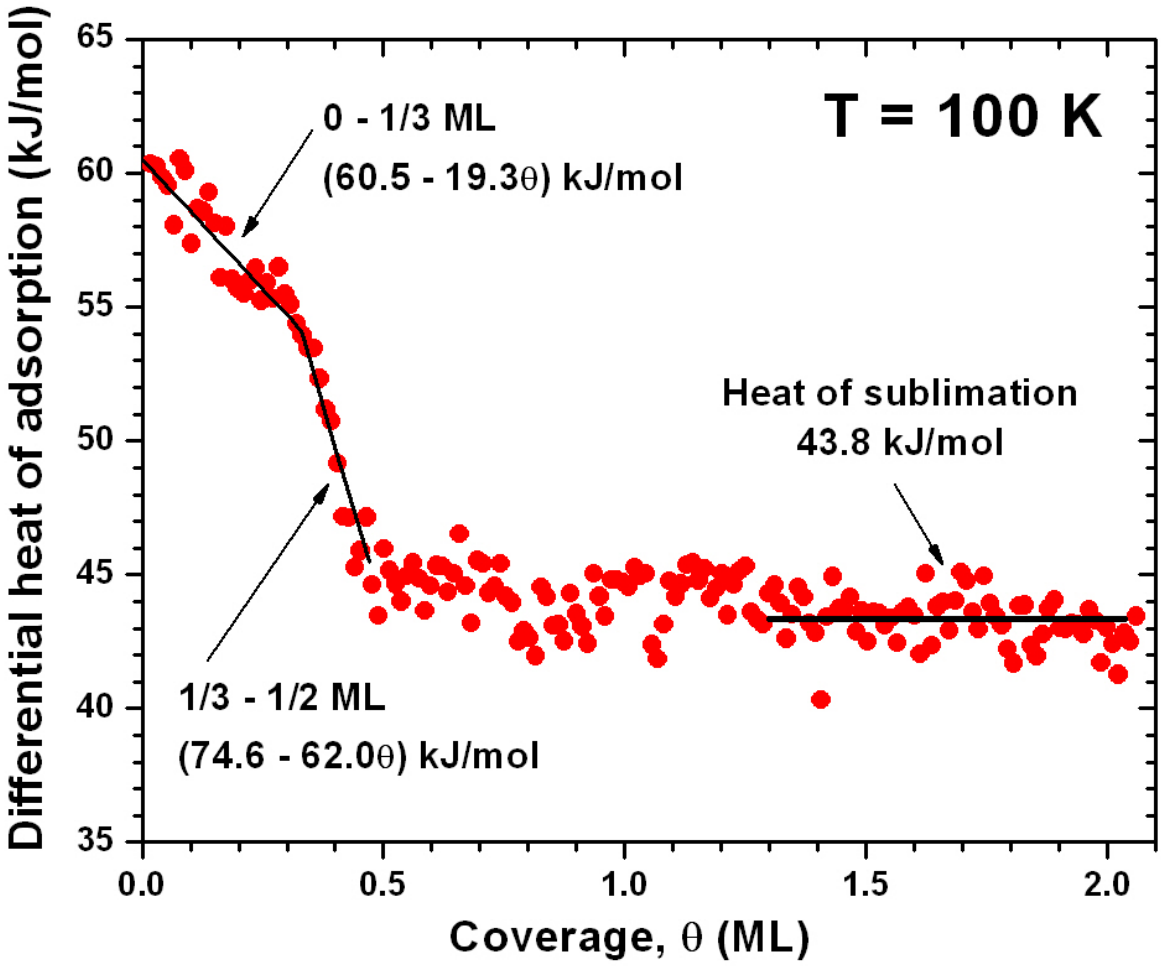

Figure 3.3: Differential heat of adsorption of methanol on clean Pt(111) at 100 K versus total methanol coverage. Each data point represents a pulse of 0.01 ML of methanol gas and is a result of averaging 10 experimental runs.

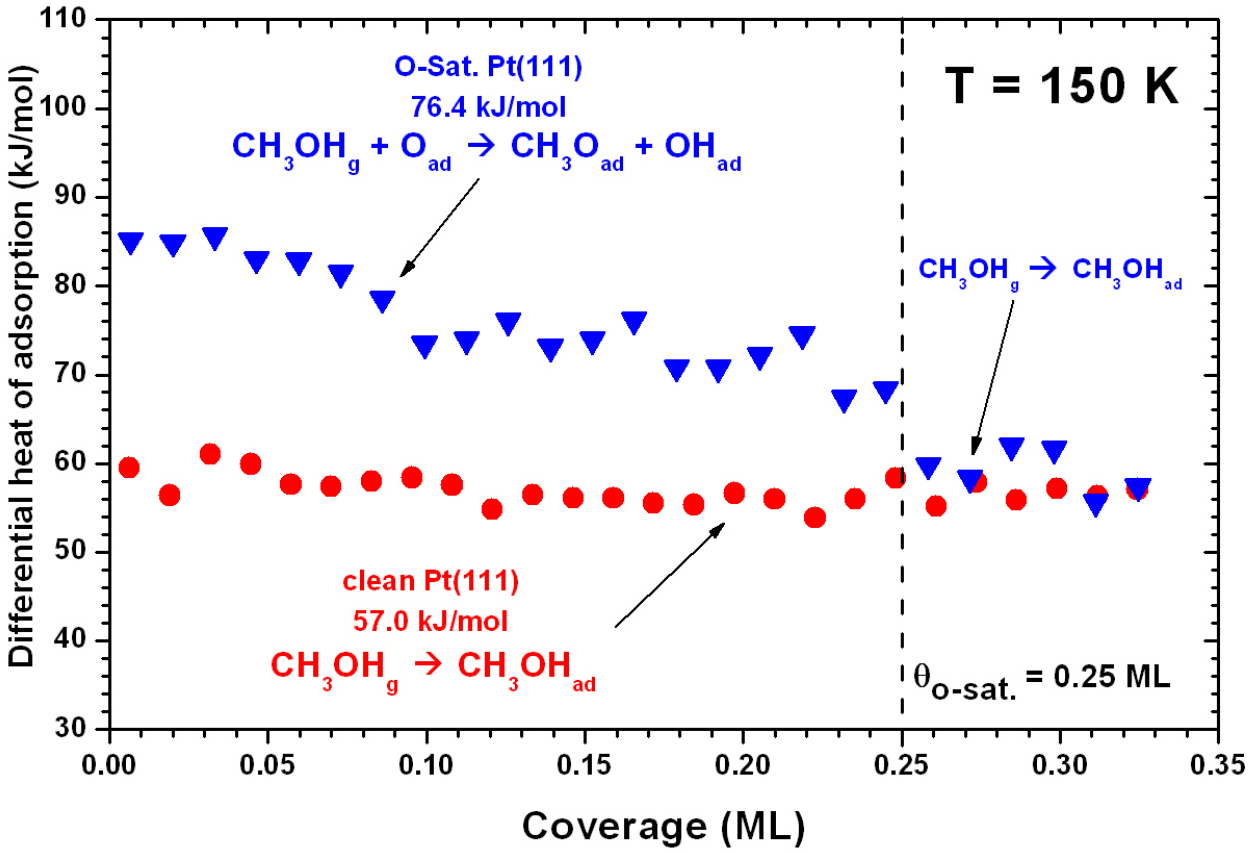

Figure 3.4: Differential heat of adsorption of methanol versus total methanol coverage on clean (filled circles) and oxygen-saturated (filled triangles) Pt(111) at 150 K. On the oxygen-saturated surface, methanol reacts to form adsorbed methoxy and hydroxyl species, giving an average heat of reaction of 76.4 kJ/mol. This reaction takes place only when adsorbed oxygen is still present, which is only up to a coverage of 0.25 ML (or to the dashed line, which indicates the total amount of O_{ad} predosed to the surface.) On clean Pt(111), methanol adsorbs molecularly, giving an average heat of 57.0 kJ/mol.

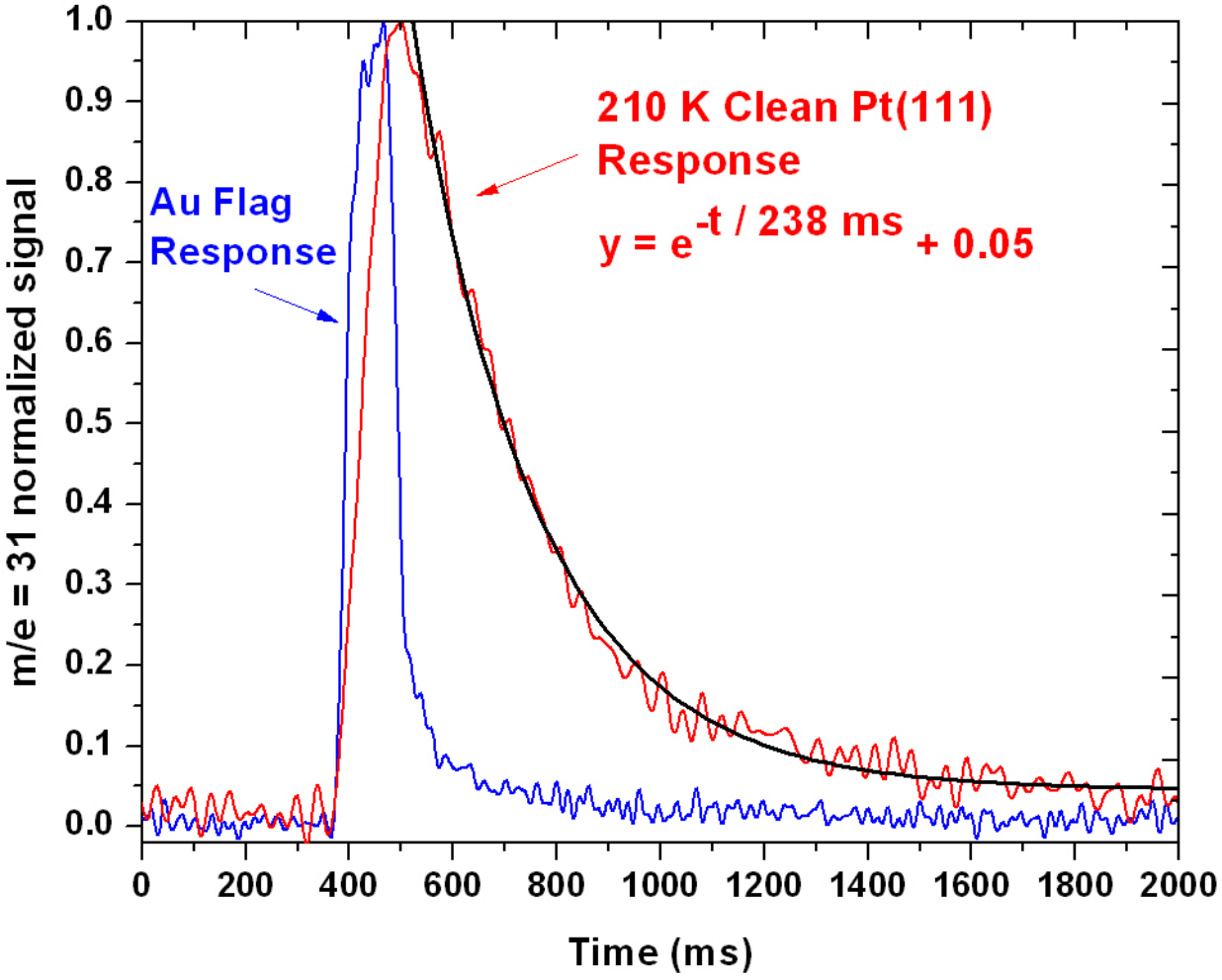

Figure 3.5: The normalized mass spectrometer signal versus time during the 2000 ms pulse cycle of methanol gas impinging on a Pt(111) surface held at 210 K, averaged over the first 30 pulses at the lowest coverage. The 100 ms pulse strikes the surface from ~380 to 480 ms on this scale. The slow desorption of methanol from the Pt(111) surface is apparent in the broad tail of the mass spectrometer response after this (red trace), which is fitted to an exponential decay with a 238 ms time constant (smooth black curve). For reference, the signal from the same 100 ms pulses of methanol after impinging on a room-temperature Au flag, where the molecules desorb rapidly, is also shown (blue trace).

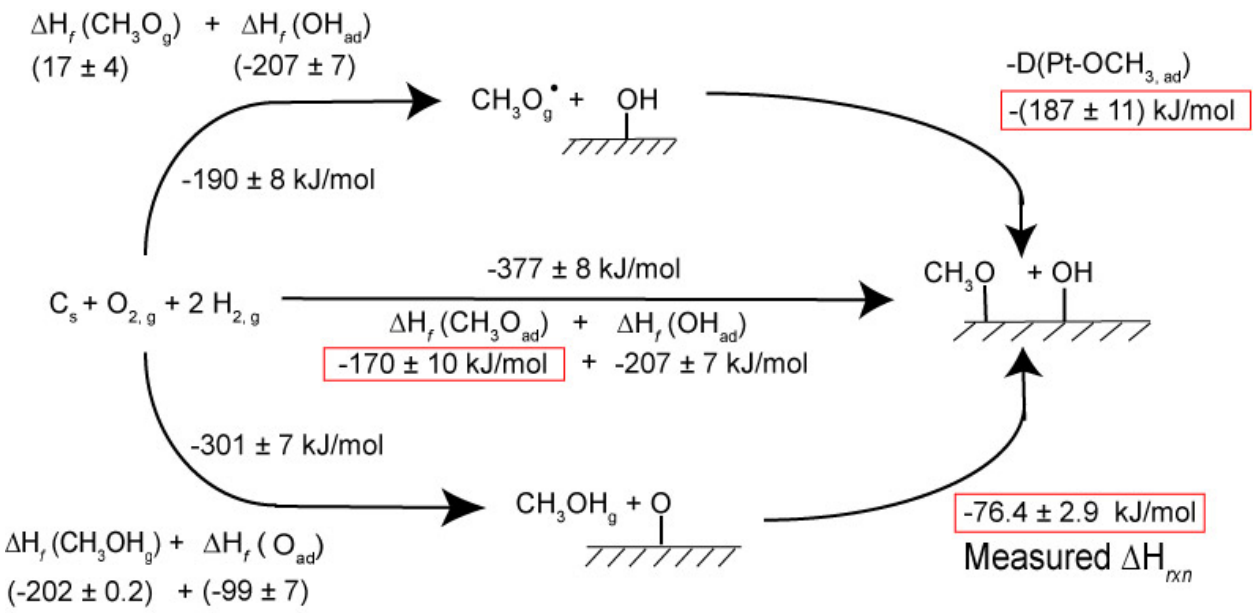

Figure 3.6: The thermodynamic cycle at 150 K used in calculating the bond enthalpy and standard heat of formation of adsorbed methoxy. Here the -76.4 kJ/mol is the measured enthalpy of the reaction $CH_3OH_g + O_{ad} \rightarrow OCH_{3,ad} + OH_{ad}$, from the data shown in Fig. 4, integrated over the coverage range up to 0.25 ML of each product (corresponding to a starting coverage of 0.25 ML of O_{ad}). The calculations from this cycle give a standard heat of formation for adsorbed methoxy ($OCH_{3,ad}$) on Pt(111) at 150 K of -170±10 kJ/mol and a Pt-O bond enthalpy of 187±11 kJ/mol for methoxy to the Pt(111) surface, both for a coverage of 0.25 ML of $OCH_{3,ad}$ coadsorbed with 0.25ML of OH_{ad}.

Chapter 4

Energetics of Adsorbed CH_3 and CH on Pt(111) by Microcalorimetry: the Dissociative Adsorption of CH_3I

The heat of adsorption and sticking probability of methyl iodide were measured on Pt(111) at 95, 215, 270, 300, and 320 K using Single Crystal Adsorption Calorimetry (SCAC). On clean Pt(111) at 95 K, the heat of adsorption for molecularly adsorbd methyl iodide was found to be 98.2 ± 2.0 kJ/mol in the limit of low coverage, resulting in a standard enthalpy of formation (ΔH_f^0) of CH_3I_{ad} of -83.6 ± 2.2 kJ/mol. The rate of dissociative adsorption of methyl iodide was fast enough at 320 K for its heat to be accurately measured. The heat of adsorption measured in the low coverage regime (0 – 0.04 ML) yielded the energetics of adsorbed methyl and iodine adatoms, giving $\Delta H_f^0(CH_{3,ad})$ = -53 kJ/mol (using reported energetic for I_{ad}) and a Pt-CH_3 bond strength of 200. kJ/mol. The measured integral heat of adsorption at 0.18 ML and 320 K yielded the energetics of adsorbed methylidyne (CH_{ad}), giving $\Delta H_f^0(CH_{ad})$ = +42 kJ/mol and a Pt-CH bond strength of 552 kJ/mol. Using these enthalpies of formation, the enthalpy for the dissociation of adsorbed methane to adsorbed methyl coadsorbed with a hydrogen adatom was found to be +1 kJ/mol, almost thermo-neutral. The further reduction of $CH_{3,ad}$ to CH_{ad} + 2 H_{ad} was found to be uphill by +23 kJ/mol. Measured methane yields (which require the product H_{ad} from this step) imply that the equilibrium constant for this step lies far to the left, consistent with this reaction's enthalpy. The bond strengths measured here for $CH_{3,ad}$ and CH_{ad} are compared to previous DFT calculations.

4.1 Introduction

Adsorbed methyl ($CH_{3,ad}$) and methylidyne (CH_{ad}) are known to be key intermediates in energy-related catalysis over late transition metals, including: partial oxidation of methane, steam reforming, combustion and selective oxidations of methane and various other hydrocarbons and oxygenates, methanation, Fischer-Tropsch, methanol decomposition, and several fuel cells reactions. The simple hydrocarbon fragments $CH_{3,ad}$, $CH_{2,ad}$, and CH_{ad} are stable enough to have been isolated on both Pt supported catalysts[16] and Pt(111) single crystal surfaces in ultrahigh vacuum (UHV) conditions.[17-19] Methyl has been produced on Pt(111) through both dissociative adsorption of methyl iodide[17,59-64] and by azomethane pyrolysis[65-68] and more recently, $CH_{2,ad}$ and CH_{ad} have been isolated on Pt(111) through the dissociative adsorption of CH_2I_2.[18,19] The interactions of CH_3I with Pt(111) have been studied previously in considerable detail[17,59-64]. It is molecularly adsorbed at 100 K:

$$CH_3I_g \rightarrow CH_3I_{ad} \quad (1)$$

Some of it desorbs intact during thermal desorption spectroscopy (TDS) between 170 and 230 K. The rest decomposes to produce $CH_{3,ad}$ plus I_{ad} by 250 K:

$$CH_3I_{ad} \rightarrow CH_{3,ad} + I_{ad}. \quad (2)$$

At low initial coverage, most of the CH_3I follows this pathway, but at higher coverage, more desorbs. At about the same temperature, the $CH_{3,ad}$ product begins to dehydrogenate and hydrogenate according to the steps:

$$CH_{3,ad} \rightarrow CH_{2,ad} + H_{ad} \quad (3)$$

$$CH_{3,ad} + H_{ad} \rightarrow CH_{4,g} \quad (4)$$

Reaction (4) is rapid at 250 K, since it starts already below 200 K in TPD when $CH_{3,ad} + H_{ad}$ are coadsorbed[69]. While it was initially thought by Zaera et al.[61] that this $CH_{2,ad}$ remained intact at

250 K, later studies in Trenary's group[18] have shown that $CH_{2,ad}$ decomposes already at 130 K via:

$$CH_{2,ad} \rightarrow CH_{ad} + H_{ad} \quad (5)$$

and the CH_{ad} product remains intact up to ~500 K[18,19]. Thus, any $CH_{2,ad}$ produced in step (3), which occurs at 250-300 K in TPD[62], must quickly decompose to $CH_{ad} + H_{ad}$. The fact that CH_{ad} is produced instead of $CH_{2,ad}$ is consistent with stoichiometric ratios measured mass spectroscopically by Hendersen et al.[60] and Hugenschmidt et al.[62]. Any H_{ad} that is not consumed to make methane desorbs in TPD as $H_{2,g}$ in a broad peak that extends from 270-400 K at high coverage[60-64].

Since the important catalytic parameters of selectivity and activity depend on the thermodynamic stability of adsorbed intermediates, it is important that the energetics (heat of adsorption, bond strength, etc.) of these important adsorbates be measured. Indeed previous studies utilizing temperature programmed desorption (TPD) have estimated kinetic parameters for methyl conversion to $CH_{4,g}$ and produced estimates for the energetics of adsorbed methyl on Pt(111).[17,70] However, TPD experiments cannot directly measure the adsorption energy of methyl or methylidyne fragments, because they do not desorb reversibly from the surface.

Here, we report direct measurements of the standard enthalpies of formation of $CH_{3,ad}$ and CH_{ad} on the Pt(111) surface by calorimetric measurements of the dissociative adsorption of methyl iodide. We show that the measured energetics of adsorbed methyl from SCAC differ from what is reported in previous TPD work[70,71] and further use these values from SCAC to calculate enthalpies of reaction for methane dehydrogenation on Pt(111). The resulting energies will be useful in making predictions about the thermodynamics and activation energies of various catalytically-interesting elementary steps over Pt catalysts, and they will also serve as

important benchmarks to compare to theoretical calculations (such as density functional theory) to evaluate the energy accuracy of new computational approaches.

4.2 Experimental

Experiments were performed in a UHV chamber (base pressure <2 x 10^{-10} mbar) equipped with X-ray photoelectron spectroscopy (XPS), Auger electron spectroscopy (AES), low energy ion scattering spectroscopy (LEIS), low energy electron diffraction (LEED), and SCAC. The apparatus and procedures for SCAC have been described in previous publications[28,72] and in detail in Chapter 2.

Calorimetry was performed by exposing the surface to a pulsed molecular beam of methyl iodide (CH_3I) gas. Each pulse was 100 ms long and repeated every 5 seconds. The methyl iodide (Fisher Scientific, 99.9%, lot 080482) was outgassed by several freeze-pump-thaw cycles after being put into its reservoir on the vacuum chamber. The reservoir was shielded from light due to methyl iodide's ability to photolyze. Its purity was checked with a mass spectrometer and found to be consistent with the manufacturer's claim. The beam was created by expanding ~2.0 mbar of CH_3I_g through a microchannel array at 299±6 K (defining the gas temperature) and then collimated through a series of five liquid nitrogen cooled orifices as described previously.[29] Coverages are reported in monolayers (ML) and are defined as the number of CH_3I molecules that adsorb to the surface irreversibly, normalized by the number of platinum surface atoms in the Pt(111) surface (1.50 x 10^{19} Pt atoms / m^2). A typical methyl iodide dose was ~0.004 ML (4.64 x 10^{12} molecules) per pulse with a beam spot size previously determined to be 4.36 mm in diameter.[29] The flux of methyl iodide from the molecular beam is

measured by impinging the beam onto a liquid nitrogen cooled quartz crystal microbalance (QCM), pre-covered with multilayers of methyl iodide. Calibration of the QCM has been described previously.[29]

The heat released from the adsorption of one methyl iodide pulse is measured with a pyroelectric polymer ribbon gently pressed against the back side of the Pt(111) sample.[31,72] The sensitivity of the pyroelectric detector was calibrated after each experiment by depositing a known amount of energy into the sample using a HeNe (632.8 nm) laser.

Sticking probabilities were measured simultaneously with calorimetric measurements, using the King and Wells method.[33] A mass spectrometer, without line-of-sight to the sample, measured the background pressure increase of CH_3I_g (m/e = 142) in the chamber. A gold flag was positioned in front of the sample and used to determine the mass spectrometry signal corresponding to full reflection of methyl iodide. The sticking probability of methyl iodide is calculated by integrating the mass spectrometer signal measured from the increase in methyl iodide partial pressure above background when the molecular beam is pulsed onto the sample surface in comparison with the increase in methyl iodide partial pressure resulting when pulsed onto the inert gold flag. We report two types of sticking probabilities, the long-term sticking probability and the short-term sticking probability.[30] The long-term sticking probability, S_∞, is the probability that a gas molecule strikes the Pt(111) surface, sticks, and remains until the next gas pulse starts ~5 seconds later. This measurement is used to calculate the adsorbate coverage remaining at the start of the next gas pulse. The short-term sticking probability, $S_{102\ ms}$, is the probability that a gas molecule strikes the Pt(111) surface, sticks, and remains at least throughout the timeframe of our heat measurement (i.e. the first 102 ms). This is used to calculate the moles of gas phase reactant that contribute to the measured heat of adsorption, so we can report that

value in kJ per mole adsorbed. When there is no desorption between pulses, the two sticking probabilities are the same.

4.3 Results

Sticking probability. As described previously[30] and above, we measured two types of sticking probabilities; the long-term sticking probability, S_∞, and the short-term sticking probability, $S_{102\ ms}$. Figure 3.1 shows both of these sticking probabilities for CH_3I_g as a function of coverage on Pt(111) at 95 K, 215 K, 270 K, 300 K and 320 K. Even though dissociation is occurring at 270 K and above, the sticking probabilities and coverages in Fig. 4.1 measure the total amount of CH_3I_g that adsorbs to the surface irrespective of the final products produced. At 95 K methyl iodide is known to adsorb molecularly through its iodine atom to the Pt(111) surface[59] in the first layer and at higher coverages form a multilayer. The sticking probabilities measured here (Fig. 4.1) show that a pulse of the methyl iodide completely sticks to the Pt(111) surface for all coverages at 95 K, as seen in both short and long term sticking probabilities of 1.00 ± 0.01. This result is consistent with previous TPD studies that found a multilayer to form below ~112 K.[61-63] At 215 K only the first layer of molecularly adsorbed methyl iodide is stable enough to form, since the sample is above the multilayer and second layer desorption peak temperatures of ~112 K and ~124 K respectively, but below the first layer desorption peak temperature of ~225 K. [61-63] At 215 K we find a total saturation coverage for the first layer of 0.23 ML, close to the value of 0.19 ML reported by French and Harrison.[63] Note here the high sticking probability (>0.95) from low coverage up to 0.16 ML, indicating a precursor-mediated adsorption mechanism. This type of adsorption has also been observed for several other organic molecules on Pt(111) namely benzene[37], naphthalene[38], cyclohexene[30], methanol[73], and water[28].

As described above, methyl iodide undergoes C-I bond scission to form adsorbed $CH_{3,ad}$ and I_{ad} on Pt(111) above ~250 K (reaction (2)). The methyl product continues to react by either dehydrogenating to CH_{ad} species (reactions (3) and (5)), and/or scavenging adsorbed hydrogen, resulting in the evolution of $CH_{4,g}$ at 260-300 K (reaction (4)).[60,61] Thus, these reactions are occurring during our measurements at 270 K, 300 K, and 320 K. The saturation coverages here represent the total amount of CH_3I_g that reacted with the surface, irrespective of the products. For these temperatures, the saturation coverage is seen to decrease as the surface temperature increases giving saturation coverages of 0.23 ML, 0.20 ML and 0.18 ML for Pt(111) at 270 K, 300 K, and 320 K respectively. As shown below, less total methane is produced with increasing temperature between 270 and 320 K, due to a greater probability for methyl dehydrogenation to evolve $H_{2,g}$ rather than to scavenge H_{ad} and evolve methane. We therefore attribute the corresponding decrease in saturation coverage to the decreasing amount of methyl product that escapes the surface as methane, and thus whose products remain behind to block sites (see below).

The short-term sticking probability at saturation coverage at 270 K is ~0.7, and drops to ~0 when at 320 K. This is because, as the surface temperature increases, the rate constant for desorption of this transiently-adsorbed CH_3I_a (on top of the saturated adlayer) increases and therefore it has a shorter surface residence time. By 320 K, it is so short that it is not long enough to be counted in the short-term sticking probability (which requires a lifetime of at least 102 ms).

Heat of adsorption at 95 K. In this chapter we define the term *heat of adsorption* as the negative of the differential standard molar enthalpy change for the adsorption reaction, with the

gas and the Pt(111) being at the same temperature as the Pt(111) surface. During our experiments, the temperature of the molecular beam was ~300 K, while the Pt(111) sample was held at cryogenic temperatures (e.g., 95 K). Thus, the measured heat is corrected by the small difference in the internal energy of the gas in the *directed* molecular beam at 300 K and in a Boltzmann distribution at the sample temperature (T), and then by RT to convert from internal energy change to enthalpy change for the adsorption reaction, as described elsewhere.[30]

The heat of adsorption of CH_3I on Pt(111) at 95 K is shown in Figure 4.2. At these conditions CH_3I adsorbs molecularly through its iodine atom to the Pt(111) surface[63], initially adsorbing with a heat of 98.2±2.0 kJ/mol. Using the known enthalpy of formation of CH_3I_g[74] and the initial enthalpy of adsorption of methyl iodide on Pt(111) the standard enthalpy of formation of CH_3I_{ad} at 95 K in this low-coverage limit is found to be $\Delta H_f^0(CH_3I_{,ad}) = -83.6 \pm 2.2$ kJ/mol. As the coverage increases to 0.25 ML, the heat of adsorption decreases linearly and is well described by a best-fit line of (98.2 - 110 θ) kJ/mol, where θ is coverage in ML, yielding an average heat of 84 kJ/mol in the first ¼ ML. The first layer saturation coverage of ~0.25 ML implies only next-to-next nearest neighbor sites can be occupied in a (2 x 2)-like structure. Following Persson's model,[43] this linear decrease in adsorption energy in the first 1/4 ML can be explained by immobile adsorbates which randomly populate next-to-next nearest neighbor sites (but not closer) with repulsive interactions between adsorbates at next-to-next nearest neighbor sites (but not further) and no relaxation of this repulsion by slight movement apart for an isolated pair (i.e., Persson's $\varepsilon = 0$). Adapting Persson's model to a hexagonal lattice, the initial heat of adsorption (98.2 kJ/mol) is the heat of adsorption for a single isolated adsorbate (Persson's μ) and the slope (-110 kJ/mol per ML) is equal to $-6V_0$ per 1/4 ML, where V_0 is the pairwise repulsion between adsorbates at next-to-next nearest neighbor sites (~4.5 kJ/mol here). This is

not a surprising result since TPD studies have found the first layer desorption peak temperature to decrease with increasing coverage indicating repulsive interactions between adsorbates in the first layer.[61,63]

An abrupt ~27 kJ/mol decrease in adsorption enthalpy, down to a value near the bulk heat of sublimation, occurs as the first layer completes at ~0.25 ML, suggesting that additional CH_3I must now adsorb in the much less stable second layer. Then there is an ~10 kJ/mol increase in adsorption energy in the coverage range of 0.26 - 0.31 ML. This slight increase in stability is likely due to the growth in size of 3D clusters of CH_3I molecules on top of the first layer. That is, more CH_3I-CH_3I bonds are made as the clusters grow in size, thus increasing their stability with increasing coverage, just as we have seen for metal cluster growth on surfaces[75]. Note that just like small 3D clusters of metal atoms, these small CH_3I clusters are metastable and will sinter into larger 3D particles in time. Support for this model comes from the RAIRS data of French and Harrison[63] that found metastable overlayers of CH_3I forming at low temperatures on Pt(111).

At coverages greater than 0.31 ML, there is a slow exponential decay in the adsorption energy even though the 3D clusters of CH_3I are continuing to grow in size (but probably have already reached the large-size limit energetically). This decay in adsorption energy could be due to a decreasing long-range electronic attraction of the CH_3I adsorbates to the underlying Pt(111) substrate. As the coverage and cluster thickness grows, the average distance between the Pt substrate and newly adsorbed CH_3I molecules increases and thus the electronic attraction to the Pt diminishes and the heat of adsorption decreases. It asymptotically becomes constant at coverages greater than 0.65 ML at 37.9±2.0 kJ/mol, in excellent agreement with the heat of sublimation of bulk methyl iodide of 38.0 kJ/mol. For the bulk heat of sublimation at 95 K, we

used the CH_3I heat of sublimation measured at 207.7 K from Ref. [76], and corrected it to 95 K by using a gas-phase heat capacity of 4R and the solid heat capacity of CH_3Br, 13 cal/(mol K)[77], since the heat capacity of solid CH_3I is not available.

Reaction pathways to adsorbed methyl and to methane evolution. In order to measure the energetics of adsorbed $CH_{3,ad}$, conditions must be found where the carbon-iodine bond scission (reaction (2)) occurs cleanly and fast enough to be detected during the timescale of our heat measurement (~102 ms). The rate constant for this reaction on Pt(111) has been reported in two separate works[62,63], giving an average value of $k_{rxn} = 9x10^{10}\ s^{-1}e^{(-50.8\ kJ/mol/RT)}$. This rate constant is used to estimate the time constant of the carbon-iodine scission ($\tau = 1/k_{rxn}$) as a function of temperature. The resulting τ values show the bond scission occurs with τ = ~100 ms or faster at temperatures of 270 K and above, which is fast enough to be detected with our heat measurement. Therefore, experiments conducted at 270 K and above are likely to yield the heat of dissociative methyl iodide adsorption to form adsorbed methyl coadsorbed with iodine (reaction (2)). Unfortunately, by 270 K, we also observed the production of methane gas, which shows that we are also producing the further products of reactions (3)-(5): $CH_{4,g}$, CH_{ad}, and H_{ad}, and possibly $H_{2,g}$.

Figure 4.3 shows the time dependence of the production rate of methane gas (i.e., its partial pressure) as a single pulse of CH_3I_g is dosed onto the Pt(111) surface at different temperatures. Each pulse of CH_3I_g from the molecular beam lasts 100. ms, consists of approximately 0.0040 ML of CH_3I_g and is repeated every 5 seconds. The methane gas signal was measured using a non-line-of-sight mass spectrometer following the signal at m/e = 16. To improve the signal-to-noise ratio here, we averaged all the pulses over the total methyl iodide

coverage range from 0.04 to 0.11 ML. No methane gas was evolved in region 1, defined as the range below 0.04 ML.

Figure 4.4a displays the amount of methane gas evolved from the surface per pulse (i.e., the area under the methane peak in Fig. 4.3) as a function of the total CH_3I_g coverage for different surface temperatures. Figure 4.4b displays the total integrated amount of methane gas evolved (that is, the sum of all pulse areas, or the integral of Fig. 4.4a) versus total methyl iodide coverage.

As described above, the reaction pathways that are known to be rapid following the adsorption of CH_3I_g on Pt(111) at 270 K can be summarized as reactions (1)-(5):

$$CH_3I_g \rightarrow CH_3I_{ad} \rightarrow CH_{3,ad} + I_{ad}, \qquad (1+2)$$

$$CH_{3,ad} \rightarrow CH_{2,ad} + H_{ad} \rightarrow CH_{ad} + 2\,H_{ad}, \text{ and} \qquad (3+5)$$

$$CH_{3,ad} + H_{ad} \rightarrow CH_{4,g}. \qquad (4)$$

If we assume that hydrogen desorption is negligibly slow at 270 K, then these reactions will eventually proceed to completion, giving the net stoichometric reaction:

$$3\,CH_3I_g \rightarrow 2\,CH_{4,g} + CH_{ad} + 3\,I_{ad}. \qquad (6)$$

Thus, for every 3 methyl iodides, two methanes are produced, one CH_{ad} remains on the surface with three iodine atoms at completion of the reaction. The saturation coverage of 0.23 ML of reacted methyl iodide (Fig. 4.1b) thus yields (2/3) x 0.23 ML = 0.153 ML of methane, 0.077 ML of CH_{ad} and 0.23 ML of I_{ad}. Summing these two adsorbates's coverages gives a total saturation coverage of 0.31 ML of all adsorbed species, very close to the value of 1/3 ML expected if only nearest neighbor sites cannot be occupied by either species. We used this saturation amount of methane at 270 K (0.153 ML) to put ML units on the y axes of Fig. 4.4.

Above 270 K, the saturation coverage decreases (Fig. 4.1b). We attribute this to the fact that a new reaction pathway for H_{ad} (desorption as $H_{2,g}$) gets fast enough to compete with its reaction with $CH_{3,ad}$ to make methane as a mechanism to eliminate H_{ad}. The competition between these two pathways for H_{ad} is shown schematically in Fig. 4.5. As seen in Fig. 4.4b, the total amount of methane gas evolved correspondingly decreases to ~0.11 ML at 300 K and ~0.08 ML at 320 K. For each $CH_{3,ad}$ that is not consumed as methane, an additional CH_{ad} remains on the surface. This will thus decrease the saturation amount of reacted methyl iodide by the same amount. These decreases in methane amount (compared to 270 K) by 0.04 ML at 300 K and 0.07 ML at 320 K are close to the decrease in saturation reaction amount in Fig. 4.1b of 0.03 and 0.05 ML, respectively, supporting this explanation for the decrease in saturation coverage with temperature. Subtracting the total methane yield of Fig. 4.4b from the saturation amounts of reacted CH_3I in Fig. 4.1b gives saturation total adsorbate coverages ($CH_{ad} + I_{ad}$) of 0.29 and 0.28 ML at 300 K and 320 K, respectively. Again, these are very close to the value of 1/3 expected if nearest-neighbor sites cannot be occupied.

Figure 4.4a has two distinct coverage regions: region 1 where no methane is evolved (0 to 0.04 ML) and region 2 (above 0.04 ML) where methane evolves with increasing and then decreasing yields from the surface as successive pulses of CH_3I are dosed. We explain in the Discussion section that the absence of methane in region 1 is due to the equilibrium constant for net reaction (3+5) being very small, so that at low coverage methyl is the dominant C-containing species on the surface, but as H_{ad} is removed from the surface (by reaction with these methyls, which only occurs fast enough at higher coverages), the reaction is driven to the right, leaving CH_{ad} as the dominant C-containing species by reaction completion. This is consistent with

RAIRS results which show that the $CH_{3,ad}$ vibrational modes seen at low temperature disappear after annealing to 300 K and show modes due to CH_{ad} remain on the surface[19].

Methyl iodide undergoes disproportionation and coupling reactions on Au(111)[78], β-hydride elimination on Ag(111)[79], and Cu(111)[80] evolving longer chain alkanes / alkenes from the surface. We monitored for these products (ethane, ethylene, propane, propene, butane, and butene), but the only signal observed was methane and its respective cracking pattern, in agreement with previous work.[60,61,63] Hydrogen evolution was also undetected, but this is not unexpected. Based on the branching ratios identified above and the stoichiometry of pathway (2) (Figure 4.5) the amount of hydrogen released even at 320 K would be below our detection limits given the background signal of m/e = 2 in the chamber and the mass spectrometer's sensitivity to $H_{2,g}$.

At 270 K, the m/e=16 lineshape in Fig. 4.3 shows the $CH_{4,g}$ signal continues to rise long after the 102 ms time window typically used for the heat measurement (between the two dashed lines in Figure 4.3). This situation should result in a lineshape change in the heat detector signal[28], as indeed observed (see below). The same is true at 300 K, but to a lesser extent. In both cases, this leads to a broadening in the heat signal, which is more complicated to interpret quantitatively to extract heats, as described below. However, by 320 K, methane is evolved in region 2 sufficiently fast to reach a maximum at the end of the pulse window in Figure 4.4, meaning the signal from the heat detector at 320 K in region 2 should exhibit little to no broadening and accurately represent the chemistry occurring here.

Heat of adsorption of methyl iodide on Pt(111) at 215, 270, 300, and 320 K. Figure 4.6 displays the heat of adsorption versus coverage for methyl iodide dosed onto Pt(111) at 215 K , 270 K , 300 K and 320 K.

At 215 K the average heat of adsorption is 96.4 kJ/mol, 11 kJ/mol larger than the average heat of adsorption measured at 95 K in the same coverage range (0-0.23 ML, Fig. 4.2). Using a mass spectrometer positioned normal to the Pt(111) surface, Harrison and French[63] observed small amounts of methane evolution at this temperature indicating a small amount of decomposition of CH_3I_{ad} that could contribute to this higher heat. We did not observe any methane evolution, but because our mass spectrometer is not normal to the surface it is unlikely that our measurement is as sensitive. However, the rate constant equation listed above gives a reaction time constant of 24 seconds for the carbon-iodine bond scission at this temperature, which is much too slow to be detected during our ~100 ms heat detection window. Therefore the 11 kJ/mol higher heat at 215 K is likely the result of adsorbed CH_3I molecules in a more stable phase at 215 K than at 95 K. This could be due to the fact that the greater mobility at higher temperature allows the molecules to arrange into their most stable structure on the time scale of the heat measurement at 215 K, but not at 95 K.

The heat signal pulses at 270 K showed significant broadening compared to that from the laser calibration signal, consistent with the slow evolution of methane seen in Figure 4.3. Such pulse broadening is due to a surface reaction depositing heat on a timescale slightly longer than the 100 ms pulse width of the molecular beam, as discussed previously in detail[28]. Here, interpretation of the broadened heat signal is complicated since the observed signal is really a convolution of sequential heat events. In region 1, the lack of methane evolution (Figure 4.4a)

coupled with previous RAIRS studies showing high concentrations of $CH_{3,ad}$ species[18,19,61,63], leads to the following model of sequential reaction events that contribute to the heat:

$$CH_3I_g \rightarrow CH_3I_{ad}. \quad (1)$$

$$CH_3I_{ad} \rightarrow CH_{3,ad} + I_{ad}. \quad (2)$$

We assumed that step (1) is instantaneous at 270 K and above and that reaction (2) proceeds with a pseudo-first-order rate constant $k_2 = 1/\tau$, thus giving rise to an exponential decay function with time constant τ which is convoluted with the input from step (1), which was set equal to the molecular beam pulse shape. We were able to deconvolute our observed heat signal into these two heat components by constructing theoretical signals for each heat event and summing them together until a best fit of the measured signal was obtained. More details of this signal analysis will be presented in Ref [81]. The heat of step 1, the heat of step 2, and the time delay, τ, of step 2 were all adjusted until the resulting modeled signal (i.e. the sum of these two simulated signals) converged to fit the measured signal. This analysis provides the differential heat of steps 1 and 2, the total differential heat of the reaction, and the rate constant for step 2 where $k_2 = 1/\tau$.

At higher coverages, reactions (3)-(5) also proceed, eventually giving net reaction (6). We assume here that steps (2)-(5) can be described by a single, pseudo-first-order rate constant, so that at higher coverages, this same deconvolution analysis provides the heat for step 1, the total differential heat of the more complicated net reaction that is occurring at each coverage, and the pseudo-first-order rate constant, $1/\tau$. As shown below, this pseudo-first-order analysis works well, probably because the latter steps are fast and rate limited by step 2.

For the data at 270 K we found that τ increased linearly with coverage from ~170 ms initially to 750 ms at 0.23 ML. This corresponds to a decrease in k_2 from 5.9 s^{-1} to 1.3 s^{-1}. The

reason k_2 decreases with coverage may be that as more active sites become blocked by adsorbates, the pseudo-first-order rate constant decreases as expected if it is really the product of a true second-order rate constant and the free site concentration. Lateral interactions with co-adsorbates might also affect the activation energy for step 2. These rate constants compare well to those measured by Hugenschmidt et al.[62] and Harrison's group[63], 4.3 s^{-1} and 1.4 s^{-1} respectively.

At 320 K the kinetics were fast enough that no broadening of the heat signal line shape was detected, consistent with the methane evolution rate in region 2 at 320 K being fast enough to occur in the timeframe of the heat measurement (Figure 4.3). In Figure 4.6 the heat curves for the corrected data at 270 K and 300 K approximately follow the heat curve measured at 320 K, confirming that similar heats are measured at these temperatures just with slower kinetics at 270 K and 300 K, but as discussed previously[35], it is most reliable to perform SCAC at conditions where the reaction is fast enough to occur within the 100 ms pulse of the molecular beam, so that no deconvolution is needed.[28] Therefore, the 320 K heat curve in Figure 4.6 is assumed to be the most accurate in representing the heat released during the surface reactions. At 270 and 300 K, the data interpretation in region 2 is also complicated by the fact that most of the methane is evolved more slowly than the heat signal time constant τ.

4.4 Discussion

Energetics of adsorbed methyl on Pt(111). The lack of methane evolution in region 1 (0-0.04 ML) in Figure 4.4a, indicates that reactions (3)-(5) are not yet occurring. We show below that this is <u>not</u> because they are too slow at 270-320 K, but instead because their net equilibrium lies

far to the left. We thus take the heat in region 1 at 320 K (Figure 4.6), to represent the net heat of steps (1) plus (2) above, or net reaction (1+2):

$$CH_3I_g \rightarrow CH_{3,ad} + I_{ad} \qquad (1+2)$$

The measured integral heat of adsorption in this coverage range (212 kJ/mol) gives the enthalpy of net reaction (1+2) to be -212 kJ/mol. A thermodynamic cycle is constructed in Figure 4.7 to extract from this value the enthalpy of formation (ΔH_f^0) and Pt-C bond enthalpy for adsorbed methyl. The enthalpy of formation of adsorbed methyl is found by first starting on the left hand side of the cycle with the elements in their standard states and following the pathway of the bottom half of the cycle. The enthalpy for the lower left hand step is simply the enthalpy of formation of CH_3I_g, +14.6 kJ/mol, from ref [74]. The lower right hand step is the integral enthalpy of adsorption measured at 320 K in region 1, -212 kJ/mol. By adding the energies of the lower left and right hand steps, a total value of -197 kJ/mol is found. This is the total enthalpy change in taking the elements in their standard states to methyl co-adsorbed with an iodine adatom (both at a coverage of 0.04 ML), and therefore is equal to the sum of the enthalpy of formation of adsorbed methyl with the enthalpy of formation of adsorbed iodine. The standard enthalpy of iodine on Pt(111) is known: ΔH_f^0 = -144 kJ/mol at 0.04 ML, from the TPD work of Labayen et. al.[82] Subtracting this enthalpy of formation of adsorbed iodine from -197 kJ/mol results in the enthalpy of formation of adsorbed methyl; $\Delta H_f^0 (CH_{3,ad})$ = -53 kJ/mol.

By following the pathway depicted in the upper part of this thermodynamic cycle (Fig. 4.7) the C-Pt(111) bond enthalpy of adsorbed methyl can be extracted. This is accomplished by again starting on the left hand side of the cycle with the elements in their standard states, but now following the upper left-hand step that takes the elements in their standard states to gas phase methyl radical and adsorbed iodine. The enthalpy for this step is determined by adding the

known enthalpy of formation of gas phase methyl (+147 kJ/mol)[54] and adsorbed iodine (-144 kJ/mol at 0.04 ML)[82] giving an enthalpy for this step of +3 kJ/mol. The upper right hand step in the pathway is the adsorption of gas phase methyl onto the Pt(111) surface that has 0.04 ML of adsorbed iodine. The enthalpy for this step is found by subtracting the upper left hand step from -197 kJ/mol, giving an enthalpy of -200. kJ/mol. Thus, the H_3C-Pt(111) bond enthalpy is 200. kJ/mol based on our heat measurement in region 1 at 320 K and other known thermodynamic data. The potential error on this number is estimated to be ± 20 kJ/mol, based on the dominant error of ± 20 kJ/mol on the heat of formation of I_{ad} from TPD[82]. The coadsorption of iodine does not perturb the activation energies for reactions of the methyl groups in any significant way[17]. Further evidence comes from RAIRS data that show the band frequencies of adsorbed methyl produced through CH_3I dissociation are identical to those obtained by azomethane pyrolysis (which produces adsorbed methyl groups without the co-adsorption of iodine).[63,65]

Energetics of adsorbed methylidyne on Pt(111). As noted above, the net reaction at 270 K at reaction completion is:

$$270\ K: \qquad CH_3I_g \rightarrow 2/3\ CH_{4,g} + 1/3\ CH_{ad} + I_{ad}. \qquad (6)$$

Thus, the integral heat of adsorption at saturation coverage at 270 K should give the heat for this net reaction. The net methane yield is 2/3 of the saturation amount of reacted CH_3I (0.23 ML), or 0.153 ML. At 300 K, the methane yield decreased to 0.11 (Fig. 4.4b), since some of the H_{ad} that is used to produce methane in reaction (6) instead desorbed as $H_{2,g}$, and the saturation coverage also decreased, to only 0.20 ML. This gives the following net reaction at completion at 300 K:

$$300\ K: \qquad CH_3I_g \rightarrow 0.55\ CH_{4,g} + 0.45\ CH_{ad} + 0.175\ H_{2,g} + I_{ad} \qquad (7)$$

Similarly, only 0.08 ML of methane was produced at 320 K (Fig. 4.4b) and the saturation coverage decreased to 0.18 ML. This gives the following net stoichiometry at reaction completion and 320 K:

$$320\ \text{K:} \qquad CH_3I_g \rightarrow 0.44\ CH_{4,g} + 0.56\ CH_{ad} + 0.34\ H_{2,g} + I_{ad} \qquad (8)$$

We have analyzed our integral heats of adsorption at these temperatures assuming these stoichiometries, with two corrections: The rate of hydrogen desorption is so slow compared to the heat measurement time τ that the H_{ad} has not yet converted to gas. (Using the reported prefactor and activation energy for hydrogen desorption from Pt(111)[83] gives much longer surface residence times.) Thus we replace every $H_{2,g}$ with 2 H_{ad} for the purposes of analyzing reaction heats. Similarly, most of the methane is evolved after the heat measurement time τ at 270 and 300 K, so that we must replace $CH_{4,g}$ with $CH_{3,ad}$+H_{ad} there too.

Unfortunately, the heat curves in Fig. 4.6 do not extend all the way up to the saturation coverages of Fig. 4.1, but the heat curve comes very close at 320 K, and it decreases linearly with coverage at the highest coverages measured. Thus, we assumed that this decrease continues linearly at 320 K up to saturation coverage. This gives a final heat of adsorption of 89 kJ/mol at 320 K. We then assumed that this final heat of adsorption of 89 kJ/mol was the same at 300 and 270 K, and connected the point in Fig. 4.6 for last heat value to this saturation coverage point assuming a straight-line decrease. We then used the integrals of these (analytically continued) heat curves to calculate the integral heats of adsorption. These values are tabulated in Table 4.1 versus temperature.

Table 4.1: The integral heat, the reaction stoichiometries, and known thermodynamic data are used to calculate the $\Delta H_f^0 (CH_{ad})$ and the Pt-CH bond enthalpy listed below.

Temperature (K)	Overall Reaction	Integral Enthalpy of adsorption (kJ/mol)	$\Delta H_f^0(CH_{ad})$ (kJ/mol)	Pt-CH Bond Enthalpy (kJ/mol)
270 K	$CH_3I_g \rightarrow 2/3\ (CH_{3,ad} + H_{ad}) + 1/3\ CH_{ad} + I_{ad}$	-163	+109	485
300 K	$CH_3I_g \rightarrow 0.55\ (CH_{3,ad}+H_{ad}) + 0.45\ CH_{ad} + 0.35\ H_{ad} + I_{ad}$	-167	+79	512
320 K	$CH_3I_g \rightarrow 0.44\ CH_{4,g} + 0.56\ CH_{ad} + 0.68\ H_{ad} + I_{ad}$	- 171	+42	552

Using the total integral heats measured at each temperature from Table 4.1 together with the reactions stoichiometries outlined above, we calculated the standard enthalpy of formation of CH_{ad}, $\Delta H_f^0 (CH_{ad})$, at each temperature, also listed in Table 4.1. This calculation required the standard enthalpy of formation of all the other reactants and products in these reactions. For adsorbed iodine, we used the coverage dependent heat of formation: a value of -125 kJ/mol at 0.23 ML for the reaction at 270 K, -128 kJ/mol at 0.2 ML for the reaction at 300 K and -130 kJ/mol at 0.18 ML of coverage for the reaction at 320 K. These coverage dependent heats of formation of iodine adatoms are found from the reported heat of adsorption of iodine extracted from careful analysis of TPD data[82]. We also used here the reported enthalpy of adsorption of $H_{2,g}$ (-72 kJ/mol)[30] for the standard heat of formation of 2 H_{ad}. Since methane is known to be produced by reaction (4) with 18.7 kJ/mol of excess enthalpy (above that expected for a Boltzmann distribution at the surface temperature)[84], we corrected its standard heat of formation taken from the literature (-75 kJ/mol [85]) by this amount. For CH_3I_g, the standard heat of formation is +14.6 kJ/mol[74]. As seen in Table 4.1, the results at these three temperatures give different heats of formation for CH_{ad}: +109 kJ/mol at 270 K, +79 kJ/mol at 300 K, and + 42 kJ/mol at 320 K. The differences could be due to the value of $\Delta H_f^0 (CH_{3,ad})$ used in these

calculations at 270 and 300 K, which is the value measured at low coverage (0.04 ML, see above) but applied here to the full coverage range up to saturation, where $CH_{3,ad}$ is probably substantially less stable due to adsorbate-adsorbate repulsions. Another factor that could contribute to these differences is the larger iodine to CH ratio at 270 K (3 to 1) and at 300 K (2.2 to 1) than at 320 K (1.8 to 1). More iodine adatoms could also be destabilizing the CH_{ad}. Additionally, from figure 3 the time constant for methane evolution at 270 K and 300 K is approximately 7 and 5 times longer, respectively, than the time constant for the heat signal. Thus, a fraction of the methane evolution is captured in the heat measurement at 270 K and 300 K and not accounted for there. Therefore we assume that the data at 320 K, where there is no time constant associated with the heat signal and methane evolves promptly, is the most accurate. It gives a ΔH_f^0 (CH_{ad}) of +42 kJ/mol and a bond strength of 552 kJ/mol (listed in Table 4.1).

We also list in Table 4.1 the HC-Pt(111) bond enthalpy for CH_{ad}, calculated at each temperature by subtracting the ΔH_f^0 (CH_{ad}) from the standard enthalpy of formation of CH_g (594 kJ/mol[85]).

It is rather surprising that the adsorption of methyl iodide initially produces mainly $CH_{3,ad}$ (plus I_{ad}) at low coverages for all three of these temperatures, but at high coverages the only surface product remaining is CH_{ad} (plus I_{ad}). We next prove that this is a natural consequence of the very small equilibrium constant for net reaction (3+5):

$$CH_{3,ad} \rightleftharpoons CH_{ad} + 2\ H_{ad}, \qquad (3+5)$$

at low coverage methyl is the dominant C-containing species on the surface, but, as H is removed from the surface (by reaction with these methyls to make methane gas, which only occurs fast enough at higher coverages), the reaction is driven to the right, so that CH_{ad} is the dominant C-

containing species by reaction completion. This push to the right is an example of Le Chatelier's Principle.

In Fig. 4.8 we show the coverages of $CH_{3,ad}$, CH_{ad} and H_{ad} versus methyl iodide coverage calculated to simulate the exact conditions of our calorimetry experiment at 270 K. These coverages were calculated by incrementally changing the adsorbate coverages with each methyl iodide gas pulse (starting from zero initially) based on the following simple model:

1. The methyl coverage was first increased by the measured amount of methyl iodide that adsorbed in that pulse period (i.e., its flux times its long-term sticking probability).
2. The coverages of $CH_{3,ad}$ and H_{ad} were each decreased by the measured amount of methane gas evolved during that pulse period (also plotted in Fig. 4.8).
3. The net reaction (3+5) was then assumed to come to equilibrium with an equilibrium constant:

$$K_{3+5} = ([CH][H]^2)/[CH_3] = 4x10^{-5}\ ML^2,$$

where [i] represents the surface coverage of species i in ML. This value for K_{3+5} was estimated by first using our measurements to calculate the enthalpy of reaction (3)+(5), giving 23 kJ/mol ($\Delta H^0_{rxn\ 11}$, see below), and then neglecting the entropy difference between reactants and products so that $K_{3+5} = \exp(-\Delta H^0_{rxn\ 11} / RT)$. The final equilibrium coverages of $CH_{3,ad}$, CH_{ad} and H_{ad} at the end of the pulse period were calculated based on their initial values (i.e., after step 2) and this equilibrium constant. Steps 1-3 were repeated for each gas pulse.

As seen in Fig. 4.8, this simple model leads to the following interesting and non-intuitive results. Initially, almost 100% of the MeI that adsorbs is used to build up the coverage of $CH_{3,ad}$ below 0.06 ML, but above 0.09 ML, that $CH_{3,ad}$ is removed almost as rapidly and there is a similar rapid buildup in the coverage of CH_{ad}. This transition occurs when the amount of

methane gas evolved per pulse gets large. This trend continues until essentially all the $CH_{3,ad}$ is consumed, and the methane gas evolution also drops to near zero.

The slopes of +0.56 for CH_{ad} and -0.66 for $CH_{3,ad}$ in the coverage range 0.11-0.17 ML in Fig. 4.8 are close to the values of 1/2 and -1/2 expected for the following net stoichiometry: 2 $CH_3I_g + CH_{3,ad} \rightarrow CH_{ad} + 2\ CH_{4,g} + 2\ I_{ad}$. However, there seems to be some small contribution from the following stoichiometry as well: $CH_3I_g + 2\ CH_{3,ad} \rightarrow CH_{ad} + 2\ CH_{4,g} + I_{ad}$, which would give larger slopes of +1 and -2 if occurring alone.

It is also surprising that methane gas does not appear already at lower coverage. We next show that this is a natural consequence of the kinetics of reaction (4) that produces methane from surface methyl plus H, provided that its activation energy decreases linearly with coverage by a small amount. The rate of reaction (4) should be proportional to the product $[CH_3][H]$ and a rate constant, k_4. In Fig. 4.8, we plot also the product $[CH_3][H]$. It maximizes at a much lower coverage than the measured methane evolution rate (amount per pulse). However, if we assume that k_4 has an activation energy that decreases with coverage by 94 kJ/mol per ML of MeI, we instead get the calculated rate of CH_4 production shown in Fig. 4.8. This maximizes at much higher coverage and semi-quantitatively reproduces the coverage dependence of the measured rate. This decrease in activation energy by 94 kJ/mol per ML of MeI corresponds to only 19 kJ/mol for the whole coverage range plotted here. This small amount is entirely reasonable, given the fact that both reactants ($CH_{3,ad}$ and H_{ad}) are certainly greatly destabilized relative to the product as coverage increases, due to adsorbate-adsorbate repulsions.

Predicted reaction enthalpies. The enthalpy of formation of methyl and methylidyne measured in this work allow the following reaction enthalpies of methane dehydrogenation steps on Pt(111) to be calculated:

$$CH_{4,g} \rightarrow CH_{3,ad} + H_{ad} \qquad \Delta H^0_{rxn\ 9} = -14\ kJ/mol \qquad (9)$$

$$CH_{4,ad} \rightarrow CH_{3,ad} + H_{ad} \qquad \Delta H^0_{rxn\ 10} = +1\ kJ/mol \qquad (10)$$

$$CH_{3,ad} \rightarrow CH_{ad} + 2H_{ad} \qquad \Delta H^0_{rxn\ 11} = +23\ kJ/mol \qquad (11)$$

The enthalpy of reaction (9), taking gas phase methane to a methyl fragment plus a hydrogen adatom on Pt(111), is found to be downhill by -14 kJ/mol. This reaction enthalpy is calculated using the known $\Delta H_f^0 (CH_{4,g}) = -75$ kJ/mol[85], the $\Delta H_f^0 (H_{ad}) = -36$ kJ/mol at low coverage[30], and the $\Delta H_f^0 (CH_{3,ad}) = -53$ kJ/mol measured in this work. In Ref [70,71], rate measurements of methane formation from methyl coadsorbed with hydrogen were used in conjunction with the activation energy for dissociative adsorption of methane from molecular beam studies[86] to estimate an enthalpy for reaction (9) of +48 kJ/mol. Note that this reaction enthalpy is 62 kJ/mol larger than what we report here using our calorimetrically measured heats for adsorbed methyl. The reaction enthalpy reported in Ref. [71] and [70] implies that the Pt-CH_3 bond enthalpy is only 138 kJ/mol, much less than measured here by SCAC and much less than any DFT calculation predicts in Table 4.2 (below).

In reaction (10), the reaction enthalpy for removing a single hydrogen atom from an adsorbed methane molecule to form adsorbed methyl coadsorbed with a hydrogen adatom is calculated to be, $\Delta H^0_{rxn\ 10} = +1$ kJ/mol, implying reaction (10) is approximately thermo-neutral. To calculate the enthalpy of reaction (10), the $\Delta H_f^0 (CH_{4,ad}) = -90.1$ kJ/mol is used, which comes from the $\Delta H_f^0 (CH_{4,g}) = -75$ kJ/mol[85] and the desorption energy of methane from Pt(111) (15.1

kJ/mol, measured by TPD[86]). DFT calculations utilizing the PW91 functional find a reaction enthalpy for reaction (10) of -7.7 kJ/mol[87], close to the +1 kJ/mol reaction enthalpy from the present experiment.

The reaction enthalpy for removing two hydrogen atoms from adsorbed CH_3 in reaction (11) is found to be uphill, $\Delta H^0_{rxn\ 11}$ = +23 kJ/mol (using here the $\Delta H_f^0(CH_{ad})$ = +42 kJ/mol from Table 4.1). Thus the addition of the reaction enthalpies for reactions (10) and (11) give a total enthalpy change of +24 kJ/mol converting an adsorbed methane molecule to adsorbed methylidyne coadsorbed with three hydrogen adatoms. DFT calculates a reaction enthalpy for this reaction of -45 kJ/mol[87].

The energetics of reactions (9)-(11) are summarized in Fig. 4.9. The energy of $CH_{2,ad}$ is not known, but only shown as less stable than $CH_{ad} + H_{ad}$ since it decomposes into these products already at 130 K[18,19].

Comparison to DFT. The bond enthalpies measured in this work provide a benchmark for comparison to DFT calculations of methyl and methylidyne on Pt(111). Table 4.2 lists calculated bond energies for these adsorbates on Pt(111) using cluster and periodic DFT calculations. Here the calculations for methyl on 35 and 10 Pt atom cluster using the B3LYP functional find a bond energy of 209 kJ/mol, which is in good agreement with the measured bond energy of 197 kJ/mol (calculated by subtracting RT from our bond enthalpy of 200 kJ/mol, Figure 4.7). The 10 and 8 Pt atom cluster calculations using the PW91 and B3LYP functional are less accurate, overestimating the bond energy of adsorbed methyl by 35 and 28 kJ/mol respectively. Periodic DFT calculations using the PW91 and PBE functionals found a bond energy of adsorbed methyl on Pt(111) of 197 and 192 kJ/mol in excellent agreement with the

measured value. However, the periodic DFT calculation that used the RPBE functional underestimates the bond energy by 34 kJ/mol.

For methylidyne, the cluster calculations all overestimate the bond energy regardless of the functional used. The most accurate cluster calculation uses the RPBE functional, finding a bond energy of 569 kJ/mol, which is an overestimation of only 19 kJ/mol (the measured bond energy is 550 kJ/mol, calculated by subtracting RT from the bond enthalpy of 552 kJ/mol, Table 4.1). The least accurate cluster calculation uses the PW91 functional with a 10 Pt atom cluster, predicting a bond energy for adsorbed methylidyne of 728 kJ/mol, 178 kJ/mol too high. Periodic DFT calculations using the PW91 and PBE functionals, also overestimate the bond energy of methylidyne by 70 and 93 kJ/mol respectively.

Cluster calculations that used the B3LYP functional give values closer to the measured value as the cluster size increases, but the cluster calculations that used the PW91 functional perform poorly and greatly overestimate the bond strengths of both $CH_{3,ad}$ and CH_{ad} to Pt(111). However, caution must be used when comparing the measured bond energy of methylidyne from this work to DFT calculations, because the HC-Pt(111) bond energy measured here is for CH coadsorbed with ~0.18-0.23 ML of I_{ad} and while it is known that the coadsorption does not significantly affect neighboring $CH_{3,ad}$ groups, at least in their reaction rates as measured by TPD[17] it is not known if iodine adatoms perturb neighboring methylidyne adsorbates.

Table 4.2: Bond energies of methyl and methylidyne to the Pt(111) surface reported from previous DFT calculations.

Species	Functional	Coverage	Bond Energy (kJ/mol)	Reference
$CH_{3,ad}$ (atop)	B3LYP	35 Pt atom cluster	209	[88]
	B3LYP	10 Pt atom cluster	209	[89]
	PW91	10 Pt atom cluster	232	[89]
	B3LYP	8 Pt atom cluster	225	[90]
	PW91	¼ ML	197	[91]
	RPBE	¼ ML	163	[91]
	PBE	1/9 ML	192	[92]
CH_{ad} (fcc hollow)	B3LYP	35 Pt atom cluster	613	[88]
	B3LYP	10 Pt atom cluster	678	[89]
	PW91	10 Pt atom cluster	728	[89]
	B3LYP	8 Pt atom cluster	697	[90]
	PW91	¼ ML	620	[91]
	RPBE	¼ ML	569	[91]
	PBE	1/9 ML	643	[92]

4.5 Conclusion

Single crystal adsorption calorimetry of methyl iodide adsorption on Pt(111) at 95 K, 270 K, 300 K, and 320 K has yielded the energetics of molecularly adsorbed methyl iodide, adsorbed methyl, and adsorbed methylidyne.

At 95 K, methyl iodide adsorbs to Pt(111) molecularly through its iodine atom, forming a (2 x 2) like structure with repulsive dipole-dipole interactions between adsorbates resulting in a decreasing heat of adsorption that is well fit by (98.2-110 θ) kJ/mol up to 0.25 ML of coverage. These results give a $\Delta H_f^0 (CH_3I_{,ad})$ = -83.6 ± 2.2 kJ/mol for adsorbed methyl iodide in the limit of low coverage. Above 0.25 ML, methyl iodide adsorbs in a second layer structure forming 3D clusters of CH_3I that increase in stability as their size grows with coverage. At coverages greater than 0.6 ML methyl iodide adsorbs with a constant heat of adsorption equal to the heat of

sublimation of methyl iodide. At 215 K, only the first 0.23 ML of methyl iodide adsorbs, giving an integral heat of molecular adsorption that is 11 kJ/mol higher than observed at 100 K in this coverage range.

At temperatures of 270-320 K, methyl iodide dissociatively adsorbs, forming $CH_{3,ad}$ coadsorbed with iodine adatoms in the coverage range 0 – 0.04 ML. As the coverage increases past 0.04 ML, dehydrogenation of these methyl groups results in the formation of methane and H_2 gas, which ultimately leaves CH_{ad} coadsorbed with iodine adatoms. The kinetics of these reactions are fast enough at 320 K to be accurately measured in the 100 ms window of our heat detector. The heat measurement in the low coverage region (region 1, 0 – 0.04 ML) gave ΔH_f^0 ($CH_{3,ad}$) = -53 kJ/mol and a Pt-CH_3 bond enthalpy of 200 kJ/mol and the integral heat measurements from 0 ML to saturation coverage at 270 K , 300 K, and 320 K provided the energetics of adsorbed methylidyne, giving ΔH_f^0 (CH_{ad}) = +42 kJ/mol and a Pt-CH bond enthalpy of 552 kJ/mol at 320 K.

The measured bond enthalpies of Pt-CH_3 and Pt-CH were compared to previous DFT calculations. Cluster calculations using the B3YLP functional were found to routinely overestimate the bond strength of both $CH_{3,ad}$ and CH_{ad} but these calculations move closer to the measured value as the cluster size increases. Cluster calculations that employed the PW91 functional overestimated the bond energy of $CH_{3,ad}$ and CH_{ad} by 35 kJ/mol and 176 kJ/mol respectively. Periodic DFT calculations using the PW91 functional performed remarkably well, exactly predicting the bond energy of adsorbed methyl measured in this work but overstimating the bond energy of adsorbed methylidyne by 68 kJ/mol. Periodic DFT using PBE also performed well, predicting the bond energy of $CH_{3,ad}$ within 5 kJ/mol, but also overestimated the

bond energy CH_{ad} by 91 kJ/mol. Finally, periodic DFT with RPBE underestimated the bond energy of $CH_{3,ad}$ by 34 kJ/mol but overestimated the bond energy of CH_{ad} by only 17 kJ/mol.

From the measured enthalpy of formation of adsorbed methyl and methylidyne the enthalpy of reaction of methane dehydrogenation on Pt(111) was calculated, giving an enthalpy of reaction of adsorbed methane to methyl coadsorbed with a hydrogen adatom (reaction (10)) of +1 kJ/mol, almost thermo-neutral. The reaction enthalpy for further dehydrogenation of adsorbed methyl to methylidyne coadsorbed with two hydrogen adatoms (reaction (11)) was found to be uphill by +23 kJ/mol.

4.6 Figures

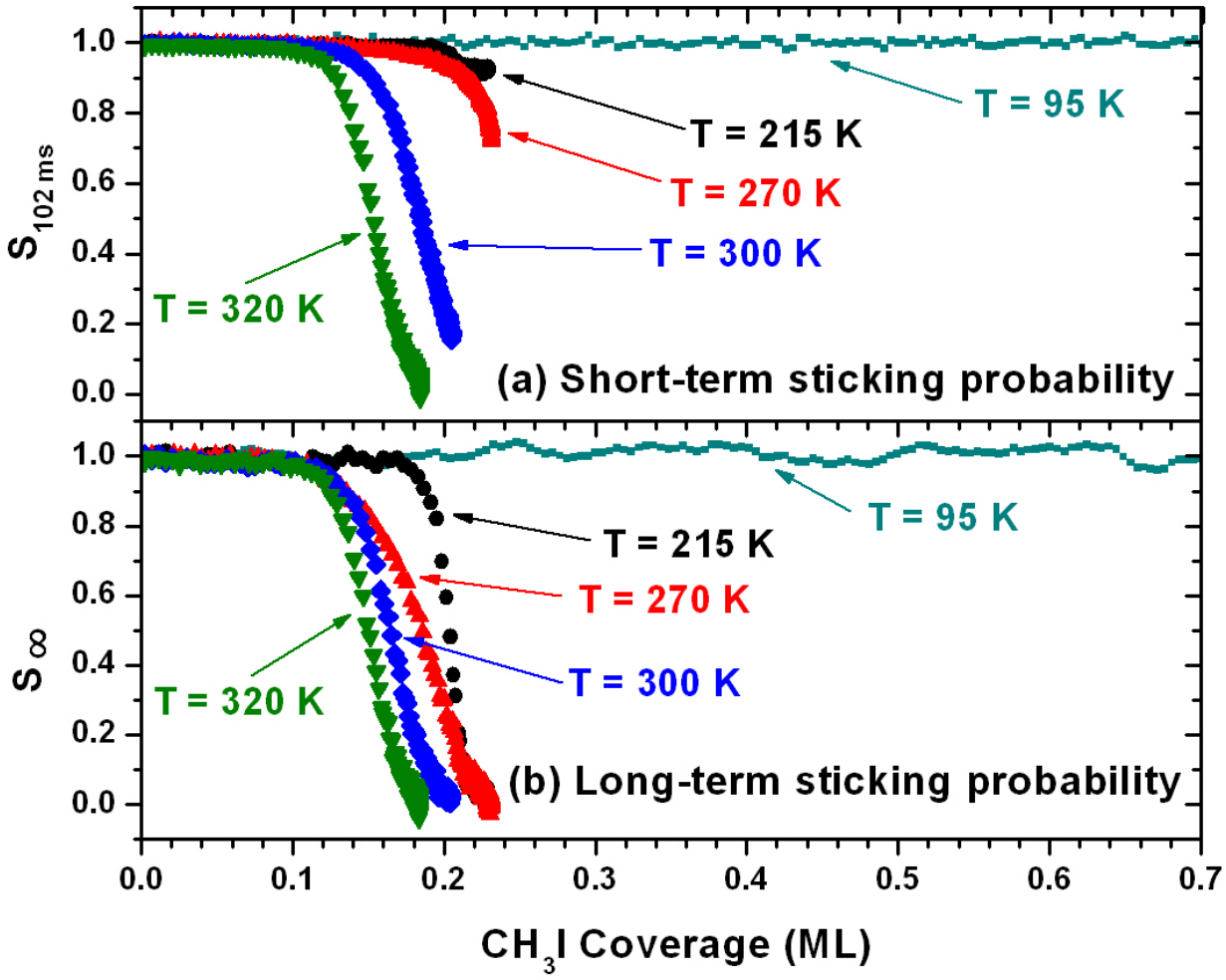

Figure 4.1: The average short term (a) and long-term (b) sticking probability of CH_3I on Pt(111) at 95 K (squares), 215 K (circles), 270 K (triangles), 300 K (diamonds), and 320 K (inverted triangles). The long-term sticking probability at 95 K has been smoothed with a 7-point moving average for presentational purposes.

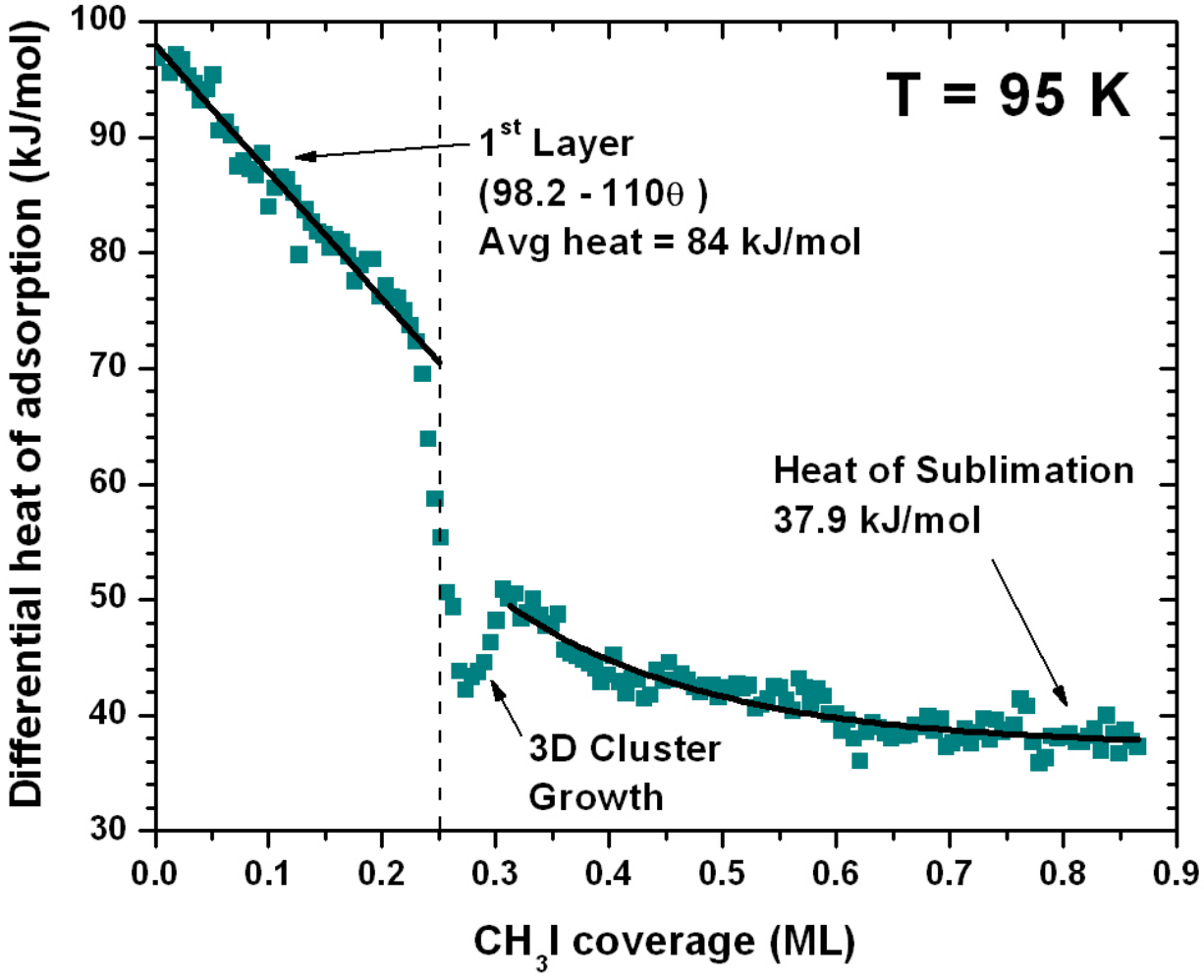

Figure 4.2: Differential heat of adsorption of CH_3I on Pt(111) at 95 K as a function of coverage. Each data point represents a pulse of 0.004 ML of CH_3I gas and is the result of averaging five experimental runs. At low coverages ($\theta < 0.25$ ML), CH_3I adsorbs molecularly to the Pt(111) surface, and the heat of adsorption exhibits large changes as the coverage increases. At high coverages ($\theta > 0.65$ ML) additional pulses of CH_3I adsorb onto solid CH_3I, and the average heat of adsorption becomes constant at 37.9±2.0 kJ/mol, in agreement with bulk values for the heat of sublimation.

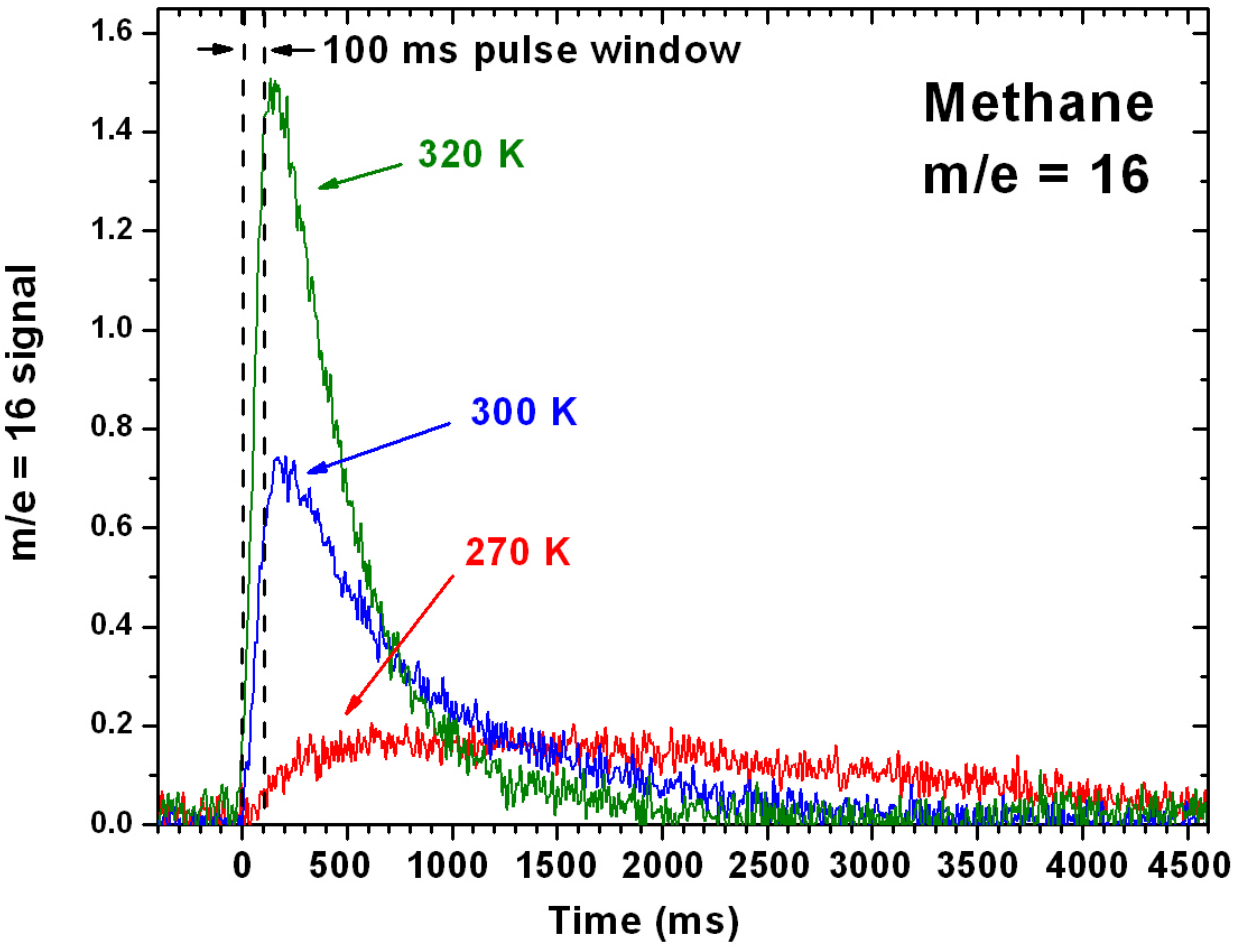

Figure 4.3: The average lineshape of the methane (m/e = 16) mass spectrometer signal for all pulses in the total methyl iodide coverage range from 0.04 to 0.11 ML (region 2) for different temperatures. The dashed lines at 0 and 100 ms define the time window of our heat measurements at 320 K, where the dose of CH_3I begins at 0 ms and ends at 100 ms. Longer heat measurement times are used at 270-300 K (see text in chapter 3).

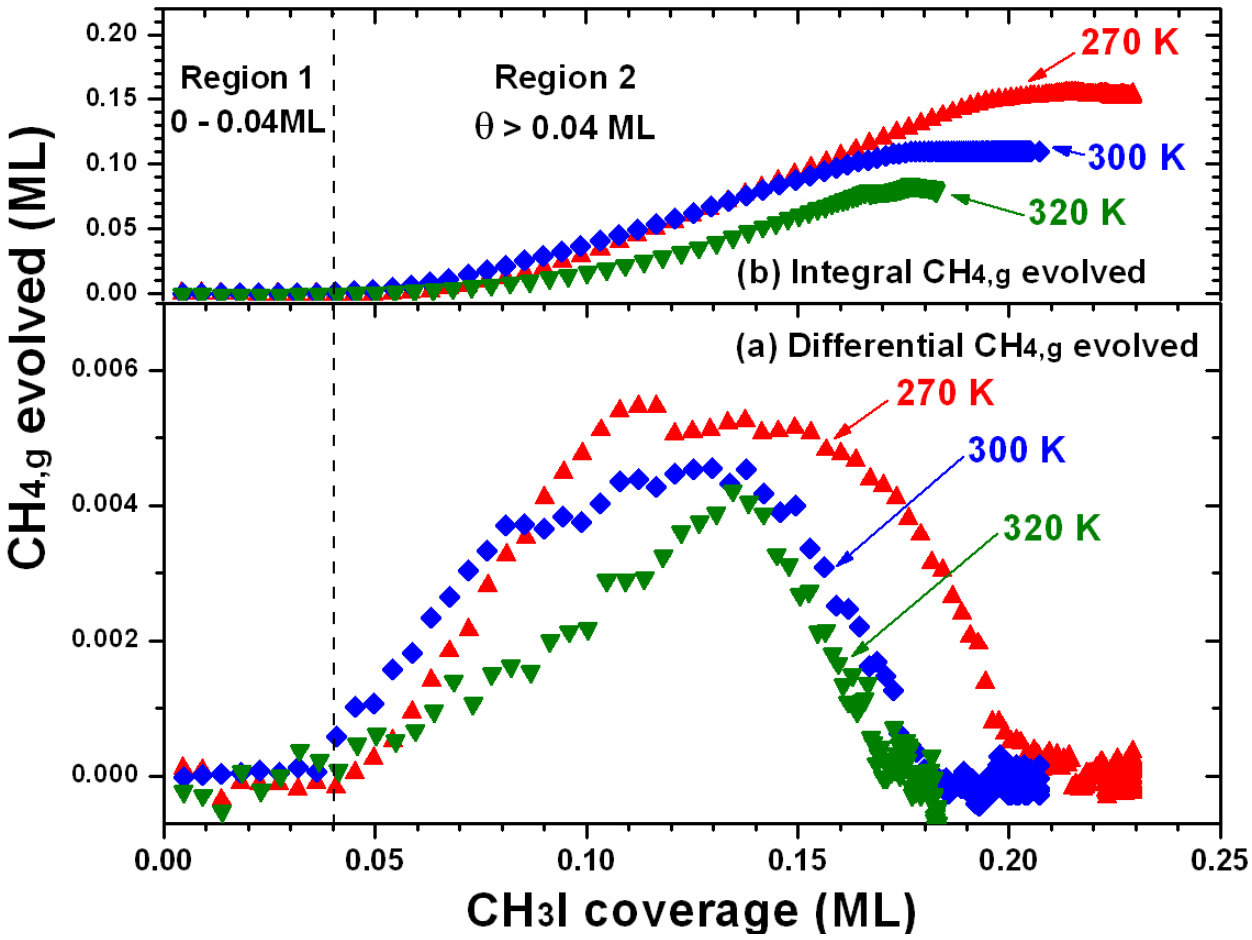

Figure 4.4: (a) The differential amount of methane gas evolve after each dose of CH_3I_g as a function of coverage for 270 K, 300 K, and 320 K and (b) The total integrated amount of methane gas evolved as a function of CH_3I coverage. Two distinct regions are present: region 1 (0 to 0.04 ML) where no methane is evolved, and region 2 (> 0.04 ML) where methane evolves in increasing and then decreasing amounts.

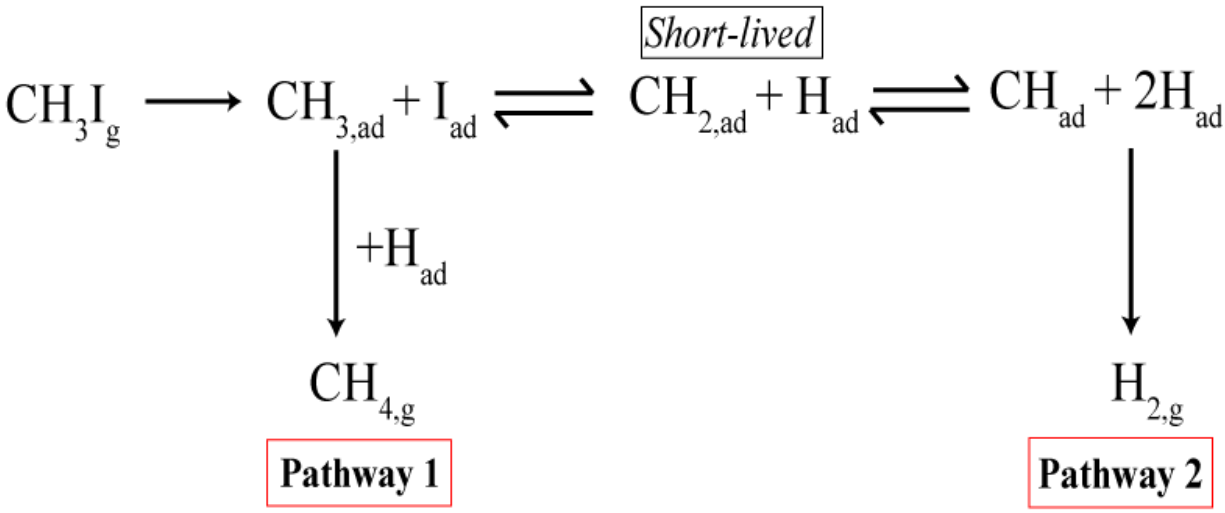

Figure 4.5: Reaction pathways of CH_3I decomposition on Pt(111), emphasizing the competing pathways by which H_{ad} can be eliminated. Pathway 2 is negligibly slow at 270 K, but starts competing with Pathway 1 at 300 K and above. As outlined in the Discussion section, adsorbed methyl is in rapid equilibrium with the CH_{ad} and $2H_{ad}$ species on the right at 270-320 K, but the equilibrium constant for this reaction is very small, so that methyl is heavily favored initially. However, at higher coverages H adatoms are eliminated from the surface via pathways (1) and (2), which forces the equilibrium to the right, ultimately leaving only CH_{ad} and I_{ad} on the surface.

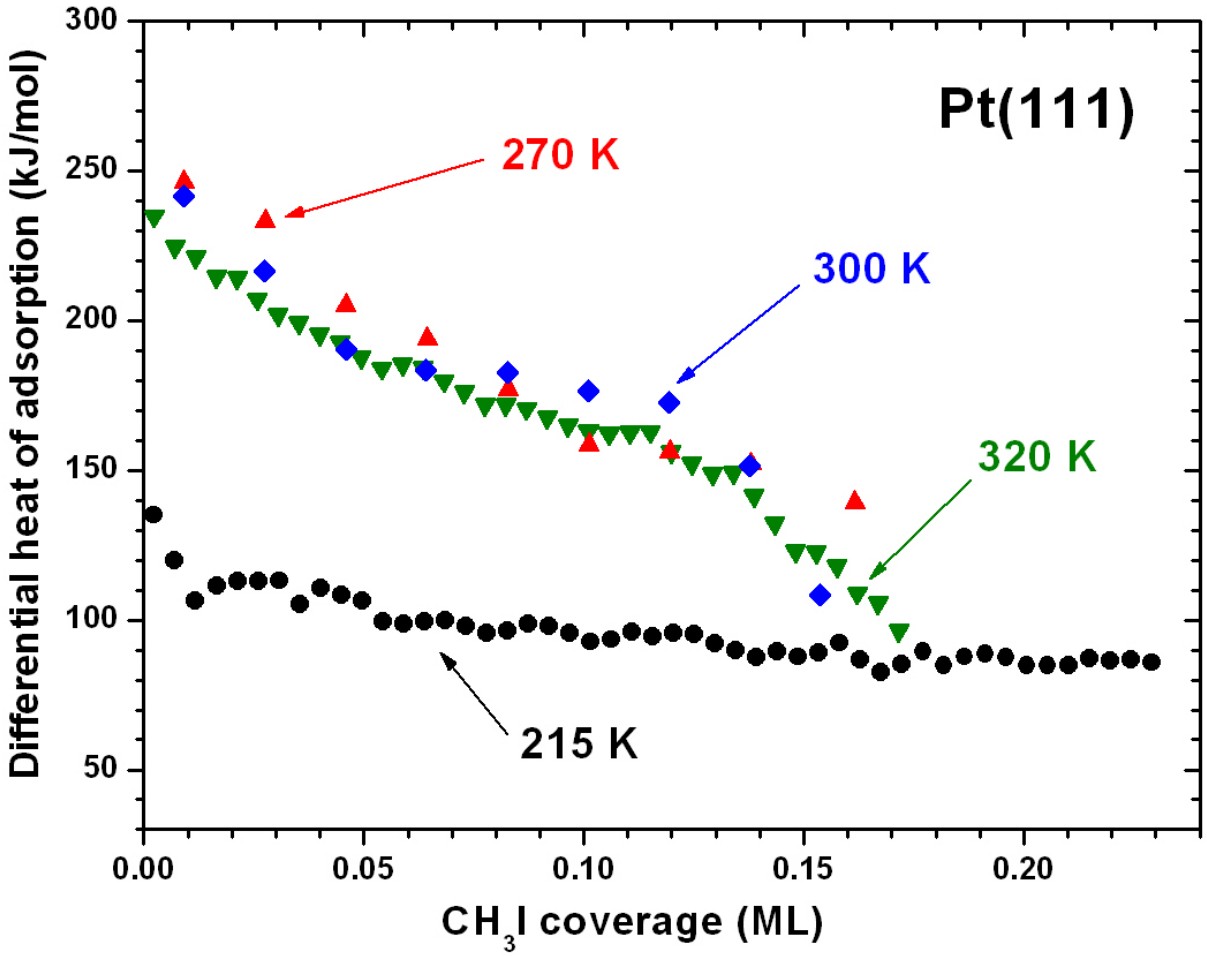

Figure 4.6: Differential heat of adsorption of CH_3I on Pt(111) versus coverage in the temperature range 215 - 320 K. The data points at 215 K and 320 K represent a pulse of ~0.004 ML of CH_3I gas and are the results of averaging five experimental runs. As described in the text, the data at 270 K and 300 K have been corrected for a broadened lineshape that resulted from slow reaction kinetics depositing heat on a timescale longer than the window of the molecular beam pulse.

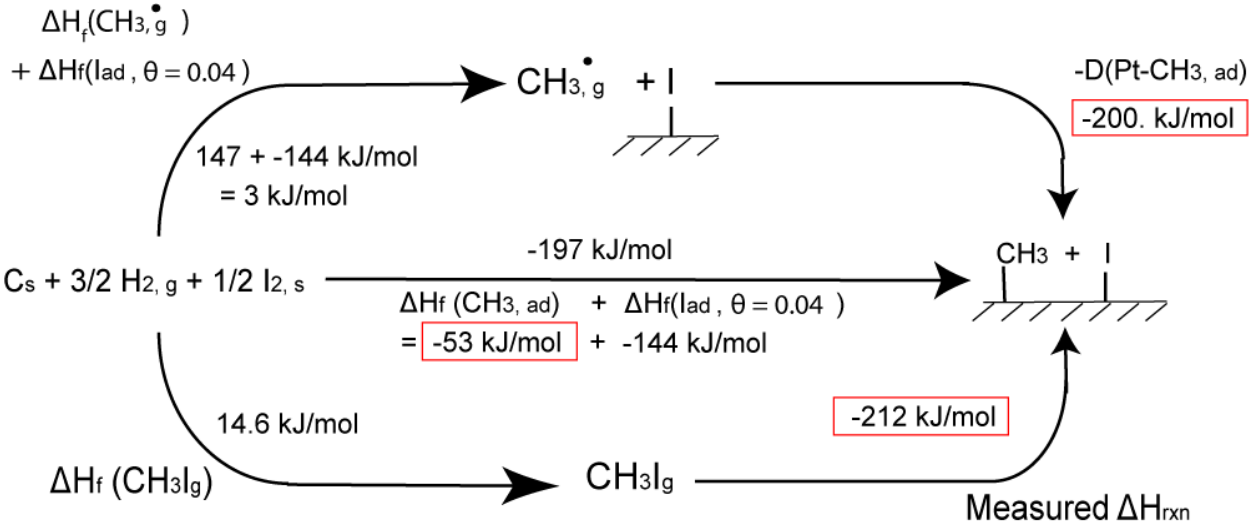

Figure 4.7: The thermodynamic cycle used in calculating the bond energy and heat of formation of adsorbed methyl to the Pt(111) surface. Here the -212 kJ/mol is the integral enthalpy of reaction for $CH_3I \rightarrow CH_{3,ad} + I_{ad}$ measured at 320 K in region 1 (i.e., for methyl and iodide coverages of 0.04 ML).

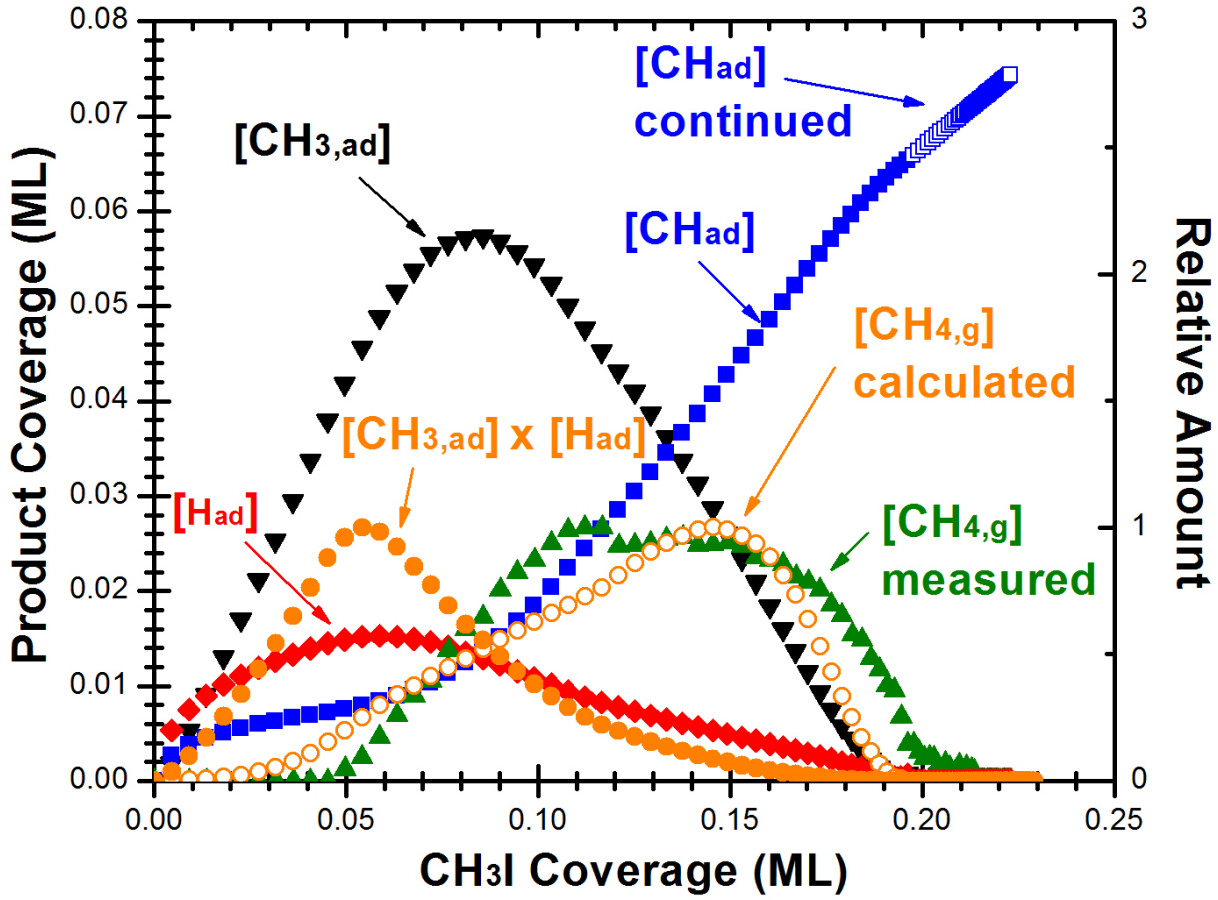

Figure 4.8: . Calculated coverages of $CH_{3,ad}$, H_{ad} and $CH_{ad,}$ assuming an equilibrium constant of $4x10^{-5}$ for reaction (3+5) and using the measured amount of methane evolved (also shown). Shown here is the product $[CH_3][H]$ and the rate of CH_4 evolution calculated form this product assuming that the rate constant k_4 has an activation energy that decreases linearly by 19 kJ/mol as coverage increase across this plot. Above the methyl iodide coverage where the methyl coverage drops to nearly zero (0.19 ML), the measured amounts of methane evolved and methyl iodide adsorbed become so small compared to the noise that the calculation of coverages became mathematically degenerate. However, since there is no more methyl to consume at these higher coverages, we know that the net stoichiometry at each pulse must be that given by reaction (6), so we analytically continued the coverage of CH_{ad} above there by assuming a slope of 1/3 as predicted by this stoichiometry (open squares).

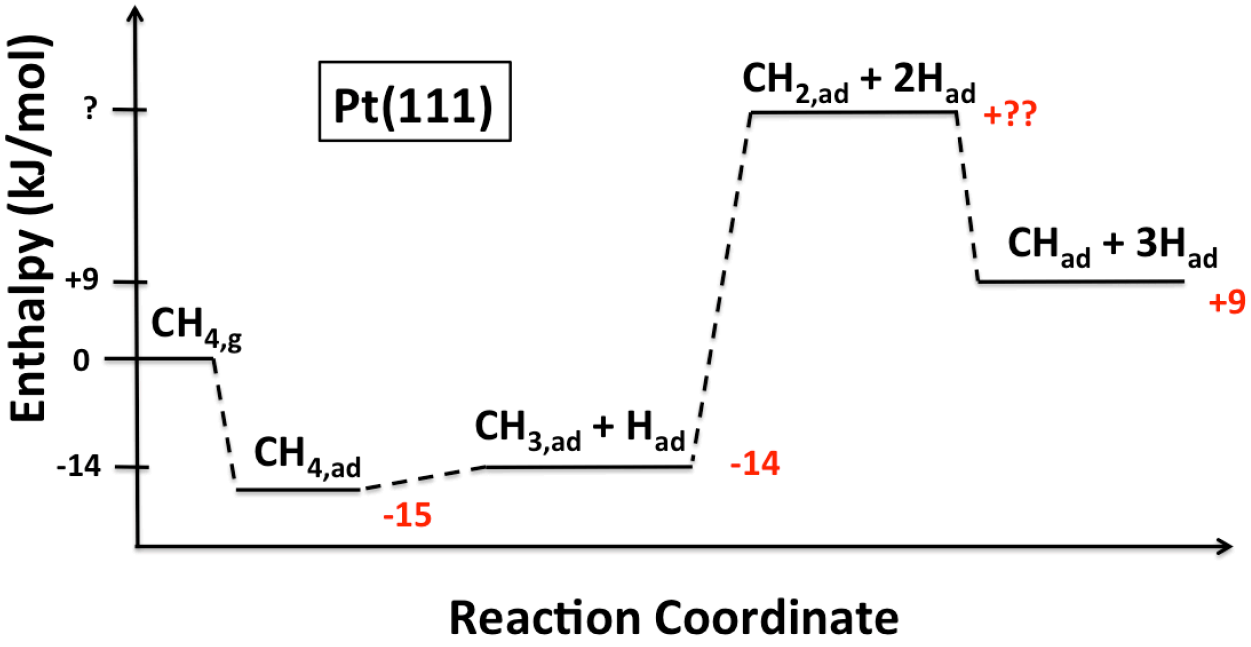

Figure 4.9: . Reaction enthalpy landscape for three steps of methane dehydrogenation on Pt(111) calculated from the heats of formation of methyl fragments measured in this work and referenced to methane gas. The enthalpy change taking methane gas to adsorbed methyl plus a hydrogen adatom is downhill in energy by 14 kJ/mol. The further dehrydrogenation of methane gas to CH_{ad} + 3 H_{ad} is found to be uphill in energy by +9 kJ/mol. Note here that the enthalpy for dehydrogenation of methane gas to to $CH_{2,ad}$ and 2 hydrogen adatoms is unknown, but is shown here higher than CH_{ad} + $3H_{ad}$ since methylene is known to decompose at low temperatures (~130 K) to CH_{ad} + H_{ad}.

Chapter 5

The energetics of oxygen adatoms, hydroxyl species and water dissociation on Pt(111)

Calorimetric measurements of the adsorption enthalpy of $O_{2,g}$ to make 2 O_{ad} on Pt(111) were performed by Fiorin et al..[93] However, we show that they used a calibration value for the optical reflectivity of Pt(111) that was incorrectly reported in the literature. This error in reflectivity led to a 40% error in the adsorption energies originally reported. We use our more accurate reflectivity of 76% to recalibrate their oxygen adsorption enthalpy data and show that it gives nearly identical results below 0.15 ML to the heats of adsorption determined from the temperature programmed desorption (TPD) experiments of two separate groups[51-52]. Differences arise above 0.15 ML, but we attribute these to the very low sticking probability of $O_{2,g}$ on Pt(111) (< 0.05) above 0.15ML, which can lead to large errors in the adsorption energies measured by calorimetry. Given this, we propose that the most reliable values for the adsorption enthalpy of oxygen on Pt(111) up to ¼ ML are those derived from TPD experiments, rather than the more recent calorimetry data. The best values are well described by (-217+151θ) kJ/mol O_2 below ¼ ML, where θ is the O_{ad} coverage in ML (where 1 ML is defined as 1 adsorbate per surface Pt atom). We also report calculations of coverage-dependent adsorption energies for oxygen on Pt(111) from density functional theory (DFT-RPBE) and find the results to be within ca. 20 kJ/mol of the integral heats measured by TPD. We further use these corrected adsorption enthalpies to amend the energetics of hydroxyl species on Pt(111) that we previously measured[35]. This gives revised values for the standard enthalpies of formation of the coadsorbed $(D_2O{-}OD)_{ad}$

complex of -511 ± 7 kJ/mol and a Pt-OD bond energy of 248 ± 7 kJ/mol for the OD species within this complex. DFT compares reasonably well, calculating an enthalpy of formation for the $(H_2O{-}OH)_{ad}$ complex of -456 kJ/mol and an O-Pt bond energy of 217 kJ/mol for the OH species within this complex. These revised values are used to estimate reaction enthalpies for the dissociation of adsorbed water and hydroxyl on Pt(111), and compared to DFT.

5.1 Introduction

Beautiful measurements of the adsorption enthalpy of $O_{2,g}$ to make 2 O_{ad} on Pt(111) were performed using single crystal adsorption calorimetry (SCAC) by Fiorin et al..[93] We show here that there was a calibration error in those measurements due to an incorrect value for the reflectivity of Pt(111) taken from the literature, which led to a 40% error in those adsorption enthalpies. We correct those adsorption enthalpies here, and show that, when corrected, they agree with TPD measurements by Campbell et al.[51] and Parker et al.[52] at low coverages, and differ only when the error in SCAC becomes large at high coverage due to the very low sticking probability. In our previous study of the heat of formation of adsorbed hydroxyl (OH_{ad}) on Pt(111) [35], it was produced by dosing water vapor to O_{ad}, and therefore the adsorption enthalpy of O_{ad} from Fiorin et al..[93] was used to extract the enthalpy of formation and Pt-O bond enthalpy for OH_{as}. Since that value for the adsorption enthalpy of O_{ad} is shown here to have a large error, we report here also corrections to our earlier values for the enthalpy of formation and Pt-O bond enthalpy for hydroxyl species on Pt(111), and use these values to estimate the reaction enthalpies for several reactions involving OH_{ad} on Pt(111). Finally, we compare all these enthalpies to new DFT calculations reported here, and to previous DFT calculations.

5.2 Experimental and Theoretical Methods

All experimental results presented here are from previous publications and cited as such. The experimental methods are outlined thoroughly in those citations. Here, we re-evaluate some of the energies and enthalpies presented in those papers as described in detail in the Results section below.

DFT calculations were performed using the GPAW code[94], and the RPBE functional[95] including zero-point energy (ZPE) corrections, with a grid spacing of 0.18 Å. Surfaces were modeled by four layers, where the two bottom layers were fixed to their bulk positions while the top two layers and the adsorbates were allowed to relax. A *k*-point sampling of 4x4x1, and 2x2x1 was used for slabs consisting of 2x2 and 3x3, and 4x4 and 6x6 Pt atoms in the x and y direction, respectively.

5.3 Results

The enthalpy of dissociative O_2 adsorption on Pt(111)

Beautiful SCAC measurements of the adsorption enthalpy of $O_{2,g}$ to make 2 O_{ad} on Pt(111) were performed by Fiorin et al..[93] However, Fischer-Wolfarth et al.[96] from Schauermann and Freund's group at the Fritz-Haber Institute, in collaboration with our group, have since uncovered a systematic error in the calorimetry measurements on Pt(111) by that group. The error originates from their use of an incorrect value for the optical reflectivity of Pt(111) at 633 nm in calibrating the heat signal. Fiorin et al. used a reflectivity of 66% for Pt(111), based on an incorrectly reported value listed in the Handbook of Chemistry and Physics (still present in the current version[97]), and in the original paper by Weaver [98] cited there, as an inset in the main graph. (This source of their value was learned through private communication with Dr. V.

Fiorin.) The main graph shows a value of 75% [98], almost identical to the value we measured (see below).

From integrating-sphere measurements, we found the reflectivity of Pt(111) to be 76%[37], very close to the value independently measured by Fischer-Wolfarth et al.[96] . If we use our more accurate reflectivity of 76% to recalibrate the oxygen adsorption enthalpy data originally reported by Fiorin et al., we obtain the corrected results versus coverage shown in Fig. 5.1. For comparison, we show the heat of adsorption as determined from activation energies for desorption of oxygen from Pt(111) measured in TPD experiments by two separate groups (Campbell et al.[51] and Parker et al.[52]) with nearly identical results. Here we assume that the activation barrier for adsorption is negligibly small (as indeed reported[52]), but add the required correction of ½ RT (where T is the desorption temperature) described elsewhere.[23] Note the near perfect agreement between the corrected calorimetric heats of adsorption and those determined by TPD below 0.15 ML. This same correction in reflectivity applied to the calorimetric heats of adsorption for CO on Pt(111) measured by that same group also led to near perfect agreement with our own more recent calorimetric measurements for CO on Pt(111) with Fischer-Wolfarth et al.[96] For O_2, the difference that arises above 0.15 ML in Fig. 5.1 is likely because the sticking probability of O_2 on Pt(111) drops rapidly to < 0.05 at ~0.15ML, making it very difficult to accurately measure adsorption energies by calorimetry. Given this, we propose that the most reliable values for the adsorption enthalpy of oxygen on Pt(111) are those presented in Fig. 5.1 derived from those TPD experiments[51,52] rather than the more recent calorimetry data, except below 0.15 ML where they agree after this calibration correction (but were approximately 40% too high as originally reported)[93].

We calculated oxygen adsorption enthalpies on Pt(111) for different coverages ranging from 1/36 to 1/2 monolayers (ML) using density functional theory (DFT), with O_{ad} always in 3-fold hollow sites and at the greatest possible O-O separations. The energy of gas-phase O_2, for which the RPBE functional performs poorly, was calculated using the DFT energies for H_2 and H_2O and the literature value for the reaction energy for 2 H_2 + O_2 → 2 H_2O, as described elsewhere[99]. Fig. 5.1 shows the integral enthalpies of adsorption for O_2 on Pt(111) by DFT. These calculated enthalpies of adsorption extrapolate to -237 kJ/mol in the low-coverage limit, but decrease with coverage to -217 kJ/mol at ¼ ML and -163 kJ/mol at ½ ML. (Note that the integral adsorption enthalpies oscillate slightly with coverage in the low coverage regime. The differential values presented here were calculated by the best-fit curve through these integral adsorption enthalpies, shown in Figure 5.1.) As seen, these heats are ~20 kJ/mol larger than the experimental heats by TPD below ¼ ML. Getman and Schneider[100] also calculated coverage-dependent adsorption energies for oxygen on Pt(111) using DFT. Their results were ~18 kJ/mol higher than our DFT results presented in Fig. 5.1 but otherwise produced a nearly identical trend in adsorption enthalpy vs. coverage. The small difference may be associated with differences in the details of the calculation method and/or ZPE corrections.

Using the corrected adsorption enthalpy for O_{ad} to revise the energetics of the $(H_2O\text{-}OH)_{ad}$ complex and related hydroxyl species on Pt(111)

In our previous study of the heat of reaction of D_2O with oxygen-dosed Pt(111), a thermodynamic cycle was constructed using measured reaction heats to calculate the standard heats of formation, ΔH^o_f, of the coadsorbed (D_2O-OD) complex and adsorbed OD, and from that the Pt(111)-OD bond enthalpy (Figure 5 within ref[35]). This cycle used a value of -266 kJ/mol for

the integral adsorption enthalpy of $O_{2,g}$ at 0.17 ML of O_{ad}, which was obtained from calorimetric measurements on Pt(111) from Fiorin et al.[93], but which we noted above included a calibration error. We now use these more reliable values from TPD in Fig. 5.1 to amend these standard enthalpies of formation of the coadsorbed (D_2O-OD) complex and adsorbed OD and the Pt(111)-OD bond enthalpy we reported in ref.[35]. Replacing the value of -266 kJ/mol for the integral adsorption enthalpy of $O_{2,g}$ at 0.17 ML of O_{ad} from the uncorrected calorimetry data of Fiorin et al. with the value of -204 kJ/mol from Fig. 5.1 based on TPD data, we obtain the improved values listed in Table 5.1, along with the original values reported in ref.[35] for comparison. The value for OD_{ad} within the (D_2O-OD) complex was estimated from ΔH^o_f for this complex, assuming that the D_2O in this complex has the same ΔH^o_f as the most stable structure of a pure D_2O adlayer, as originally done in ref.[35]. Table 5.1 also includes our calorimetric results for ΔH^o_f of D_2O_{ad} in its most stable (i.e., high-coverage) structure on Pt(111) (-301 ± 7 kJ/mol[28]).

These measurements report the energetics of deuterated hydroxyl and water, from which we can also calculate the energetics of the corresponding H isotope by correcting for the zero-point energy difference between Pt-OD and Pt-OH. Using known vibrational frequencies for H-H, D-D, O-H and O-D stretches[101] the zero-point reaction energy difference between H_2 + ½ O_2 → H_2O and D_2 + ½ O_2 → D_2O is 5.2 kJ/mol in the gas phase, resulting in a difference of 2.6 kJ/mol in the heat of formation for each OH bond in the products (with OH species being less stable than the corresponding OD species). This implies that the standard heats of formation of the coadsorbed (H_2O-OH) complex and adsorbed OH should be smaller than their D analogues by 7.8 and 2.6 kJ/mol, respectively. Values for these H isotope species calculated from the D isotope results using these zero-point corrections are also listed in Table 5.1.

Experimental values for isolated OH_{ad} and H_2O_{ad} are also listed in Table 5.1. These were estimated from the experimental values for their high-coverage structures described above, by correcting for the energy change with coverage estimated from the DFT values listed in Table 5.1 (see below). This was necessary since these species form islands of these high-coverage structures even at low coverage, so low local coverage is not experimentally accessible. Finally, Table 5.1 also includes a value for the hydrogen adatom, which was experimentally measured at low local coverage.

DFT estimates of the formation enthalpies of the $(H_2O\text{-}OH)_{ad}$ complex and hydroxyl species on Pt(111)

Table 5.1 also includes our DFT results for the heats of formation of the coadsorbed (H_2O-OH) complex, adsorbed H_2O and adsorbed OH on Pt(111). The results in Table 5.1 show that the $(H_2O{-}OH)_{ad}$ complex is ~47 kJ/mol less stable by DFT than in the experiment, but this error drops to only 20 kJ/mol after subtracting the enthalpy of adsorbed water to estimate the heat of formation of the OH_{ad} within this $(H_2O{-}OH)_{ad}$ complex. Note that our calculations of OH_{ad} in a water environment on Pt(111), using this same DFT method, were also found to be in good agreement with electrochemical measurements of the oxygen reduction reaction on Pt(111).[102,103] Our calculated DFT adsorption energy for high-coverage H_2O is for a √3 structure at 2/3 ML, which is known to give a DFT adsorption energy very close to that in the more complex, slightly higher-coverage (√39x√39)R16.1° structure[104]. This DFT value in Table 5.1 gives high-coverage H_2O_{ad} to be ~24 kJ/mol less stable than the experimental value.

Experimental values for "isolated" adsorbates could not be measured, but are available with DFT. To provide our best estimate of experimental values in the low-coverage limit, the

measured values for the high-coverage cases described above were corrected by adding the energy difference between this structure and the low-coverage limit as estimated by DFT, shown in parentheses in Table 5.1.

Estimates of O-Pt(111) bond enthalpies for surface O, OH and H_2O, and comparisons to DFT

Table 5.1 also lists the experimental and DFT values for the O-Pt(111) bond enthalpies for adsorbed O_{ad}, OH_{ad} and H_2O_{ad}, calculated from the difference between their heats of formation listed here and that for the corresponding gas-phase species. Bond enthalpies to Pt(111) are thus defined here to include all metal-adsorbate and adsorbate-adsorbate interaction energies. As seen, the O-Pt(111) bond enthalpy for OH_{ad} within $(H_2O{-}OH)_{ad}$ complex is ~31 kJ/mol weaker according to DFT than the experimental value of 248 kJ/mol; and that for H_2O_{ad} is ~21 kJ/mol weaker according to DFT than the experimental value of 51.3 kJ/mol. The difference is most likely due to small errors in calculating the binding of H_2O to the Pt(111) surface. Most of this interaction is due to van der Waals forces that are not described well by the functional used in this study. (When we instead used BEEF, a functional that is known to better describe van der Waals interactions[105] the binding energy of H_2O to the Pt(111) surface in the low coverage regime increases by 24 kJ/mol, much closer to experiment.)

Enthalpies for reactions involving surface hydroxyls on Pt(111)

The enthalpies of formation in Table 5.1 allow us to estimate reaction enthalpies (ΔH^o_{rxn}) for the following reactions involving surface hydroxyls on Pt(111):

$$H_2O_{ad} \rightarrow OH_{ad} + H_{ad} \qquad \Delta H^0_1 = 50 \text{ kJ/mol}, \qquad (1)$$

$OH_{ad} \rightarrow O_{ad} + H_{ad}$ $\Delta H^0_2 = 62$ kJ/mol, (2)

and

$2\ OH_{ad} \rightarrow O_{ad} + H_2O_{ad}$ $\Delta H^0_3 = 12$ kJ/mol. (3)

The values listed above were calculated using the experimental values of ΔH^o_f each adsorbate in its most stable structures, which for O_{ad} and H_{ad} are the low-coverage limits, but for H_2O_{ad} is its high-coverage structure and for OH_{ad} is in the $(H_2O{-}OH)_{ad}$ complex. These elementary steps have been proposed to take place in many important catalytic reactions over Pt. Note that Reactions (1) and (2) are rather endothermic, and therefore probably rather slow steps in these catalytic mechanisms.

Table 5.2 summarizes these reaction energies, and compares them to values based on DFT energies and values for the adsorbates in their low-coverage limit, estimated as described. The energy for Reaction (1) is accurately estimated with DFT, but Reaction (2) is less uphill by 27 kJ/mol, and Reaction (3) is estimated to be 14 kJ/mol exothermic by DFT, but 12 kJ/mol endothermic experimentally.

The reaction energies in Table 5.2 can also be compared to earlier DFT calculations by Mavrikakis's group, who found the following energies for Reactions (1) through (3) at 1/4ML coverage of 50 kJ/mol, 15 kJ/mol, and -36 kJ/mol, respectively.[106]

5.4 Conclusion

Corrected heats of O_2 adsorption on Pt(111) using the more accurate reflectivity of 76% are nearly identical to the heats of adsorption determined from TPD experiments below 0.15 ML.[51,52] These corrected adsorption enthalpies were used to amend the energetics of hydroxyl species on Pt(111) that we previously measured[35], giving revised values for the standard enthalpies of

formation of the coadsorbed (H_2O-OH) complex of -503 ± 7 kJ/mol. From this, we estimate a O-Pt(111) bond enthalpy in adsorbed hydroxyl of 248 ± 7 kJ/mol within this complex. This value is an upper bound, since it assumes that the H-bonding interactions between OH_{ad} and H_2O_{ad} are the same in the complex as in a pure H_2O adlayer, but the very fact that OH_{ad} and H_2O_{ad} combine into a stable 1:1 complex proves they are more stable in the complex. Using the difference in DFT values for the O-Pt(111) bond enthalpies for OH_{ad} of 217 kJ/mol within the (H_2O-OH) complex (estimated with this same assumption) and of 179 kJ/mol for isolated OH_{ad} to approximately correct this assumption gives an estimate of 210 ± 7 kJ/mol for the experimentally measured O-Pt(111) bond strength in isolated OH_{ad}. These revised values are used to estimate reaction enthalpies for the dissociation of adsorbed water and hydroxyl on Pt(111). The DFT value for water dissociation is in good agreement, but the DFT value for OH_{ad} dissociation is 27 kJ/mol less endothermic.

5.5 Figures

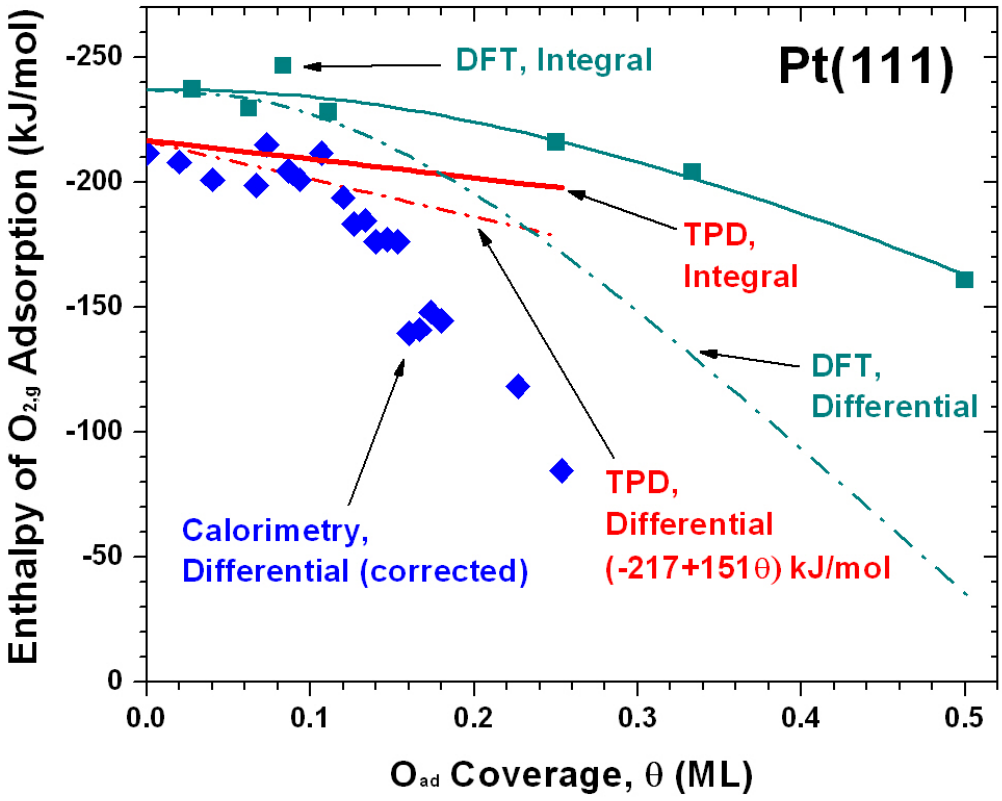

Figure 5.1: The enthalpy of $O_{2,g}$ adsorption on Pt(111) versus O_{ad} coverage measured by Fiorin et al. using single crystal adsorption calorimetry[93], after correction for an error in reflectivity as described in text (filled diamonds) compared to that determined from the TPD experiments of ref. [51] and [52] (dashed red line). We have averaged the TPD measurements of ref [51] and [52] and added ½ RT for direct comparison to adsorption enthalpies, as described in text, giving ΔH_{ads} = (-217+151θ) kJ/mol, where θ is the coverage. Also presented is the integral heat of adsorption calculated by DFT as a function of coverage (filled squares) and, for comparison, the integral heat of adsorption from TPD (solid line).

Table 5.1: Standard enthalpies of formation at 298 K (ΔH^o_f) of O adatoms, adsorbed hydroxyl and the coadsorbed hydroxyl-water complex (both D and H isotopes) on Pt(111) at the specified coverages, and the corresponding O-Pt(111) bond enthalpies calculated from the corrected enthalpy of O_2 adsorption (TPD-based data in Fig. 1) and the thermodynamic cycle of Figure 5 within ref.[35]. Numbers in italics are the original values reported in ref. [35] before correction (which in the case of O_{ad} corresponds to the uncorrected heats originally reported by Fiorin et al.[93]). Values for OD_{ad} and OH_{ad} were estimated from the values for the corresponding hydroxyl-water complex, assuming that the water in this complex has the same heat of formation as the most stable structure of a pure water adlayer, as describe in ref.[35]. Conversion of experimental enthalpies, which were all for the D isotope, to the H isotope used the known difference in zero-point energies, as described in text.

Adsorbate	Coverage (ML)	Experimental ΔH^o_f (kJ/mol)	O-Pt(111) Bond Enthalpy (kJ/mol)	DFT ΔH^o_f (kJ/mol)	DFT O-Pt(111) Bond Enthalpy (kJ/mol)
O_{ad}	0 ML	-109 ± 7 (*-150 ± 7*)	358 ± 7*	-119	362
	0.17 ML	-102 ± 7 (*-133 ± 7*)	351 ± 7*	-114	357
	0.25 ML	-99 ± 7 (*-125 ± 7*)	348 ± 7*	-109	352
$(D_2O{-}OD)_{ad}$	1/3 ML	-511 ± 7 (*-527 ± 7*)	-	-	-
$(H_2O{-}OH)_{ad}$	1/3 ML	-503 ± 7	-	-456	-
OD_{ad} within $(D_2O{-}OD)_{ad}$ complex	1/3 ML	-210 ± 7 (*-226 ± 7*)	248 ± 7 (*263 ± 7*)	-	-
OH_{ad} within $(H_2O{-}OH)_{ad}$ complex	1/3 ML	-207 ± 7	248 ± 7	-187	217**
OH_{ad} Isolated	1/16 ML	(-169± 7)***	(210± 7)***	-149	179**
D_2O_{ad} High Coverage	~2/3 ML	-301 ± 7	51.3 ± 7	-	-
H_2O_{ad} High Coverage	~2/3 ML	-293 ± 7	51.3± 7	-269	30
H_2O_{ad} Isolated	1/16 ML	(-273 ± 7)***	(31.3 ± 7)***	-249	10

H_{ad} Isolated	~1/16ML	-36	-	-33	-

* The bond enthalpies listed here for O_{ad} are the entire O-Pt(111) bond enthalpy, which sums the bonding to three Pt atoms since O_{ad} sits in a 3-fold hollow site.[107] We use here the known standard heat of formation of O_g of +249.2 ± 0.1 kJ/mol.[108] Bond enthalpies for adsorbed hydroxyl and water to Pt(111) are defined here to include all adsorbate-adsorbate interaction energies.

** This uses the DFT value for $\Delta H^o_f(OH_g)$ of 30.3 kJ/mol.(Experimental value = 39.0 kJ/mol[85].)

*** The experimental values for "isolated" adsorbates are written in parentheses here, since they were estimated by correcting the measured value for the high-coverage case by adding the energy difference between this and the low-coverage limit as estimated by DFT.

Table 5.2: Reaction enthalpies (ΔH^{o}_{rxn}) on Pt(111) for three reactions involving adsorbed OH, comparing experimental values with those estimated by DFT on Pt(111) terraces. These reaction enthalpies were calculated from the heats of formation of all the adsorbates in two situations with respect to surface coverage: in their lowest-coverage state and in their most stable situation, which for H_2O_{ad} corresponds to the high-coverage pure water adlayer and for OH_{ad} corresponds to its presence in the coadsorbed (H_2O-OH) complex, assuming that the water in this complex has the same heat of formation as in that most stable pure water adlayer. (Note that this "most stable" case is equivalent to replacing each OH_{ad} in each reaction as written below with $(H_2O\text{-}OH)_{ad}$, and adding an H_2O_{ad} to the other side of the reaction, which is a more rigorous way to represent these reaction in that case.) The experimental values were only determined in this "most stable" situation. The experimental low-coverage limits are written in parentheses here, since they were estimated by correcting this ΔH^{o}_{rxn} value for the most stable case by adding the difference in ΔH^{o}_{rxn} between this and the low-coverage limit as estimated by DFT.

Reaction	Coverage	Experimental ΔH_{rxn} (kJ/mol)	DFT ΔH_{rxn} (kJ/mol)
$H_2O_{ad} \rightarrow OH_{ad} + H_{ad}$	Low-Coverage Limits	(68)	67
	Most Stable Adsorbates	50	49
$OH_{ad} \rightarrow O_{ad} + H_{ad}$	Low Coverage Limits	(24)	-3
	Most Stable Adsorbates	62	35
$2OH_{ad} \rightarrow O_{ad} + H_2O_{ad}$	Low-Coverage Limits	(-44)	-70
	Most Stable Adsorbates	12	-14

Chapter 6

A Trend in the Bond Strengths of Adsorbates to the Pt(111) Surface

Understanding and predicting the functionality of catalytic materials is a major challenge in the fields of chemistry and chemical engineering. Such knowledge would allow more rapid development of the next generation of catalysts in chemical production and in renewable energy applications. Much work in computational chemistry, like Density Functional Theory (DFT), has been dedicated to developing trends from fundamental parameters to predict the catalytic activity of new materials. However, there are very few trends in fundamental parameters, especially for metal surfaces, developed from empirical data.

One of the key interactions related to the activity of a catalyst is the strength of bonding between organic molecules and metals. In organometallic chemistry, equilibria measurements yielded the bond energetics of many ligands to metal centers and these bond strengths have subsequently been compiled into a trend allowing the prediction of many other ligand to metal center bond strengths. This trend, discovered by Bryndza et. al.[25], shows that the strength with which a metal center bonds a ligand correlates linearly with a slope of ~1.0 with the corresponding gas-phase hydrogen-ligand bond strength (see Fig. 6.1). This relationship allows the bond strength of many other ligands to metal centers in organometallic complexes to be predicted simply by knowing the gas phase hydrogen-ligand bond strength, for which much data exists.

Using bond strengths of three oxygen-bound adsorbates to Pt(111), recently measured from Single Crystal Adsorption Calorimtery (SCAC) we show for the first time that this trend

also holds for metal surfaces, in this case Pt(111). Table 6.1 lists our calorimetrically measured Pt(111) to O bond strength and the corresponding gas phase hydrogen ligand bond enthalpy for methoxy ($-OCH_3$), monodentate formate (-O(O)CH), and deuterated hydroxyl (-OD). The measured Pt(111) to adsorbate bond enthalpy is plotted versus the corresponding hydrogen to ligand bond enthalpy in Figure 6.2, similarly to the work of Bryndza et. al., and a line with slope 1 is fit through these three measured points. The equation for this line is:

(Pt(111)-OR bond enthalpy) = (H-OR bond enthalpy) - 252 kJ/mol Eq.(1)

The excellent agreement of these measured points and the fitted line is remarkable. It is not too surprising that this trend is holding for adsorbates on metal surfaces, since a similar bonding situation arises as with ligands bound to metal centers in organometallic complexes. Here these measured adsorbates are bound through a single bond to atop sites on the Pt(111) surface. This is a similar bonding picture to a ligand bound with a single bond to a metal center in an organometallic complex, thus the observation of this trend for these adsorbates on Pt(111) is not completely unexpected.

The fitted line in Figure 6.2 does allow the bond enthalpy of several other oxygen bound adsorbates to be predicted from their known bond enthalpies to H. Table 6.2 lists the predicted bond enthalpy of several larger alkoxy species and the hydroperoxy species to the Pt(111) surface are listed along with their corresponding known gas-phase hydrogen-ligand bond strengths, and their heats of formation.

From these values, insight can be gained into the thermodynamics of potential chemical pathways on Pt(111). Of particular importance in proposed pathways for electrochemical and photocatalytic water splitting on Pt-based catalysts is the hydroperoxy species, whose energetics on Pt(111) are predicted from this trend. Note that the predicted bond enthalpy of OOH_{ad} to

Pt(111) is 104 kJ/mol, close to what has been calculated from DFT (99.7 kJ/mol)[109]. This adsorbate has relevance in PEM fuel cells where the oxygen reduction reaction occurs over a Pt based catalyst, but during this reaction hydrogen peroxide is formed as an unwanted byproduct that degrades the polymer membrane. Two chemical pathways have been proposed involving the hydroperoxy intermediate (reactions (1) and (2) below) whose reaction enthalpies can be calculated on Pt(111) from the empirical heats of formation of OH_{ad}[35,36] O_{ad} [36] and the predicted OOH_{ad} energetics in Table 6.2:

$$OH_{ad} + O_{ad} \rightarrow OOH_{ad} \qquad \Delta H_{rxn\,1}{}^{0} = +212 \text{ kJ/mol} \qquad (1)$$

$$O_{2,g} + H_{ad} \rightarrow OOH_{ad} \qquad \Delta H_{rxn\,2}{}^{0} = -68 \text{ kJ/mol} \qquad (2)$$

From the reaction energies associated with reactions (1) and (2) it is clear that the most energetically favorable route to form OOH_{ad} is through reaction (2), or the insertion of $O_{2,g}$ into an adsorbed hydrogen adatom on Pt(111) to form the OOH_{ad} species. A spectroscopic study by MacNaughton et. al.[110] seems to be consistent with the thermodynamics of the above reactions finding that H_{ad} promotes the formation of the OOH_{ad} species.

Another interesting insight from these reaction enthalpies comes from the inverse of reaction (1), or the decomposition of an OOH_{ad} to OH_{ad} and O_{ad}, shown as reaction (3) below:

$$OOH_{ad} \rightarrow O_{ad} + OH_{ad} \qquad \Delta H_{rxn\,3}{}^{0} = -212 \text{ kJ/mol} \qquad (3)$$

Taking the sum of reactions (2) and (3) yields a downhill in energy pathway (by -280 kJ/mol) for $O_{2,g}$ to produce O_{ad}. This reaction energy of -280 kJ/mol is consistent with using the heats of

formation of OH_{ad}, O_{ad}, and H_{ad} reported in Chapter 5 (See table 5.1) thus providing an internal consistency check for the reaction energies reported here.

From the thermodynamic insight gained in the above reaction pathways and the values in Table 6.2, one can certainly see the value in this relationship and it is very likely that this trend also holds for adsorbates species that are bound to the surface through other atoms like carbon. However, because Pt tends to bond to carbon more strongly than oxygen it may be that this line with slope one is shifted up (i.e larger intercept) than the line for these oxygen bound species. On other metal surfaces that are more oxophilic, like copper, it is likely that the oxygen line may shift up significantly.

There are unfortunately some limitations to the predictive ability of this trend. For adsorbates that form multiple bonds to the surface (like bidentate formate[111] or methylidyne[32]) this trend does not hold, because the x-axis value in Figure 6.1 no longer applies. Additionally, it is unlikely that this relationship can predict the energetics of large molecules that have strong van der waals interactions with the surface, since this trend is really only predicting the chemical bond between one atom on the adsorbate and the surface.

Still the excellent agreement here for these oxygen bound species on Pt(111) is promising and certainly yields insight into the energetics of many adsorbates and surface reactions, but more calorimetric data of adsorbates on single crystal surface must be collected to draw these trends for other metals.

Table 6.1: Calorimetrically measured heat of formation and bond strengths of three oxygen-bound adsorbates on Pt(111) and the corresponding gas-phase H—OR bond strengths.

Adsorbate	Measured Pt(111)—OR Bond Enthalpy (kJ/mol)	Known H—OR Bond Enthalpy (kJ/mol)	ΔH_f^0 (kJ/mol)
OD	248 ± 7 [35,36]	500. [112]	-210 ± 7 [36]
O(O)CH	224 ± 16 [111]	469 ± 12.6 [113]	-353 ± 10 [111]
OCH_3	187 ± 11 [114]	440 [112]	-170 ± 10 [114]

Table 6.2: Bond strengths and heats of formation of several oxygen-bound adsorbates on Pt(111), as predicted from Eq. (1) and their known bond enthalpies to H in the gas phase. For $\Delta H_f^0(OOH_{ad})$, the heat of formation of the OOH gas-phase radical (+2.09 kJ/mol[85]) was added to the negative of the predicted bond enthalpy.

Adsorbate	Predicted Pt(111)—OR Bond Enthalpy (kJ/mol)	Known H—OR Bond Enthalpy (kJ/mol)	ΔH_f^0 (kJ/mol)
tButoxy	193	445 [115]	-279
ethoxy	184	436 [112]	-200
propoxy	181	433 [112]	-222
butoxy	179	431 [112]	-243
OOH (hydroperoxy)	104	356 [85]	-102

6.1 Figures

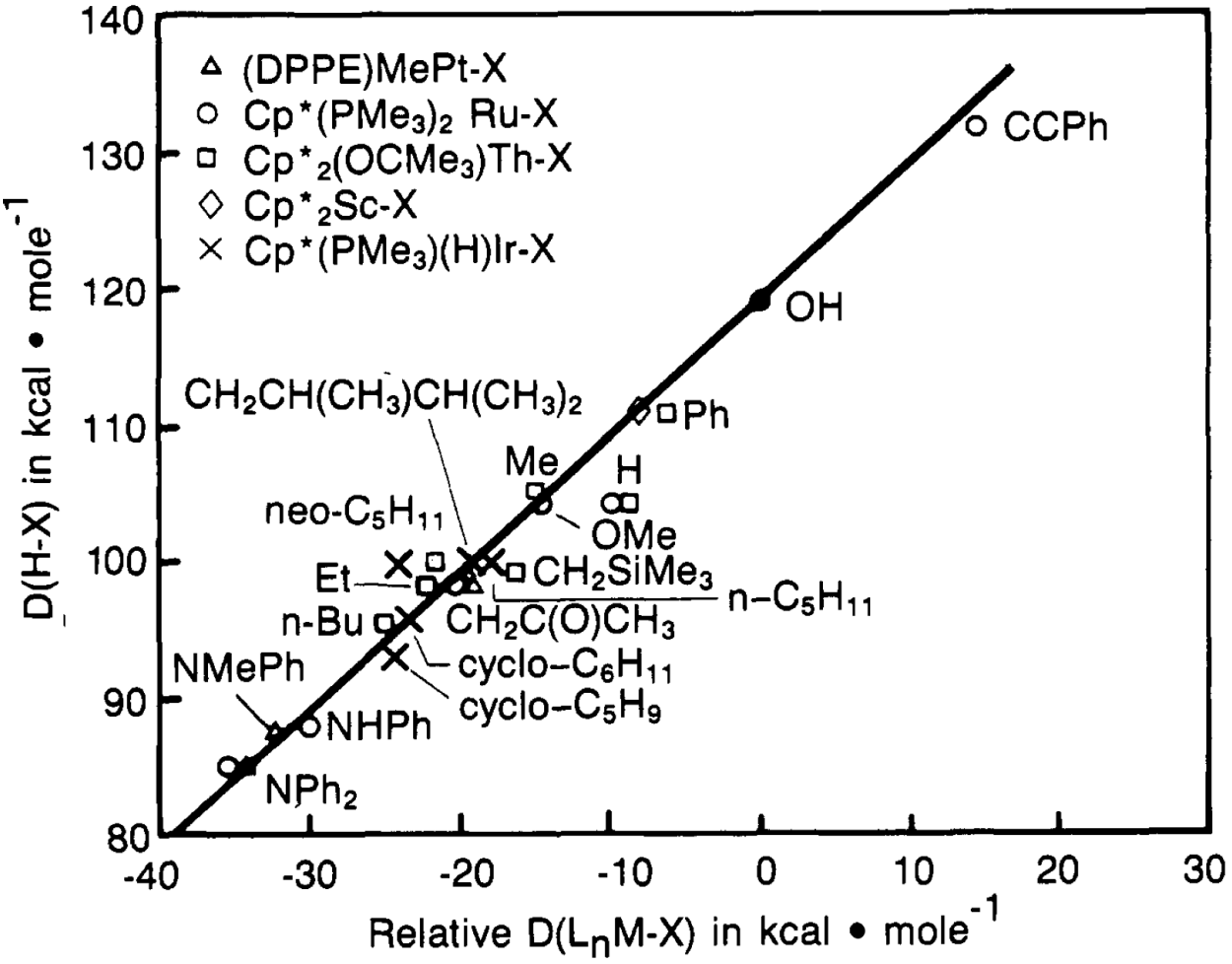

Figure 6.1: Cumulative plot of H-X vs. relative L,M-X bond strengths discussed in ref. [25]. Good 1:1 correlation of H-X and L_nM-X bond strengths is noted. (Figure taken with permission from ref. [25])

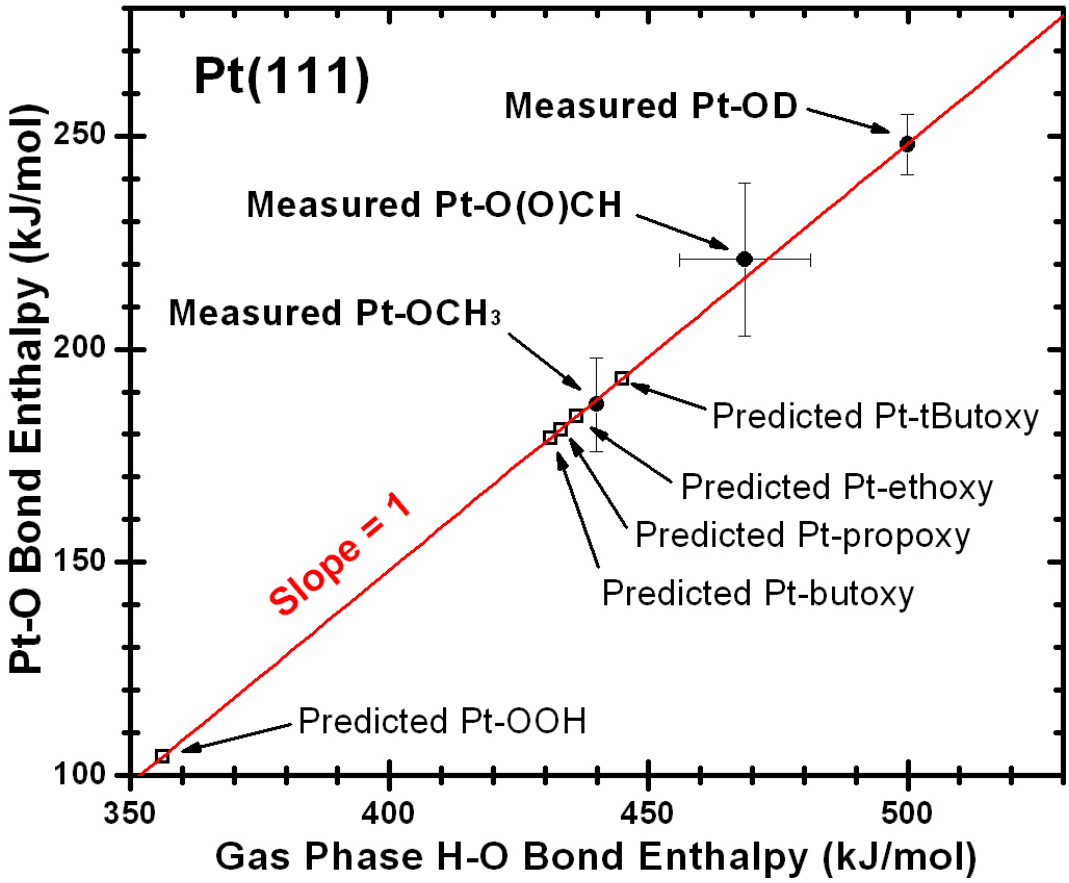

Figure 6.2: The calorimetrically measured bond strength of three oxygen bound adsorbates (hydroxyl, methoxy, and monodentate formate) to Pt(111) (filled circles) versus their corresponding gas phase hydrogen-OR bond strengths. A line with slope equal to 1 is fit through these three points showing that these measured adsorbates fall on this line. This allows the prediction of the bond strength of other important oxygen bound adsorbates on Pt(111) that have not or cannot be measured (open squares), such as other alkoxies and the hydroperoxy adsorbate. The error bars on the measured points represent the 95% confidence interval on each measurement.

Chapter 7 Conclusion

Single Crystal Adsorption Calorimetry (SCAC) is a powerful technique for measuring the energetics of well-defined adsorbates on metal surfaces. The work presented in this dissertation has yielded the bond strengths and heats of formation of $CH_{3,ad}$, CH_{ad}, CH_3O_{ad}, H_2O_{ad}, and OH_{ad} on Pt(111), which are all key chemical intermediates in many industrially important reactions on Pt based catalysts. These results are summarized in Table 7.1 below.

Table 7.1: Compilation of the thermodynamic parameters (ΔH_f^0 and bond enthalpy) of several adsorbates on Pt(111) measured from the SCAC work presented in this dissertation.

Adsorbate	ΔH_f^o (kJ/mol)	Bond Enthalpy (kJ/mol)
O_{ad} (0 ML)	-109 ± 7	358 ± 7
OH_{ad} (isolated)	-169 ± 7	210 ± 7
OH_{ad} within $(H_2O{-}OH)_{ad}$ complex	-207 ± 7	248 ± 7
H_2O_{ad}	-293 ± 7	51.3 ± 7
$OCH_{3,ad}$	-170 ± 10	187 ± 11
OOH_{ad}*	-102	104
$CH_{3,ad}$	-53	200.
CH_{ad}	+42	552

*Predicted from the trend developed in Chapter 6.

The values obtained through this work will serve as vital benchmarks for comparison to theory, thus facilitating the improvement of theoretical methods, like Density Functional Theory, that routinely calculate adsorbate energetics to predict the energetics of reaction pathways for developing new catalytic materials. In Table 7.2 the measured bond enthalpies of these adsorbates in Table 7.1 are compared to DFT calculations available for each adsorbate.

Table 7.2: The bond energies of the adsorbates measured from SCAC on Pt(111) are compared to the most accurate DFT calculations available in the literature. The bond energy for each measured value was found by subtracting RT from the bond enthalpy in table 6.1.

Adsorbate	Measured Bond Energy (kJ/mol)	DFT Bond Energy (kJ/mol)	Calculation Details
O_{ad} (0 ML)	358 ± 7	362	0 ML coverage RPBE functional
OH_{ad} (isolated)	210 ± 7	179	RPBE functional
OH_{ad} within $(H_2O{-}OH)_{ad}$ complex	248 ± 7	217	1/3 ML coverage RPBE functional[36]
H_2O_{ad}	51.3 ± 7	30	2/3 ML coverage RPBE functional[36]
HOC_3H_{ad}	58.6 ± 2.2	43.2	¼ ML Coverage PW-91 Functional[58]
$OCH_{3,ad}$	186 ± 11	161	¼ ML Coverage PW-91 Functional[58]
OOH_{ad}*	104	99.7	35 Pt atom cluster B3YLP Functional[109]
$CH_{3,ad}$	197.	197	¼ ML Coverage PW-91 Functional[91]
CH_{ad}	550	569	¼ ML Coverage RPBE Functional[91]

In Table 7.2 the agreement between the measured bond energies and these DFT calculations are not that bad (within 14% on average). The worst case scenario is that of OH_{ad} within the $(H_2O\text{-}OH)_{ad}$ complex which is predicted by DFT to be 31 kJ/mol less stable than it is measured to be. However, it must be noted that the calculated DFT values in Table 7.2 are from different computational studies that gave the closest predictions to our measured bond energies. There are

many examples of similar calculations that even used the same functional for these same adsorbates to find values much different than those in Table 7.2. For example, a 10 Pt atom cluster calculation using the PW-91 functional found a bond energy for CH_{ad} of 728 kJ/mol (see Chapter 4, Table 4.2), which is 178 kJ/mol higher than measured. Here we find that some functionals are better at predicting certain adsorbate energies. For example, the PW-91 functional does an excellent job of calculating the binding energy of $CH_{3,ad}$, but the RPBE functional is much better for the CH adsorbate.

Another interesting observation from the results in Table 7.2 is that regardless of the functional used, the bond energy of adsorbates bound through an oxygen atom (H_2O_{ad}, HOC_3H_{ad}, OH_{ad}) are all underestimated by DFT. This could be related to the difficulty DFT methods have in treating oxygen, especially in the gas phase.

Finally, and most importantly, the differences observed between the measured bond energy and the calculated bond energy are <u>not</u> systematically different. Take, for example, the results of the DFT study in Ref. [58] which finds bond energies of 43.2 and 161 kJ/mol for adsorbed methanol and methoxy on Pt(111) respectively. The calculated adsorbed methanol bond energy is 15.4 kJ/mol less stable than measured and the calculated methoxy bond energy is 25 kJ/mol less stable than measured. These differences, while not too large, are clearly not systematic and this has adverse consequences when applying DFT to predicting reaction pathways on metal surfaces. For example, the reaction enthalpy for the combination of $2OH_{ad}$ to from adsorbed water and an oxygen adatom (from Chapter 5) is actually predicted to be exothermic from DFT while it is endothermic using measured values (shown below).

$$2OH_{ad} \rightarrow O_{ad} + H_2O_{ad} \qquad \Delta H_{rxn,\ measured} = +12 \text{ kJ/mol} \qquad \Delta H_{rxn,\ DFT} = -14 \text{ kJ/mol}$$

The reason for these large differences in reaction energies predicted from DFT come from the fact that each adsorbate's calculated binding energy has a non-systematic error associated with it and when the reaction energy is calculated (energy of products minus energy of reactants) these errors can compound to give a reaction energy that can be significantly different than what is measured experimentally.

A clear example of this issue comes from the computational studies of methanol decomposition on Pt(111) in references [55,56]. In Figure 7.1 (below) three possible reaction pathways for methanol decomposition to CO and hydrogen on Pt(111) are calculated from DFT using the PW-91 functional. Here the lowest energy pathway predicted is the abstraction of a hydrogen atom from the carbon atom of the bound methanol to form the carbon bound hydroxymethyl intermediate (blue pathway in Figure 7.1), and the other pathway that involves abstraction of the acidic proton to produce a methoxy intermediate (red pathway) is found to be less energetically favorable. This prediction of the lowest energy pathway does not reflect the observations seen in UHV conditions where the decomposition of methanol on Pt(111) is known to go through a methoxy intermediate[116]. The reasons for this could be that DFT seems to routinely underestimate the binding energy of oxygen bound adsorbates on Pt(111) (Table 7.2). Thus, these calculations routinely underestimate the stability of the oxygen bound methoxy and select the hydroxymethyl adsorbate to be more energetically favorable.

These results highlight the importance of using the data available from SCAC measurements to assess the performance of computational methods, and for their use as benchmarks for the improvement of these methods. Using this SCAC data to improve the accuracy of DFT will hopefully allow computational methods to accurately predict adsorption energetics, making them incredibly powerful tools for catalyst discovery and development.

However, more SCAC data must be collected not just for the improvement of DFT, but also to develop more fundamental trends in the strength with which adsorbates bind to metals surfaces (like the trend developed in Chapter 6). These types of trends can lead to enormous physical insight in the interaction between organics and metal surfaces, which is crucial information needed to develop the next generation of catalysts.

There are many possible directions for the future SCAC work. One direction is measuring the heat of adsorption of organic molecules on oxide surfaces (like ceria), which are notoriously difficult systems to handle with DFT. Another direction could be measuring the energetics of organic molecules on metal nanoparticle catalysts to measure how the size of nanoparticles affects the stability of bound organics, providing a crucial link between the structure / function relationship of metal supported catalysts. With these possible directions for the future work of SCAC it is hoped that the work presented in this dissertation, for several chemical intermediates on Pt(111), has provided important information for the improvement of computational methods and has provided an excellent starting point to extend the complexity of systems with which SCAC can be applied.

7.1 Figures

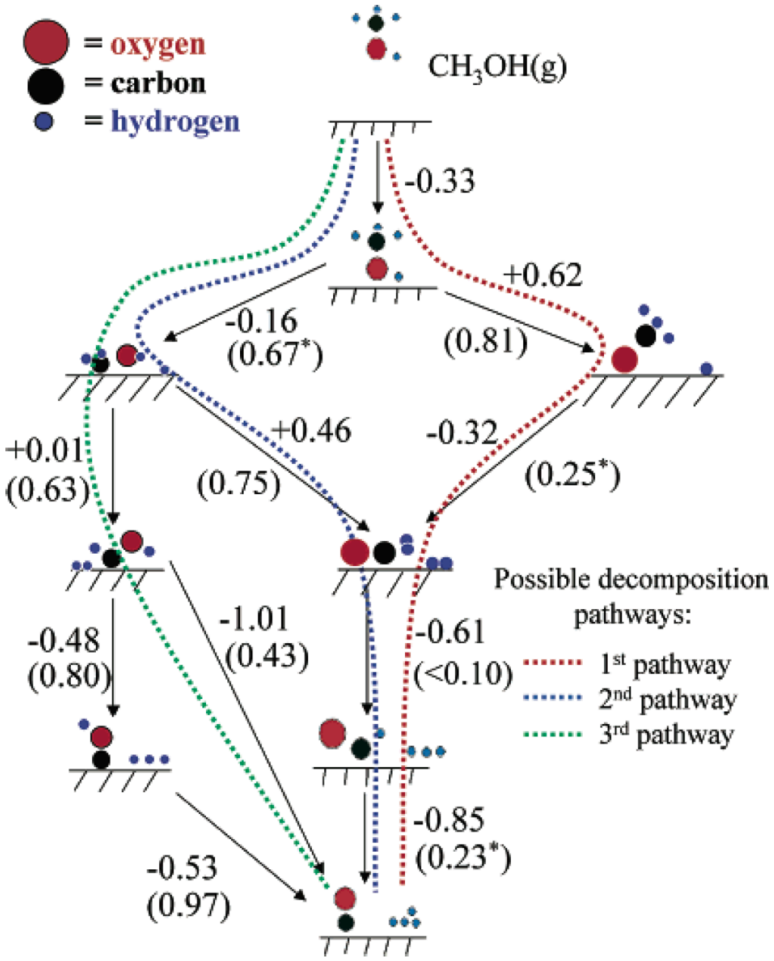

Figure 7.1: Schematic summary of the reaction network for methanol decomposition through C-H and O-H bond scission in methanol on Pt- (111). Values without parentheses are energy changes of the indicated elementary steps (negative values indicate exothermic steps). Values in parentheses are activation energy barriers. The energies do not include zero- point energy corrections. The dotted lines correspond to likely decomposition pathways for methanol, as indicated in the figure legend. Number is parenthesis are activation energy barriers (Figure and caption taken with permission from Reference [55])

References

(1) Hammer, B.; Norskov, J. K. *Surface Science* **1995**, *343*, 211.

(2) Hammer, B.; Norskov, J. K. *Advances in Catalysis, Vol 45: Impact of Surface Science on Catalysis* **2000**, *45*, 71.

(3) Greeley, J.; Norskov, J. K.; Mavrikakis, M. *Annual Review of Physical Chemistry* **2002**, *53*, 319.

(4) Norskov, J. K.; Bligaard, T.; Logadottir, A.; Bahn, S.; Hansen, L. B.; Bollinger, M.; Bengaard, H.; Hammer, B.; Sljivancanin, Z.; Mavrikakis, M.; Xu, Y.; Dahl, S.; Jacobsen, C. J. H. *Journal of Catalysis* **2002**, *209*, 275.

(5) Gokhale, A. A.; Kandoi, S.; Greeley, J. P.; Mavrikakis, M.; Dumesic, J. A. *Chemical Engineering Science* **2004**, *59*, 4679.

(6) Kandoi, S.; Greeley, J.; Sanchez-Castillo, M. A.; Evans, S. T.; Gokhale, A. A.; Dumesic, J. A.; Mavrikakis, M. *Topics in Catalysis* **2006**, *37*, 17.

(7) Brogan, M. S.; Cairns, J. A.; Dines, T. J.; Rochester, C. H. *Spectrochimica Acta Part a-Molecular and Biomolecular Spectroscopy* **1997**, *53*, 943.

(8) Evin, H. N.; Jacobs, G.; Ruiz-Martinez, J.; Graham, U. M.; Dozier, A.; Thomas, G.; Davis, B. H. *Catalysis Letters* **2008**, *122*, 9.

(9) Cao, C. D.; Hohn, K. L. *Applied Catalysis a-General* **2009**, *354*, 26.

(10) Jacobs, G.; Davis, B. H. *Applied Catalysis a-General* **2005**, *285*, 43.

(11) Sexton, B. A. *Surface Science* **1981**, *102*, 271.

(12) Sexton, B. A.; Rendulic, K. D.; Hughes, A. E. *Surface Science* **1982**, *121*, 181.

(13) Akhter, S.; White, J. M. *Surface Science* **1986**, *167*, 101.

(14) Peck, J. W.; Beck, D. E.; Mahon, D. I.; Koel, B. K. *Journal of Physical Chemistry B* **1998**, *102*, 3321.

(15) Peck, J. W.; Mahon, D. I.; Beck, D. E.; Bansenaur, B.; Koel, B. E. *Surface Science* **1998**, *410*, 214.

(16) McGee, K. C.; Driessen, M. D.; Grassian, V. H. *Journal of Catalysis* **1996**, *159*, 69.

(17) Zaera, F. *Accounts of Chemical Research* **1992**, *25*, 260.

(18) Deng, R. P.; Herceg, E.; Trenary, M. *Surface Science* **2004**, *573*, 310.

(19) Herceg, E.; Celio, H.; Trenary, M. *Review of Scientific Instruments* **2004**, *75*, 2545.

(20) Borronibird, C. E.; King, D. A. *Review of Scientific Instruments* **1991**, *62*, 2177.

(21) Borronibird, C. E.; Alsarraf, N.; Andersson, S.; King, D. A. *Chemical Physics Letters* **1991**, *183*, 516.

(22) Alsarraf, N.; Stuckless, J. T.; Wartnaby, C. E.; King, D. A. *Surface Science* **1993**, *283*, 427.

(23) Brown, W. A.; Kose, R.; King, D. A. *Chemical Reviews* **1998**, *98*, 797.

(24) Dixonwarren, S. J.; Kovar, M.; Wartnaby, C. E.; King, D. A. *Surface Science* **1994**, *307*, 16.

(25) Bryndza, H. E.; Fong, L. K.; Paciello, R. A.; Tam, W.; Bercaw, J. E. *Journal of the American Chemical Society* **1987**, *109*, 1444.

(26) Crowe, M. C.; Campbell, C. T. *Annual Review of Analytical Chemistry, Vol 4* **2011**, *4*, 41.

(27) Lew, W.; Lytken, O.; Farmer, J. A.; Crowe, M. C.; Campbell, C. T. *Review of Scientific Instruments* **2010**, *81*, 9.

(28) Lew, W. D.; Crowe, M. C.; Karp, E.; Campbell, C. T. *Journal of Physical Chemistry C* **2011**, *115*, 9164.

(29) Ajo, H. M.; Ihm, H.; Moilanen, D. E.; Campbell, C. T. *Review of Scientific Instruments* **2004**, *75*, 4471.

(30) Lytken, O.; Lew, W.; Harris, J. J. W.; Vestergaard, E. K.; Gottfried, J. M.; Campbell, C. T. *Journal of the American Chemical Society* **2008**, *130*, 10247.

(31) Stuckless, J. T.; Frei, N. A.; Campbell, C. T. *Sensors and Actuators B-Chemical* **2000**, *62*, 13.

(32) Karp, E. M.; Silbaugh, T. L.; Campbell, C. T. *unpublished results* **2012**.

(33) King, D. A.; Wells, M. G. *Surface Science* **1972**, *29*, 454.

(34) Gong, J.; Flaherty, D. W.; Ojifinni, R. A.; White, J. M.; Mullins, C. B. *Journal of Physical Chemistry C* **2008**, *112*, 5501.

(35) Lew, W.; Crowe, M. C.; Karp, E.; Lytken, O.; Farmer, J. A.; Arnadottir, L.; Schoenbaum, C.; Campbell, C. T. *Journal of Physical Chemistry C* **2011**, *115*, 11586.

(36) Karp, E. M.; Studt, F.; Abild-Pedersen, F.; Nørskov, J. K.; Campbell, C. T. *Submitted* **2012**.

(37) Ihm, H.; Ajo, H. M.; Gottfried, J. M.; Bera, P.; Campbell, C. T. *Journal of Physical Chemistry B* **2004**, *108*, 14627.

(38) Gottfried, J. M.; Vestergaard, E. K.; Bera, P.; Campbell, C. T. *Journal of Physical Chemistry B* **2006**, *110*, 17539.

(39) Ehlers, D. H.; Spitzer, A.; Luth, H. *Surface Science* **1985**, *160*, 57.

(40) Panja, C.; Saliba, N.; Koel, B. E. *Surface Science* **1998**, *395*, 248.

(41) Bondi, A. *Journal of Physical Chemistry* **1964**, *68*, 441.

(42) Lee, J.; Cowin, J. P.; Wharton, L. *Surface Science* **1983**, *130*, 1.

(43) Persson, B. N. J. *Surface Science* **1991**, *258*, 451.

(44) Lawton, T. J.; Carrasco, J.; Baber, A. E.; Michaelides, A.; Sykes, E. C. H. *Physical Review Letters* **2011**, *107*, 5.

(45) Lawton, T. J.; Carrasco, J.; Baber, A. E.; Michaelides, A.; Sykes, E. C. H. *Physical Chemistry Chemical Physics* **2012**.

(46) Carlson, H. G.; Westrum, E. F. *Journal of Chemical Physics* **1971**, *54*, 1464.

(47) Thermodynamics Research, C.; U.S. Dept. of Commerce, Technology Administration, National Institute of Standards and Technology: Boulder, CO, 1986.

(48) Tauer, K. J.; Lipscomb, W. N. *Acta Crystallographica* **1952**, *5*, 606.

(49) Green, S. D.; Bolina, A. S.; Chen, R.; Collings, M. P.; Brown, W. A.; McCoustra, M. R. S. *Monthly Notices of the Royal Astronomical Society* **2009**, *398*, 357.

(50) Gland, J. L.; Sexton, B. A.; Fisher, G. B. *Surface Science* **1980**, *95*, 587.

(51) Campbell, C. T.; Ertl, G.; Kuipers, H.; Segner, J. *Surface Science* **1981**, *107*, 220.

(52) Parker, D. H.; Bartram, M. E.; Koel, B. E. *Surface Science* **1989**, *217*, 489.
(53) Chao, J.; Rossini, F. D. *Journal of Chemical and Engineering Data* **1965**, *10*, 374.
(54) Tsang, W. *ChemInform* **1997**, *28*, no.
(55) Greeley, J.; Mavrikakis, M. *Journal of the American Chemical Society* **2002**, *124*, 7193.
(56) Greeley, J.; Mavrikakis, M. *Journal of the American Chemical Society* **2004**, *126*, 3910.
(57) Skoplyak, O.; Menning, C. A.; Barteau, M. A.; Chen, J. G. G. *Topics in Catalysis* **2008**, *51*, 49.
(58) Desai, S. K.; Neurock, M.; Kourtakis, K. *Journal of Physical Chemistry B* **2002**, *106*, 2559.
(59) Henderson, M. A.; Mitchell, G. E.; White, J. M. *Surface Science* **1987**, *184*, L325.
(60) Henderson, M. A.; Mitchell, G. E.; White, J. M. *Surface Science* **1991**, *248*, 279.
(61) Zaera, F.; Hoffmann, H. *Journal of Physical Chemistry* **1991**, *95*, 6297.
(62) Hugenschmidt, M. B.; Domagala, M. E.; Campbell, C. T. *Surface Science* **1992**, *275*, 121.
(63) French, C.; Harrison, I. *Surface Science* **1995**, *342*, 85.
(64) Panja, C.; Samano, E. C.; Saliba, N. A.; Koel, B. E. *Surface Science* **2004**, *553*, 39.
(65) Fairbrother, D. H.; Peng, X. D.; Viswanathan, R.; Stair, P. C.; Trenary, M.; Fan, J. *Surface Science* **1993**, *285*, L455.
(66) Jentz, D.; Peng, X. D.; Stair, P.; Trenary, M. *Abstracts of Papers of the American Chemical Society* **1994**, *207*, 22.
(67) Jentz, D.; Trenary, M.; Peng, X. D.; Stair, P. *Surface Science* **1995**, *341*, 282.
(68) Berlowitz, P.; Yang, B. L.; Butt, J. B.; Kung, H. H. *Surface Science* **1986**, *171*, 69.
(69) Fairbrother, D. H.; Peng, X. D.; Trenary, M.; Stair, P. C. *Journal of the Chemical Society-Faraday Transactions* **1995**, *91*, 3619.
(70) Zaera, F. *Surface Science* **1992**, *262*, 335.
(71) Zaera, F. *Catalysis Letters* **1991**, *11*, 95.
(72) Lew, W.; Lytken, O.; Farmer, J. A.; Crowe, M. C.; Campbell, C. T. *Review of Scientific Instruments* **2010**, *81*, 024102.
(73) Karp, E. M.; Silbaugh, T. L.; Crowe, M. C.; Campbell, C. T. *to be published* **2012**.
(74) Cox, J. D.; Pilcher, G. *Thermochemistry of organic and organometallic compounds*; Academic Press, 1970.
(75) Farmer, J. A.; Campbell, C. T. *Science* **2010**, *329*, 933.
(76) Wren, D. J.; Vikis, A. C. *Journal of Chemical Thermodynamics* **1982**, *14*, 435.
(77) Egan, C. J.; Kemp, J. D. *Journal of the American Chemical Society* **1938**, *60*, 2097.

(78) Paul, A.; Yang, M. X.; Bent, B. E. *Surface Science* **1993**, *297*, 327.
(79) Wu, G.; Stacchiola, D.; Collins, M.; Tysoe, W. T. *Surface Review and Letters* **2001**, *8*, 303.
(80) Lin, J. L.; Bent, B. E. *Journal of Physical Chemistry* **1993**, *97*, 9713.
(81) Silbaugh, T. L.; Karp, E. M.; Campbell, C. T. *to be published* **2012**.
(82) Labayen, M.; Furman, S. A.; Harrington, D. A. *Surface Science* **2003**, *525*, 149.
(83) Poelsema, B.; Mechtersheimer, G.; Comsa, G. *Surface Science* **1981**, *111*, 519.
(84) Donald, S. B.; Harrison, I. *Physical Chemistry Chemical Physics* **2012**, *14*, 1784.
(85) Chase, M. W.; National Institute of Standards and, T. *NIST-JANAF thermochemical tables*; American Chemical Society ; American Institute of Physics for the National Institute of Standards and Technology: [Washington, D.C.]; Woodbury, N.Y., 1998.
(86) Meixner, D. L.; George, S. M. *Surface Science* **1993**, *297*, 27.
(87) Michaelides, A.; Hu, P. *Journal of the American Chemical Society* **2000**, *122*, 9866.
(88) Jacob, T.; Goddard, W. A. *Journal of Physical Chemistry B* **2005**, *109*, 297.
(89) Psofogiannakis, G.; St-Amant, A.; Ternan, M. *Journal of Physical Chemistry B* **2006**, *110*, 24593.
(90) Kua, J.; Goddard, W. A. *Journal of the American Chemical Society* **1999**, *121*, 10928.
(91) Ford, D. C.; Xu, Y.; Mavrikakis, M. *Surface Science* **2005**, *587*, 159.
(92) Yang, M. L.; Zhu, Y. A.; Fan, C.; Sui, Z. J.; Chen, D.; Zhou, X. G. *Journal of Molecular Catalysis a-Chemical* **2010**, *321*, 42.
(93) Fiorin, V.; Borthwick, D.; King, D. A. *Surface Science* **2009**, *603*, 1360.
(94) Enkovaara, J.; Rostgaard, C.; Mortensen, J. J.; Chen, J.; Dulak, M.; Ferrighi, L.; Gavnholt, J.; Glinsvad, C.; Haikola, V.; Hansen, H. A.; Kristoffersen, H. H.; Kuisma, M.; Larsen, A. H.; Lehtovaara, L.; Ljungberg, M.; Lopez-Acevedo, O.; Moses, P. G.; Ojanen, J.; Olsen, T.; Petzold, V.; Romero, N. A.; Stausholm-Moller, J.; Strange, M.; Tritsaris, G. A.; Vanin, M.; Walter, M.; Hammer, B.; Hakkinen, H.; Madsen, G. K. H.; Nieminen, R. M.; Norskov, J.; Puska, M.; Rantala, T. T.; Schiotz, J.; Thygesen, K. S.; Jacobsen, K. W. *Journal of Physics-Condensed Matter* **2010**, *22*, 24.
(95) Hammer, B.; Hansen, L. B.; Norskov, J. K. *Physical Review B* **1999**, *59*, 7413.
(96) Fischer-Wolfarth, J. H.; Hartmann, J.; Farmer, J. A.; Flores-Camacho, J. M.; Campbell, C. T.; Schauermann, S.; Freund, H. J. *Review of Scientific Instruments* **2011**, *82*, 15.
(97) Weaver, J. H.; Frederikse, H. P. R. In *CRC*; CRC Press: Boca Raton, Fl, 2008, p 12.
(98) Weaver, J. H. *Physical Review B* **1975**, *11*, 1416.
(99) Rossmeisl, J.; Logadottir, A.; Norskov, J. K. *Chemical Physics* **2005**, *319*, 178.
(100) Getman, R. B.; Schneider, W. F. *Chemcatchem* **2010**, *2*, 1450.

(101) McQuarrie, D. A. *Statistical mechanics*; University Science Books: Sausalito, Calif., 2000.

(102) Stamenkovic, V. R.; Fowler, B.; Mun, B. S.; Wang, G. F.; Ross, P. N.; Lucas, C. A.; Markovic, N. M. *Science* **2007**, *315*, 493.

(103) Rossmeisl, J.; Karlberg, G. S.; Jaramillo, T.; Norskov, J. K. *Faraday Discussions* **2008**, *140*, 337.

(104) Meng, S.; Xu, L. F.; Wang, E. G.; Gao, S. W. *Physical Review Letters* **2003**, *91*.

(105) Wellendorff, J.; Lundgaard, K. T.; Møgelhøj, A.; Petzold, V.; Landis, D. D.; Nørskov, J. K.; Bligaard, T.; Jacobsen, K. W. *Physical Review B* **2012**, *85*, 235149.

(106) Grabow, L. C.; Gokhale, A. A.; Evans, S. T.; Dumesic, J. A.; Mavrikakis, M. *Journal of Physical Chemistry C* **2008**, *112*, 4608.

(107) Jerdev, D. I.; Kim, J.; Batzill, M.; Koel, B. E. *Surface Science* **2002**, *498*, L91.

(108) Cox, J. D.; Wagman, D. D.; Medvedev, V. A.; Hemisphere Pub. Corp.: New York, 1989.

(109) Jacob, T. *Fuel Cells* **2006**, *6*, 159.

(110) MacNaughton, J. B.; Naslund, L. A.; Anniyev, T.; Ogasawara, H.; Nilsson, A. *Physical Chemistry Chemical Physics* **2010**, *12*, 5712.

(111) Silbaugh, T. L.; Karp, E. M.; Campbell, C. T. *to be published* **2013**.

(112) McMillen, D. F.; Golden, D. M. *Annual Review of Physical Chemistry* **1982**, *33*, 493.

(113) Blanksby, S. J.; Ellison, G. B. *Accounts of Chemical Research* **2003**, *36*, 255.

(114) Karp, E. M.; Silbaugh, T. L.; Crowe, M. C.; Campbell, C. T. *Submitted JACS* **2012**.

(115) Lide, D. R. *CRC Handbook of Chemistry and Physics: A Ready-reference Book of Chemical and Physical Data*; CRC Press, 2004.

(116) Waszczuk, P.; Lu, G. Q.; Wieckowski, A.; Lu, C.; Rice, C.; Masel, R. I. *Electrochimica Acta* **2002**, *47*, 3637.

Curriculum Vitae

ERIC M. KARP
Ph.D. Candidate in Chemical Engineering
1230 N. 49th St.
Seattle WA, 98103
Tel: (270)-313-6063
karp.eric@gmail.com / karpe@uw.edu

EDUCATIONAL BACKGROUND

Dept. of Chemical Engineering — Ph.D, M.Sc.
University of Washington Seattle WA, USA — 2008 – (expected 2012)

Dept. of Chemical and Biological Engineering — B.Sc.
University of Colorado Boulder CO, USA — 2003-2007

AWARDS

- 2nd Place Oral Presentation at Graduate Student Symposium, University of Washington Chemical Engineering Dept. — 2010
- Most outstanding senior thesis, University of Colorado at Boulder — 2007
- David M. Boyd Scholarship (UC Boulder) — 2006
- J. Ranald Fox Scholarship (UC Boulder) — 2006
- Undergraduate Research Opportunities Grants (2) — 2005 - 06
- Dean's list (multiples) — 2004 - 07
- Most outstanding science project, Rose Hulman Institute of Technology — 2002

ACADEMIC EMPLOYMENT RECORD

1. University of Washington Chemical Engineering Dept. — 2008 – present
   Position: PhD Candidate / Graduate Student / Research Assistant
   Advisor: Prof. Charles T. Campbell (Tel: 206-616-6085, campbell@chem.washington.edu)
   - Fundamental surface science studies of catalytic materials which involved extensive work with thermodynamics of catalytic processes.
   - Use of many UHV analysis techniques: LEED, XPS, Auger, ISS, mass spectrometry and many others.
   - Design, construction, and maintenance of UHV equipment.
   - Kinetic measurements of catalysts using high-pressure reactors. Construction and maintenance of experimental catalytic reactor systems.
   - See publications 1,3-11

2. University of Colorado Boulder Chemical Engineering Dept. — 2004-2007
   Position: Research Assistant
   Advisor: Prof. Daniel Schwartz (Tel: 303-735-0240, daniel.schwartz@colorado.edu)
   - Atomic force microscopy, langmuir blodgett and trough techniques.

- Rebuilt Brewster angle microscope and wrote DAQ programs in Labview.
- See publication 12

3. University of Colorado Boulder Chemical Engineering Dept. 2003
Position: Research Assistant
Advisor: Prof. Will Medlin (Tel: 303-492-2418, Will.Medlin@colorado.edu)
    - Project: Structure sensitivity of fuel cell cathode reactions
    - Introduction to Molecular modeling and simulations with DFT
    - Built small computational cluster

INDUSTRIAL EMPLOYMENT RECORD

1. Pacific Northwest National Laboratory Jan – April 2012
Position: Interning Scientist
Contact: Dr. Charles (Chuck) H.F. Peden (Tel: 509-371-6501, Chuck.Peden@pnnl.gov)
    - Kinetic measurements using high temperature/pressure reactors
    - Study of metal exchanged zeolite catalysts for NO_x reduction
    - See publications 2

2. Symbios Technologies www.symbiosenergy.com 2007-2009
Position: Chemical Engineer
Contact: Justin Bzdek (Tel: 970 222-9178, justin@symbiostechnologies.com)
    - Biodiesel blending skid redesign and rebuild
    - Solar thermal plant modeling for DOE grant
    - Supercritical biomass to oil extraction (modeled and wrote phase I results and obtained SBIR for phase II funding)
    - Project successfully obtained SBIR funding

PUBLICATIONS

1. "The Mechanism and Rate of CO_2 Dissociation on Pt Black During the Reverse Water Gas Shift Reaction"
E.M. Karp, J.M. Lownsbury, T.A. Livingston Large, H.J. Sismaet, L.G. Cameron, L.Youn, T.L. Silbaugh, C.T. Campbell
(In Preparation)

2. "Probing Structure-Activity Relationships in NH_3-SCR over Cu-SSZ-13: Reaction Kinetics and EPR Studies"
F. Gao, **E.M. Karp**, C. HF. Peden
(In Preparation)

3. "Strength of Pt-OR and Pt-CR Bonds at a Pt(111) Surface by Adsorption Microcalorimetry; Predictions for Other Oxygen Containing Adsorbates"
E.M. Karp, T.L. Silbaugh, C.T. Campbell
(In preparation)

4. "Strength of Pt- CH_3 Bond at the Pt(111) Surface; Dissociative Adsorption of CH_3I by microcalorimetry"
   E.M. Karp, T.L. Silbaugh, C.T. Campbell
   (Too be submitted in ~3 weeks)

5. "Energetics of Adsorbed Formate and Monodentate Formate on Pt(111); Formic Acid on the O Predosed Pt(111) Surface"
   T.L. Silbaugh, **E.M. Karp**, C.T. Campbell
   (In Preparation)

6. "Kinetic Infromation Obtained From Microcalorimetry Through Detailed Signal Analysis"
   T.L. Silbaugh, **E.M. Karp**, C.T. Campbell
   (In Preparation)

7. "Energy of Adsorbed Methoxy on Pt(111); Methoxy on O Predosed Pt(111) Surface"
   E.M. Karp, T.L. Silbaugh, C.T. Campbell
   Submitted JACS

8. "The Energetics of Oxygen Adatoms and Hydroxyl Species on Pt(111)"
   E.M. Karp, F. Studt, J.K. Norskov, C.T. Campbell
   Submitted J. Phys. Chem. C.

9. "Energy of Adsorbed Hydroxyl on Pt(111) by Microcalorimetry"
   W. Lew, M.C. Crowe, **E.M. Karp**, C.T. Campbell
   J. Phys. Chem. C, 2011, 115, 11586-11594

10. "Insights into Catalysis by Gold Nanoparticles and their Support Effects through Surface Science Studies of Model Catalysts"
    C.T. Campbell, James C. Sharp, Y.X. Yao, **E.M. Karp**, Trent L Silbaugh
    Faraday Discuss., 2011. 152, 227-239

11. "Energy of Molecularly Adsorbed Water on Clean Pt(111) and Pt(111) with Coadsorbed Oxygen by Calorimetry"
    W. Lew, M. C. Crowe, **E.M. Karp**, C.T. Campbell
    J. Phys. Chem. C, 2011, 115, 9164-9170

12. "Langmuir Monolayers of Photo-Isomerizable Macrocycle Surfactant"
    E.M. Karp, C. Pecinovsky, D. Gin, D.K. Schwartz
    Langmuir, 2007, 23, 7923-7927

INVITED TALKS

1. Single Crystal Adsorption Calorimetry; Energetics of Catalytic Intermediates, Empirical Trends, and Benchmarks for DFT
   Argonne National Laboratory, Argonne IL, Aug 2012

2. Single Crystal Adsorption Calorimetry; Energetics of Catalytic Intermediates, Empirical Trends, and Benchmarks for DFT
   Northwestern University, Evanston IL, Aug 2012

3. Thermodynamics and kinetics of elementary reaction steps on and sintering of late transition metal catalysis,
   242nd ACS Ntnl. Meeting, Denver CO, Aug 2011

PRESENTATIONS AT SCIENTIFIC CONFERENCES

1. A trend in the strength of bonding of oxygen-containing intermediates on Pt(111) surfaces, and its implications in energy-related catalysis
   University of Washington Chemical Engineering Graduate Symposium, Sept. 2011

2. Heat of formation of adsorbed methyl on Pt(111) using adsorption microcalorimetry,
   242nd ACS Ntnl. Meeting, Denver CO, Aug 2011

3. Heat of formation of adsorbed methoxy on Pt(111),
   AVS National Symposium, Albuquerque NM, October 2010

4. Heat of formation of adsorbed methoxy on Pt(111),
   University of Washington Chemical Engineering Graduate Symposium, Seattle WA, September 2010

COMMITTEES SERVED ON

1. Distinguished Young Scientist Seminar Series Selection Committee 2011
2. American Vacuum Society, University of Washington Student Chapter 2010-present